

POLITECNICO DI TORINO

Facoltà di Ingegneria

PhD in materials science and technology

XXVII° ciclo



**Self hardening aluminum alloys for  
automotive applications**

Academic advisors:  
Prof. Mario Rosso  
Dott.ssa Ildiko Peter

PhD student:  
Christian Castella

## **Acknowledgements**

I would like to extend my deepest gratitude to my thesis advisors, Prof. Mario Rosso and Dr. Ildiko Peter and to Teksid Aluminum for their mentoring, support and help. I also wish to thank all the people that have helped me to realized this work.

*Thanks to my family that has always supported me in these years*

# Self hardening aluminium alloys for automotive applications

	Pag.
<b>INDEX</b>	2
<b>OUTLINE</b>	4
<b>CHAPTER 1: <i>Aluminium alloys used in automotive industry</i></b>	5
<b>1.1</b> Introduction	5
<b>1.2</b> Aluminium alloys	6
<b>1.2.1</b> Cast aluminum alloys	7
<b>1.2.2</b> Wrought aluminum alloys	9
<b>1.3</b> Thermal treatment used for aluminium cast alloys	10
<b>1.3.1</b> Solution treatment	12
<b>1.3.2</b> Quenching	13
<b>1.3.3</b> Ageing	15
<b>1.4</b> Defects in foundry casting	19
<b>1.5</b> Mechanical components produced with aluminum alloys in the automotive industry	29
<b>CHAPETR 2: <i>Corrosion resistance of aluminum alloys</i></b>	35
<b>2.1</b> Introduction	35
<b>2.2</b> Causes of corrosion	39
<b>2.2.1</b> Effect of the alloying elements	39
<b>2.2.2</b> Effect of the microstructure on corrosion	40
<b>2.2.2.1</b> Pitting corrosion	41
<b>2.2.2.2</b> Galvanic corrosion	44
<b>2.2.2.3</b> Intergranular corrosion	46
<b>2.2.2.4</b> Stress-corrosion cracking	49
<b>2.2.3</b> Effect of environmental variables on corrosion	53
<b>2.3</b> Corrosion prevention methods	56
<b>CHAPTER 3: <i>Self hardening aluminium alloys</i></b>	60
<b>3.1</b> Introduction	60
<b>3.2</b> Properties	61

3.3 Applications	62
<b>CHAPTER 4: <i>Real case study</i></b>	65
4.1 Introduction	65
4.2 Knuckle component	66
4.2.1 Analysis of the heat treatment costs for the production of knuckle component	67
4.3 AlZn10Si8Mg self hardening alloy as a possible alternative to A356 alloy to produce the knuckle component	70
4.3.1 Microstructural analysis	70
4.3.2 Mechanical properties	75
4.3.2.1 Tensile test	76
4.3.2.2 Brinell hardness test	78
4.3.3 Corrosion resistance evaluation	79
4.4 Modification of AlZn10Si8Mg chemical composition through the addition of Mg up to 3%wt	81
4.4.1 Microstructural analysis	82
4.4.2 Mechanical properties evolution	95
4.4.2.1 Three point bending test	95
4.4.2.2 Charpy Impact test	98
4.4.2.3 Vickers hardness test	100
4.4.3 Fracture surfaces analysis	102
4.4.4 Corrosion properties	104
4.4.4.1 Salt spray corrosion test	104
4.4.4.2 Intergranular corrosion test	108
4.4.5 Fatigue properties evaluation	118
4.4.5.1 Fracture surface analysis	119
<b>CHAPTER 5: <i>Conclusions and on-going activities</i></b>	122
<b>REFERENCES</b>	125
<b>AUTHOR'S PUBLICATIONS</b>	132

## **OUTLINE**

This PhD thesis has been carried out in collaboration with Teksid Aluminum, an aluminum foundry situated in Carmagnola near Turin, where all the samples tested in this work have been casted and produced. While the whole characterization of the specimens has been performed in the laboratories of the department of applied science and technology, of the Politecnico di Torino.

Self-hardening aluminum alloys (Al-Zn-Si-Mg alloys) represent an innovative class of light aluminum alloys. They present high mechanical properties, which make them suitable for many applications in different industrial fields, especially in transport industry. The most important and relevant feature of the self-hardening alloys is related to their good performance, without the need of any heat treatment: they are subjected to a natural ageing phenomenon at room temperature after a storage period of about 7-10 days. The possibility to avoid the heat treatment represents an important benefit, contributing to considerably reduce both the production cost of some components and the amount of energy involved in the manufacturing process. Furthermore, without heat treatment the risk of component's deformation during the production is eliminated.

The goal of this PhD Thesis was to find an alternative solution to the actually used T6 heat-treated A356 alloy for automotive component production.

The feasibility of the development, of a knuckle suspension component, starting from the self hardening alloy was evaluated and investigated. In addition, some qualitative and semi-quantitative considerations was figured out from economical point of view. The use of the self-hardening aluminum alloy allows avoiding any heat treatment, consequently an important energy saving can be reached during the manufacturing, especially in terms of gas and electricity consumption, that are important features for the environment.

## Outline

A consistent part of this thesis was focalized on the study of the structural features and mechanical properties of the self-hardening aluminum alloys. Another part was dedicated to investigate their corrosion resistance. The effect of the Mg content and of the cooling rate, on the microstructure of three different self-hardening aluminum alloys, were investigated, aiming to define the optimal alloy composition for knuckle suspension component production.

# 1 ALUMINUM ALLOYS USED IN AUTOMOTIVE INDUSTRY

## 1.1 Introduction

Aluminum is a light-weight metal and it is one of the most abundant metallic element on earth, about 8% of earth's crust, making it second after silicon (28%). The main ore of aluminum is the bauxite, primarily a mixture of  $\text{Al}_2\text{O}_3 \cdot 3\text{H}_2\text{O}$ ,  $\text{Fe}_2\text{O}_3$  and  $\text{SiO}_2$ . The aluminum could be produced as primary or secondary aluminum. For the former type production the process starts from the raw material of aluminum, namely, bauxite. Bayer process [1] is used to extract the aluminum oxide ( $\text{Al}_2\text{O}_3$ ). In this process, developed by Austrian Karl Joseph Bayer in 1892, bauxite is placed inside a solution of caustic soda, at elevated temperature and under pressure, so as a consequence alumina has dissolved out as a solution of sodium aluminate. Then the aluminum hydrate is separated by precipitation from the solution of sodium aluminate and through the calcination process is converted in aluminum oxide ( $\text{Al}_2\text{O}_3$ ). Finally by the use of the electrolytic process, known as the Hall-Héroult process, the primary aluminum is obtained. In this process alumina is dissolved in a cryolite bath.

On the other hand the improved techniques of scrap preparation and melting gave rise to the development of the secondary aluminum industry, since 1950s. There has been an increasing interest, towards the recycling of aluminum, because the energy required to re-melt aluminum scraps is only 5% of that required to produce the primary aluminum.

In the late 1800s and early 1900s, because of three important industrial developments:

- 1) development of the first internal combustion engine;
- 2) electrification;
- 3) invention of airplane by Wright brothers;

the aluminum became a very important economic competitor and the aluminum industry was subjected to an exponential growth [2-3].

The aluminum offers a wide range of properties that make it a suitable metal for many applications in different industrial fields such as: the automotive industry, the aeronautical and aerospace area, the electrical and electronic industries and so on. Some of the principal properties of this metal are:

1. its density  $\rho = 2,7 \text{ g/cm}^3$ , that is one-third that of the steel;
2. its high strength to weight ratio;
3. its high corrosion resistance under the majority of service conditions;
4. the excellent thermal and electrical conductivity;
5. the high reflectivity;
6. is a non ferromagnetic metal, which is important especially in electrical and electronic industries;
7. is nontoxic, so for this reason is used routinely for food and beverages packages;
8. is recyclable.

## 1.2 Aluminum alloys

Aluminum alloys are classified in two categories:

1. cast aluminum alloys;
2. wrought aluminum alloys.

In table 1 is reported the aluminum alloys designation system, used by the Aluminum Association of the United States, for both cast than wrought aluminum alloys. This designation system uses a four-digit numerical system to identify the different aluminum alloys. The nomenclature for wrought alloys has been accepted by most countries and is now called the International Alloy Designation System (IADS). The first digit indicates the alloy group and the last two digits identify the aluminum alloy or indicate the aluminum purity. The second digit indicates modifications of the original alloy or impurity limits. The designation of cast alloys, the first digit is essentially the

same as for wrought alloys while the second two digits serve to identify a particular composition.

**Table 1:** Designation system of aluminum alloys [4].

Alloy type <sup>a</sup>	Four-digit designation
<b>Wrought alloys</b>	
99.00% (min) aluminum	1XXX
Copper	2XXX
Manganese	3XXX
Silicon	4XXX
Magnesium	5XXX
Magnesium and silicon	6XXX
Zinc	7XXX
Others	8XXX
<b>Casting alloys</b>	
99.00% (min) aluminum	1XX.X
Copper	2XX.X
Silicon with added copper and/or magnesium	3XX.X
Silicon	4XX.X
Magnesium	5XX.X
Zinc	7XX.X
Tin	8XX.X
Others	9XX.X

<sup>a</sup> Designations are based on aluminum content or main alloying elements.

### 1.2.1 Cast aluminum alloys

Nowadays, casting aluminum alloys are finding new applications in many industry fields. About 80 % of all aluminum casting products come from aluminum scrap, percentage that is significantly higher than wrought products. In the last 10 years casting technologies have developed considerably so now it is possible to achieve higher quality alloys. The cast aluminum alloys have an increasing interest in the automotive and aerospace industries as cost-effective, environment-friendly lightweight materials. Their interesting properties such as good castability, high mechanical properties, ductility and good corrosion resistance, have allowed them to substitute steel and cast iron for the production of critical components [5]. Generally these alloys contain high percentage of alloying elements; the most important alloying elements are [6]:

- *Silicon*: is one of the most important alloying element used for cast aluminum alloys. Generally presents a content between 5-12 wt%. First of all, this alloying element,
- allows to increase the fluidity of the alloys and as a consequence enhance its castability, reduces the thermal expansion coefficient of alloys. Presents a low density ( $2.34\text{g/cm}^3$ ) determining a reduction of cast components weight and finally its low solubility in aluminum allows the precipitation of pure, hard Si particles which improve the abrasion resistance of the alloy.
- *Copper*: increases both the mechanical strength and the machinability of alloys; reduces the coefficient of thermal expansion and as most important characteristic has a negative effect on the corrosion resistance of alloys.
- *Magnesium*: allows to increase the mechanical properties through the precipitation of  $\text{Mg}_2\text{Si}$  hardening precipitates, enhance the corrosion resistance and the weldability of alloys;
- *Manganese*: improves the tensile properties as well as increase significantly the low-cycle fatigue resistance. Addition of manganese improves the corrosion resistance of the alloy.
- *Iron*: is the most common and inevitable impurity in Al-Si foundry alloys, because it can form different types of intermetallic compounds; such compounds are brittle and have a deleterious effect on the mechanical strength of components. Several types of Fe-rich phase exist, such as  $\beta\text{-Al}_5\text{FeSi}$ ,  $\alpha\text{-Al}_{15}\text{Fe}_3\text{Si}_2$  and  $\alpha'\text{-Al}_8\text{Fe}_2\text{Si}$ . When the Mn concentration in the alloy is increased the total volume fraction of intermetallic phase linearly increases, but the  $\beta\text{-Al}_5\text{FeSi}$  phase is converted into  $\alpha\text{-Al}_{15}\text{-(Fe,Mn)}_3\text{Si}_2$  phase, that is stable at low cooling rate. The  $\alpha\text{-Al}_{15}\text{-(Fe,Mn)}_3\text{Si}_2$  (Figure 1a) particles are more compact than the  $\beta$  ones (Figure 1b) and they show a Chinese script, star-like or polyhedral morphology, and for this reason they present a minor effect on the fragility of the alloy. Generally when the concentration of Mn in the alloy overcame 1%wt, the lamellar  $\beta\text{-Al}_5\text{FeSi}$  phase is completely converted in the  $\alpha$  phase.

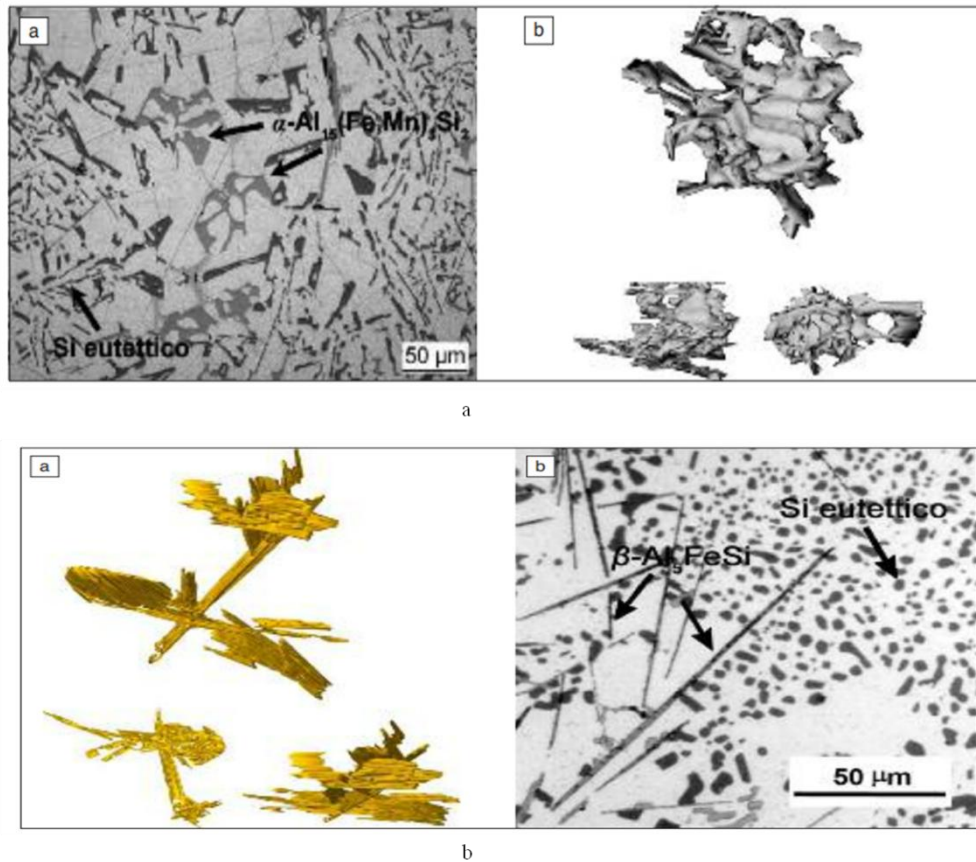


**Figure 1:** Microstructures showing: a) the  $\alpha$ -Al<sub>15</sub>(Fe,Mn)<sub>3</sub>Si<sub>2</sub> phase with Chinese script morphology and b) the  $\beta$ -Al<sub>5</sub>FeSi platelets [7].

### 1.2.2 Wrought aluminum alloys

The wrought aluminium alloys are widely used in automotive and aerospace industry to manufacture different components, thank to their mechanical properties, which are higher than those obtained for cast aluminum alloys [8-9]. Wrought aluminum alloys represent about 85% of aluminum applications. They are initially cast as ingots or billets and subsequently hot and/or cold worked mechanically into the desired form. The crystal structure of Al, face centered cubic system (fcc) offers a good cold formability. For wrought applications, the addition of alloying elements improves most of the mechanical properties; even if they have a comparatively small quantity of alloying

elements, the structure of wrought alloys offers better mechanical properties than cast alloys.

Plastic deformation have increase the degree of grain refinement and homogenize the microstructure. There are four main process applied to wrought alloys to obtain different products:

1. Rolled products: plates, flat sheets, coiled sheets, and foils.
2. Extruded products: extruded rods, solid and hollow shapes, profiles, or tubes.
3. Forming products: rolled or extruded products are formed to achieve complex shapes.
4. Forged products: they have complex shapes with superior mechanical properties.

### **1.3 Thermal treatment used for aluminum cast alloys**

Generally, heat treatments are widely used in Al foundry to increase the mechanical strength of aluminium alloys. Actually, there is a high tendency to minimize the energy consumption in order to have a minor impact on the environment. Additionally, a more strict reliability, higher performance and production costs became important features. In this scenario, optimization of heat treatments is important. This process significantly influence properties such as strength, ductility, fracture toughness, thermal stability, residual stresses, dimensional stability, resistance to corrosion and stress corrosion cracking. The most important heat treatment procedures are homogenization, annealing and precipitation hardening which involves solution heat treatment, quenching and aging.

The Aluminum association has developed the classification of temper - designation system reported in table 2.

**Table 2:** Temper - designation system used for aluminum alloys [4].

Suffix letter (indicates basic treatment or condition)	First suffix digit (indicates secondary treatment)	Second suffix digit (indicates residual hardening)
F, as fabricated		
O, annealed/wrought products only		
H, cold-worked/work-hardened	1, cold-worked only 2, cold-worked and partially annealed 3, cold-worked and stabilized	2, 1/4 hard 4, 1/2 hard 6, 3/4 hard 8, hard 9, extra hard
W, solution heat-treated		
T, heat-treated/stable	1, partial solution plus natural aging 2, annealed cast products only 3, solution plus cold work 4, solution plus natural aging 5, artificially aged only 6, solution plus artificial aging 7, solution plus stabilizing 8, solution plus cold work and artificial aging 9, solution plus artificial, aging and cold work	

a Added as suffix letters and digits to the alloy number.

This designation system, used for both cast than wrought aluminum alloys with the exception of ingots, has been developed by the Aluminum Association and is currently adopted as part of the IADS by most countries. This system is based on digits following the letters indicate subdivisions of the tempers, that significantly influence the properties of the alloy.

If the strengthening effects is not necessary, the most suitable heat treatments, for casting are the homogenization and annealing whereas, when an increase of mechanical strength is required, the heat treatments to a stable condition (T series temper state) must be applied.

The heat treatment is divided in three steps [10]:

1. Solution treatment
2. Quenching
3. Ageing

### 1.3.1 Solution treatment

The solution treatment is carried out at temperature as close as possible to the eutectic temperature in order to obtain:

- the dissolution of soluble phases, containing Cu and Mg formed during the solidification;
- the homogeneization of the alloying elements;
- the spheroidization of eutectic silicon particle.

The rate of these three processes increases as the solution treatment temperature increases. High accuracy has to be adopted to choose the temperature used for this treatment: as reported in figure 2 in the Al-Cu phase diagram the solubility of alloying elements increase when the temperature increase. The assumed temperature generally is situated between the solvus temperature and the solid temperature. For example in the case of Al-Cu alloys, the solution temperature have to be lower than 485°C in order to avoid the incipient melting, of the Cu-rich phases [11], because localized melting results in distortion and significantly can reduce the mechanical properties. Components have to be maintained at this temperature for a period of time necessary to reach a homogeneous solid solution.

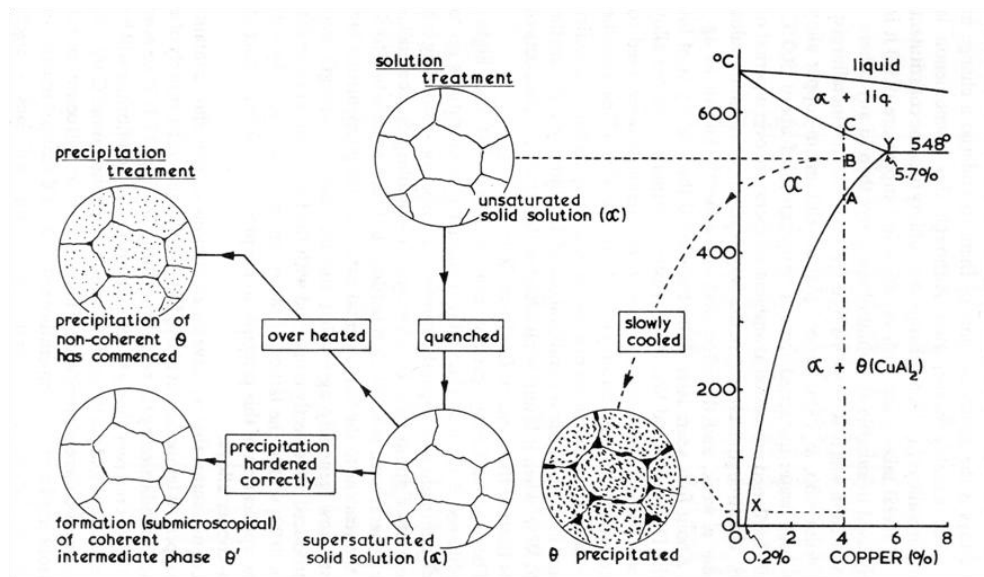


**Figure 2:** Representation of the mechanisms associated with solution, quench and aging in the case of Al-Cu alloys [12].

### 1.3.2 Quenching

The goal of the quenching is to have at room temperature the structure obtained after the solution treatment; in fact through a rapid cooling a supersaturated solution of alloying elements into the  $\alpha$ -Al matrix is obtained. It is necessary to choose accurately the quenching rate, if the cooling is too slow particles precipitated at grain boundaries and a reduction in supersaturation of solute and a lower maximum yield strength, after ageing, have been obtained, while on the other hand, a rapid cooling induces residual stresses into the components. Especially for components with severe thickness variations, rapid quenching can give rise to severe thermal gradients that determine a non-homogeneous plastic flow, which in turn induces distortion and the presence of residual stresses [13]. Generally water is used as a quenching medium to guarantee a correct cooling rate, while other quenching medium such as oil, salt baths and organic solutions can be used if a slower quench rate is necessary. To get better cooling characteristics of the quenching medium, some aqueous solutions of poly-alkylene glycol (PAG) have been recently developed [14]. Commonly the adopted PAG concentration is included

between 4 and 30% and usually is determined by the type of product being processed [14].

Recently, an innovative method, known as uphill quenching [15], has been developed to minimize the residual stress induced by the quenching. The uphill quenching consists of four steps:

1. quenching in boiling water ( $\sim 100^{\circ}\text{C}$ ) for 15 minutes;
2. quenching into liquid nitrogen for 30 min;
3. quenching in boiling water ( $\sim 100^{\circ}\text{C}$ ) for 15 minutes;
4. removing the components from the hot water and let them air cool to room temperature for the following natural ageing.

Through the adoption of this method, the main advantage obtained is to reduce the induced residual stresses and distortions, without decreasing the mechanical properties. This is reached thanks to the reduction of the  $\Delta T$  between the various steps. As a disadvantage one can mention the increasing of time necessary for the quenching and also the enhancement of the process costs, as a consequence of the use of  $\text{N}_2$  as quenching medium. Figure 3 reports a temperature versus time diagram for both conventional and uphill quenching processes.

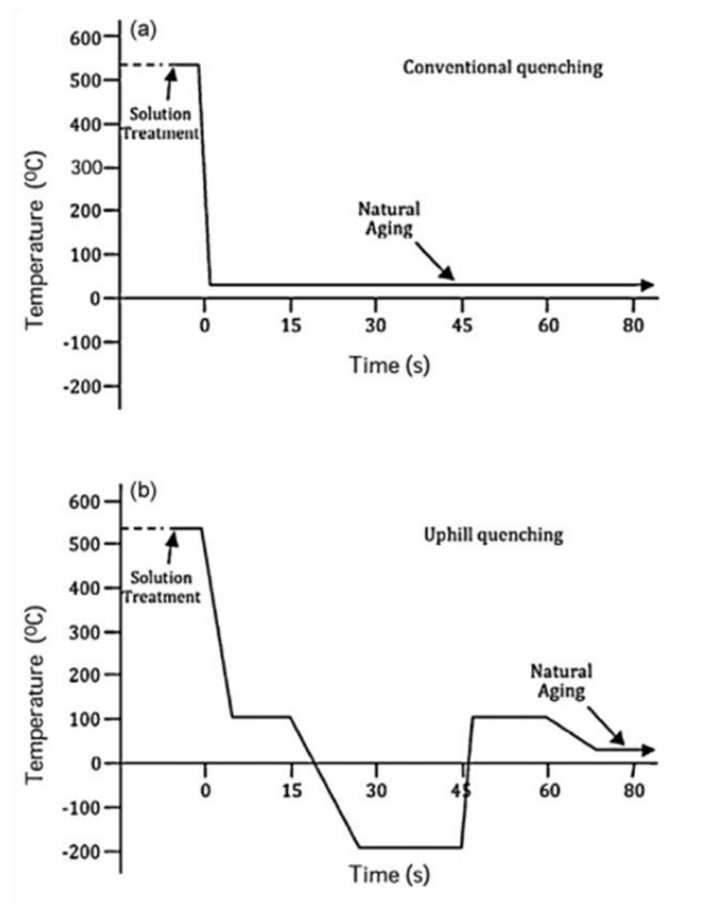


**Figure 3:** Temperature versus time diagram for: a) conventional and b) uphill quenching processes [15].

### 1.3.3 Ageing

The objective of ageing is to reach the precipitation of small hardening precipitates, uniformly distributed into the  $\alpha$ -Al matrix, in order to improve the mechanical strength of the alloys. The ageing can be performed at room temperature (natural ageing) or at high temperature in the range of 100–210 °C (artificial ageing). The improved mechanical properties of the alloys are due to the ability of precipitates to block dislocations. The size and the distribution of the precipitates, together with the coherency of the precipitates with the matrix, are fundamental to determine the high strength obtained during the ageing process. Figure 4 illustrates the Friedel effect and

the Orowan mechanism used to describe and explain, the interaction between dislocations and hardening precipitates.

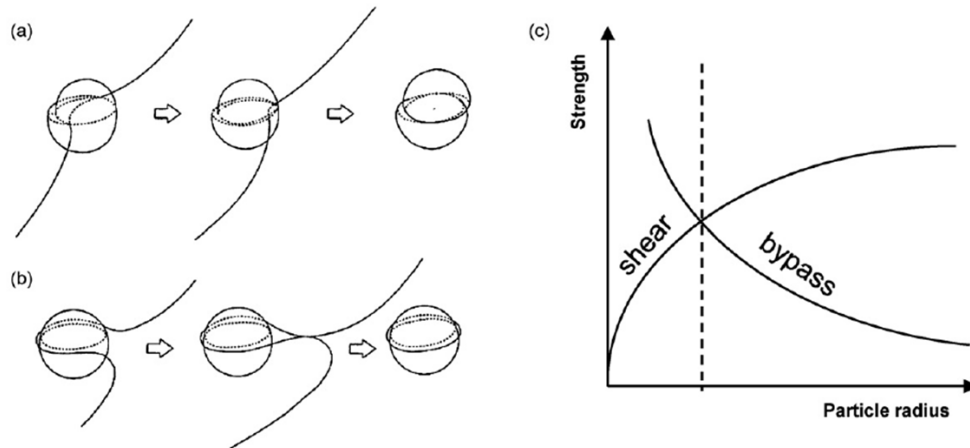


**Figure 4:** Dislocation bypass precipitates by : a) Friedel effect or b) Orowan mechanism. c) strength versus particle radius diagram [10].

If the precipitates are small and not hard they are sheared by moving dislocations (Friedel effect reported in figure 4a), whilst when their dimensions increase they are bypass by bowing the (Orowan mechanism figure 4b). As can be observed in the diagram reported in figure 4 c, when there is the same probability for the dislocations to pass the hardening precipitates, by shearing or by bowing, the maximum strength is achieved.

After the quenching process, the hardened aluminum alloy is in a un-stable condition and has a high energy level, so for this reason the alloy itself tries to achieve a low energy state, through the spontaneous transformation of the supersaturated solid solution in metastable phase or equilibrium phase. The driving force, for this transformation, is the decrease of the system's energy, which takes place through the precipitation of hardening precipitates. The precipitation process follows the traditional nucleation and growth mechanism. For the development of stable nuclei is required a certain period, after which, the process slowdown continuously because of the progressive depletion of solute atoms in the solid solution. The hardness-time curve summary of the ageing process is reported in figure 5.

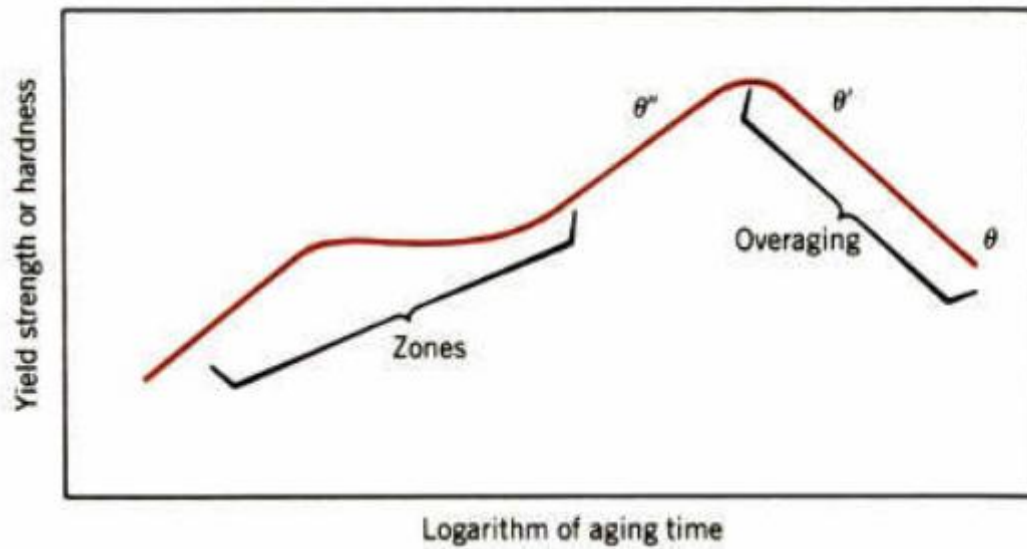


**Figure 5:** Strength and hardness as a function of the logarithm of aging time [16].

The precipitation sequence for Al-Si-Cu alloys, reported in figure 6, is the following:

- GP zones: are small aggregations of solute (clusters) called Guiner Preston zones. These zones are developed at low aging temperature and are made as a consequence of the segregation of Cu atoms in the supersaturated solid solution  $\alpha$ . The GP zones are made of areas of thickening in the form of discs of a few atoms thick (0.4-0.6 nm) and they have a diameter of about 8-10 nm.
- $\theta''$ : are precipitates with nanodimensions that are coherent with the matrix. Their dimensions ranging from about 1 to 4 nm (thickness) and 10 to 100 nm in diameter.
- $\theta'$ : are precipitates with micrometric size and are incoherent with the matrix;
- $\theta$ : is the equilibrium phase, is completely incoherent with the matrix and has the composition of  $\text{Al}_2\text{Cu}$ .

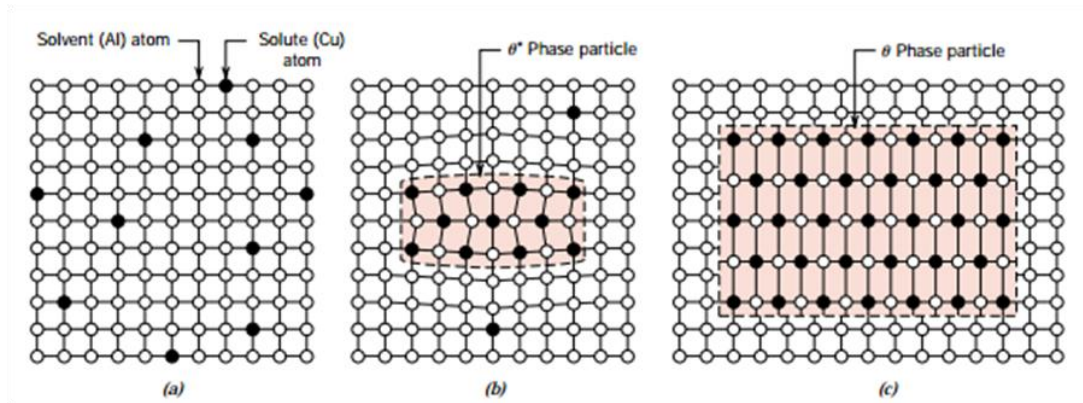


**Figure 6:** Precipitation sequence for Al-Si-Cu alloys [16].

Finally, as can be reported in figure 5, there is a decrease of the mechanical properties due to coalescence of precipitation hardening; this phenomenon is called overaging.

The hardness-tensile strength-time curves obtained at different ageing temperatures is reported in Figure 7. At high temperatures the process is more rapid and the hardness's peak is achieved in a short time, due to the major diffusion rate, but on the other hand, the maximum value of hardness decreases when the temperature increases.

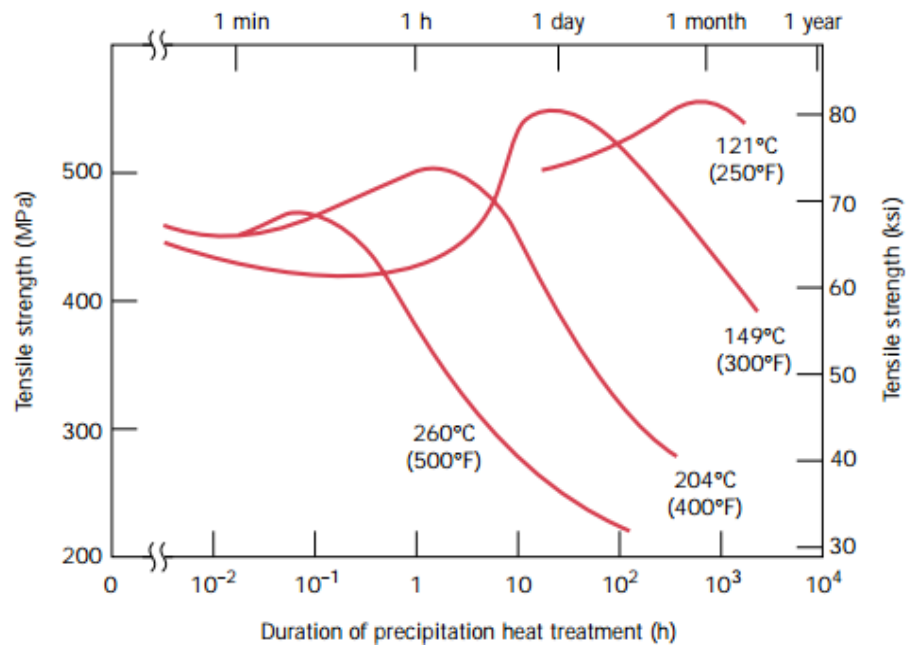


**Figure 7:** Hardness-Tensile strength-time curves at different ageing temperatures [16].

The precipitation is a diffusion phenomenon that depends exponentially from the temperature, so when the temperature is increased the time necessary for ageing decreases. This allows reducing the costs of the treatment and it is the reason why industrially, normally the ageing is artificial.

## 1.4 Defects in foundry casting

In the scientific literature, the foundry defects, especially those detected in components produced by die-casting process, have been classified according to two different approaches. The first one has been proposed by Cocks [17] and classify the defects according to their geometric position in surface defects and internal defects. Figure 8 reports the classification by Cocks.

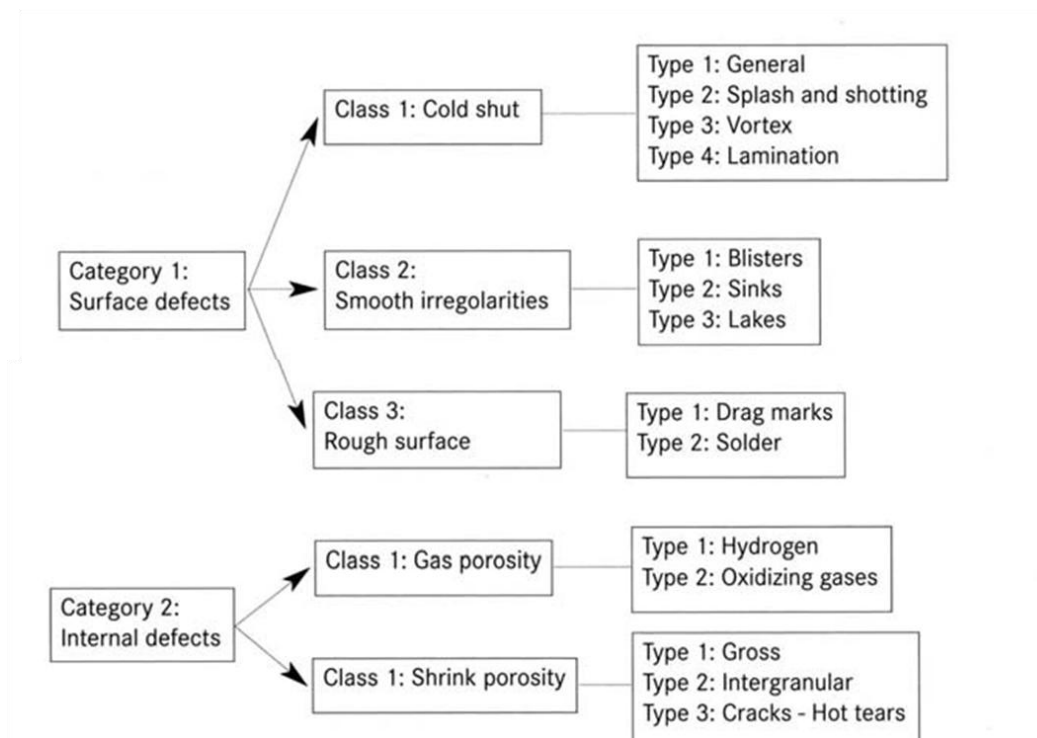


**Figure 8:** Classification of foundry defects according Cocks [17].

The second classification has been proposed by Campbell [18] and is reported in figure 9. This classification considers the defects in accordance with the metallurgical causes that have gave rise to the defects into the produced components.

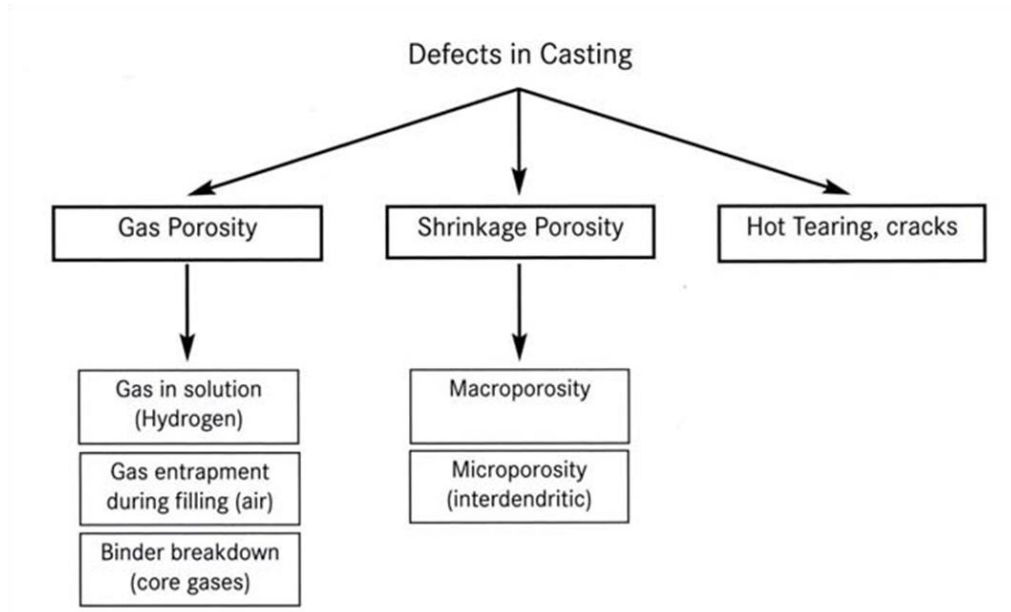


**Figure 9:** Classification of foundry defects according Campbell [18].

The most important foundry defects are:

*Gas porosity:* the main causes of these defect are [19]: air, humidity and especially hydrogen. The solubility of hydrogen in aluminum varies directly with temperature and the square root of pressure; solubility increases quickly with increasing temperature above the liquidus. Hydrogen has a greater solubility in liquid aluminum than in solid aluminum, as can be noted in figure 10. During cooling and solidification, dissolved hydrogen in excess of the extremely low solid solubility can precipitate in molecular form, resulting in the formation of primary and/or secondary voids (figure 11). This gas porosity has harmful effects on the mechanical properties of aluminum casting [20-21]. This type of porosity is usually spherical in appearance. It can be avoided through proper degassing of the molten metal, appropriate gating design and correct pouring practices.

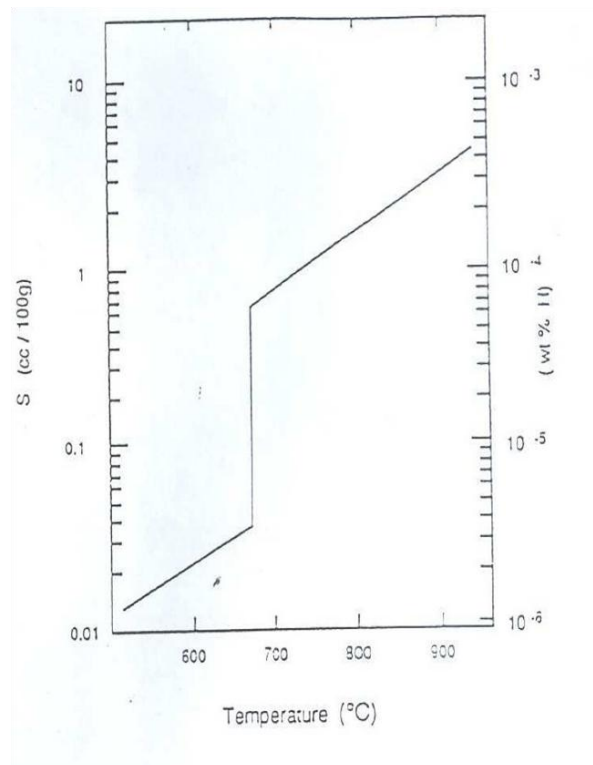


**Figure 10:** Diagram of Sievert's law.



**Figure 11:** Gas porosity (courtesy of Teksid Aluminum).

*Shrinkage porosity*: the transformation from liquid to solid state is accomplished by a decrease in volume, so because of this volumetric difference shrinkage porosity occurs during solidification. In aluminum alloys, the volumetric shrinkage that occurs during solidification varies from 3.5 to 8.5%. Shrinkage pores generally are individuated in regions suffering volume reduction, as a consequence of the phase change from liquid to solid, where the feed metal has no access. These areas are called hot spot because are islands of hot metal totally surrounded by solidified material. SEM images in figure 12 reports some shrinkage porosities.

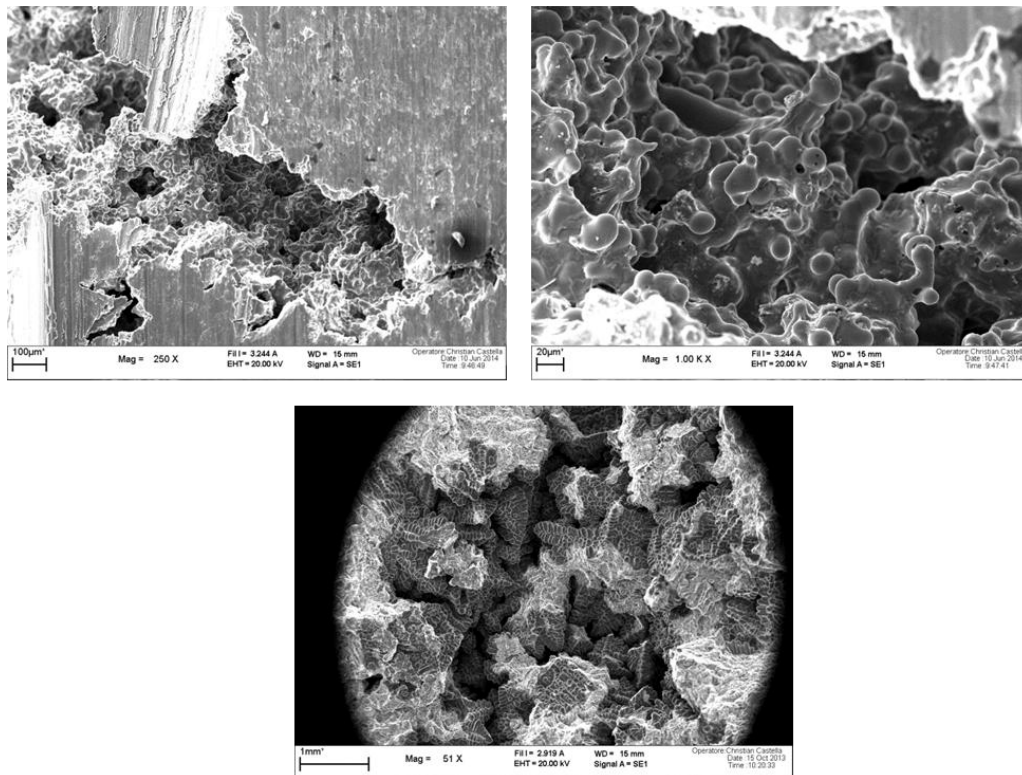


**Figure 12:** Shrinkage porosity (courtesy of Teksid Aluminum).

Shrinkage porosities can act as stresses raisers and therefore they represent the favorite nucleation site for cracks, consequently are extremely deleterious for the mechanical strength [22-23]. As can be observed in the SEM image (figure 13), the shrinkage porosities can be the nucleation site for a fatigue crack. The alloying elements that contribute to elevated-temperature strength such as iron, copper, and nickel increase resistance to surface collapse, leading to contained shrinkage voids.

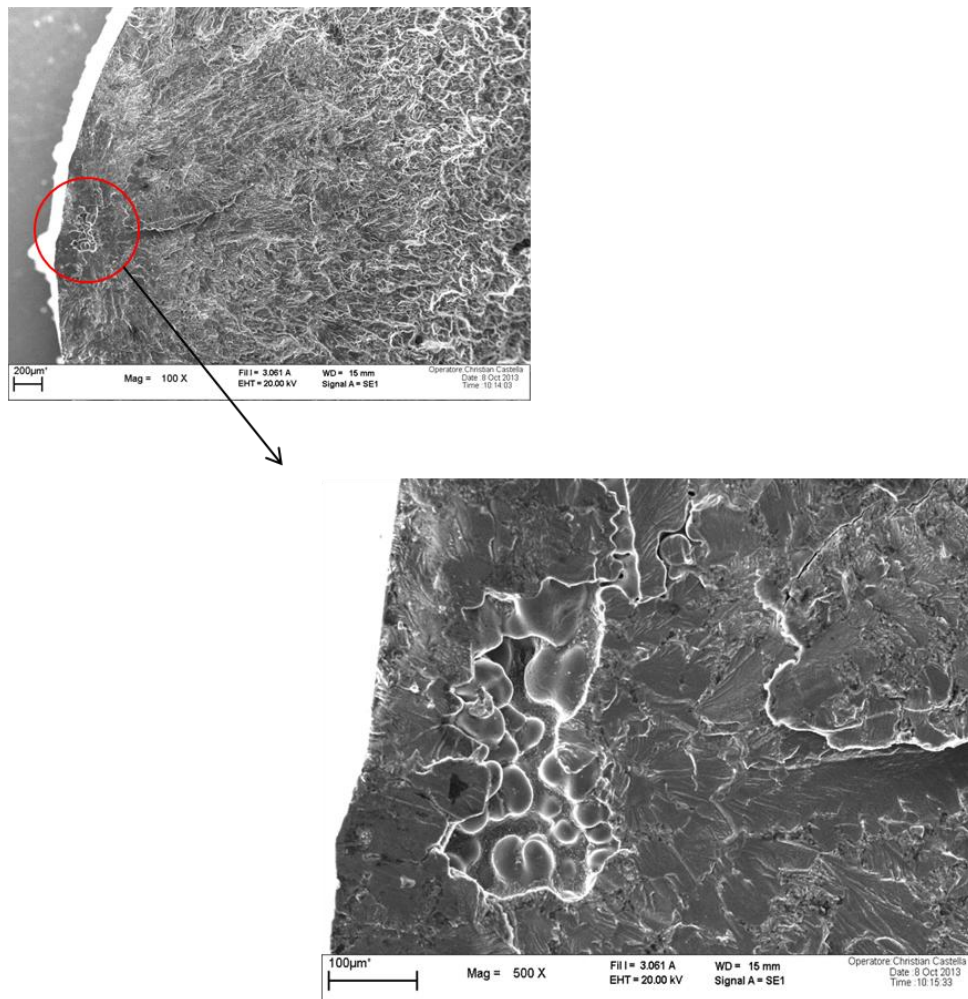


**Figure 13:** Shrinkage porosity that act as nucleation site for a fatigue crack (courtesy of Teksid Aluminum).

*Inclusions:* non metallic inclusions, particularly oxides particles, are typical in cast aluminum and are due to the high affinity between aluminum and oxygen. The oxidation rate is higher than the molten metal temperatures and increases as temperature and time of exposure increases. Figure 14 reports a SEM image with the presence of oxide particle. These inclusions affect negatively the mechanical strength of components [24-25].

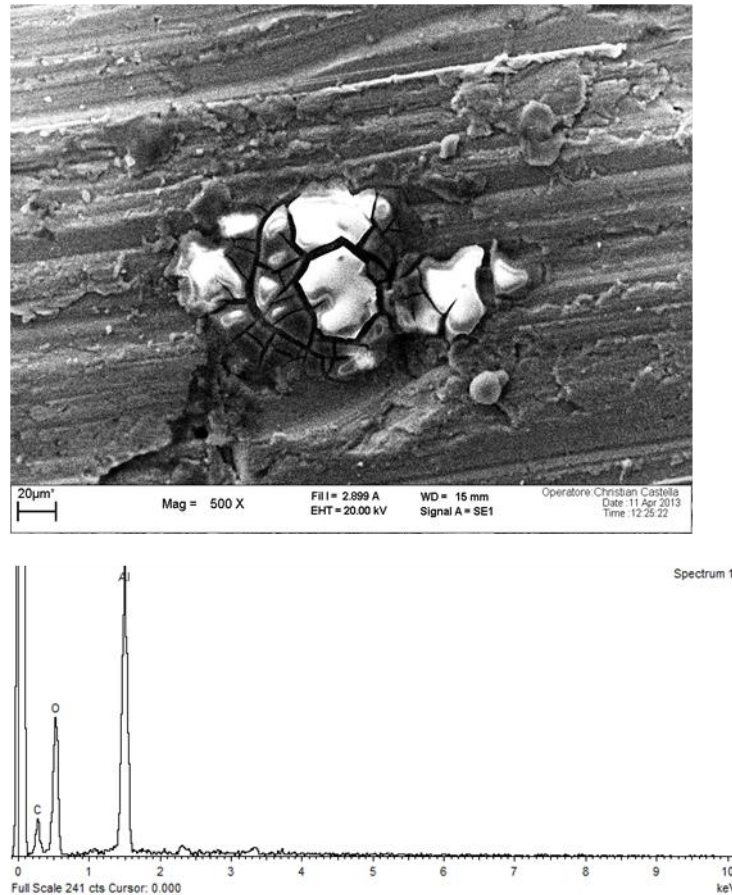


**Figure 14:** Oxide particle (source Teksid Aluminum).

*Bifilms*: the high affinity between aluminum and oxygen give rise to the formation of a layer of aluminum oxide ( $\text{Al}_2\text{O}_3$ ) on the surface of molten aluminum. This oxide layer protects the molten metal from the further oxidation. The presence of this layer becomes deleterious during the various operations which involve the molten metal, especially during casting operations. The alumina oxide as a consequence of the turbulence created could be entrapped inside the molten metal. In this way, two not wettable oxide surfaces, as can be observed in figure 15, come in contact between them and trap gas.

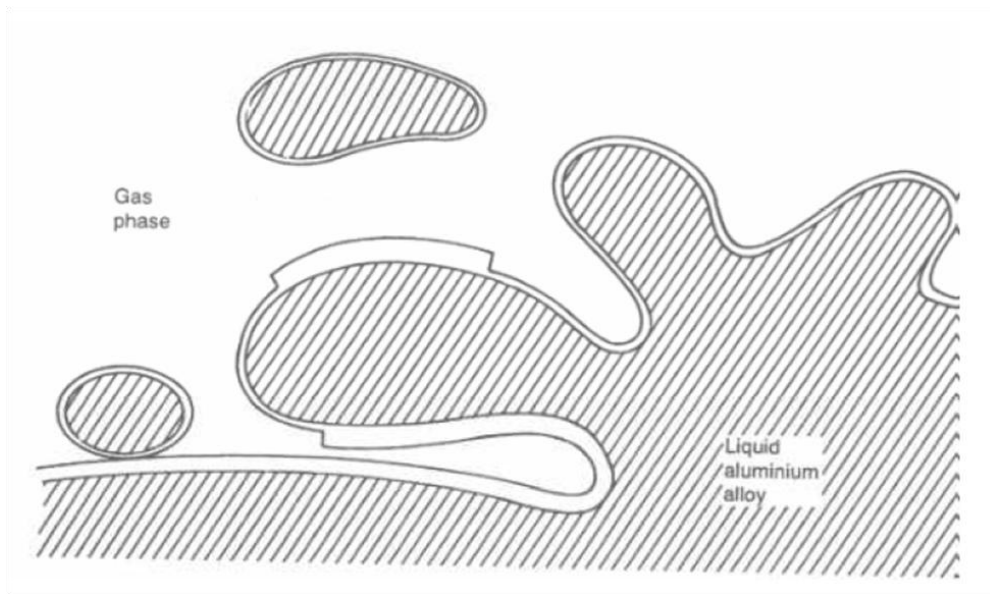


**Figure 15:** Creation mechanism of bifilm [26].

The defect, called bifilm, act as a crack and can reduces drastically the performances of aluminium alloys [27]. Figure 16 and 17 report the micrographs of some bifilms individuated in A354 (AlSi9Cu) aluminum alloy samples .

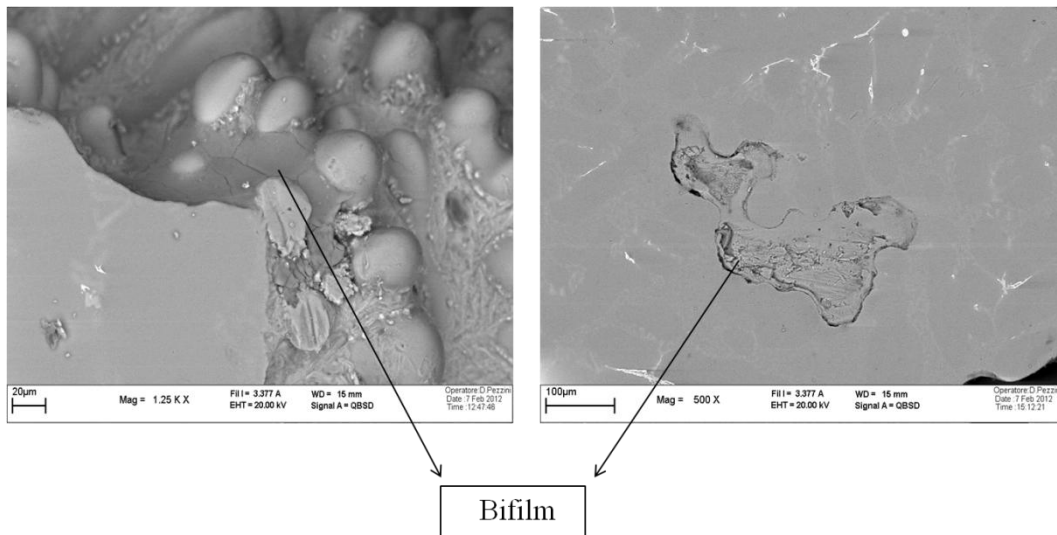


**Figure 16:** Some bifilm individuated in a A354 aluminum alloy (courtesy of Teksid Aluminum).

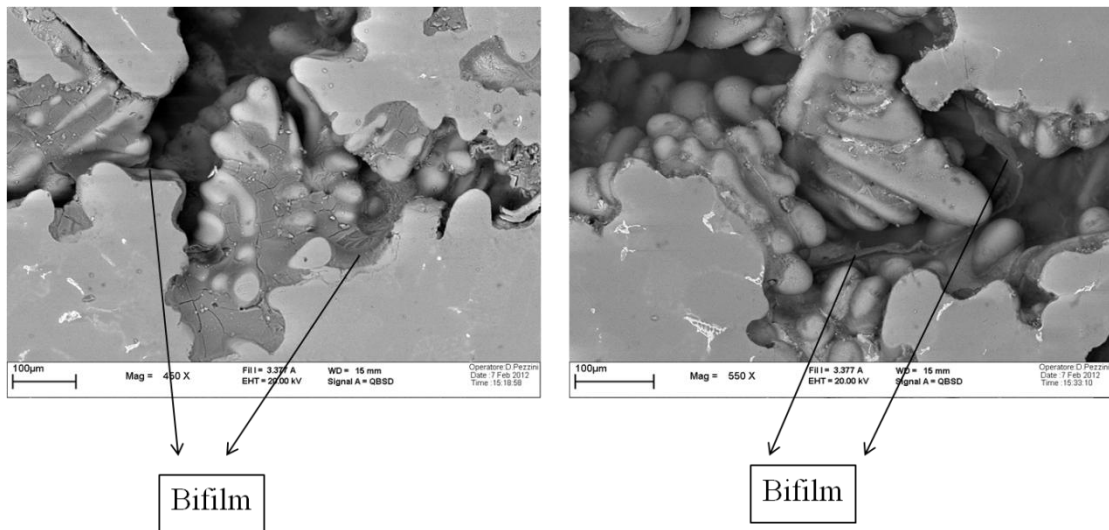


**Figure 17:** Some bifilm individuated in a A354 aluminum alloy (courtesy of Teksid Aluminum).

*Cold shut:* these defects originates in the cold area of dies, which are far from the feeding channel. In these zones there is a non-correct thermal regime so the material has a inadequate temperature for its correct solidification as a result when this partial solidified material met a flux of hotter material creates a cold shut, as can be appreciated in figure 18.



**Figure 18:** Cold shut revealed in some aluminum components [19].

*Cracks*: these defects could have different sources: differential cooling, phase transformation or heat treatments. Cracks are extremely deleterious for the mechanical performances of aluminum casting because act as stress raisers. Some cracks can be observed in the microstructure reported in figure 19.

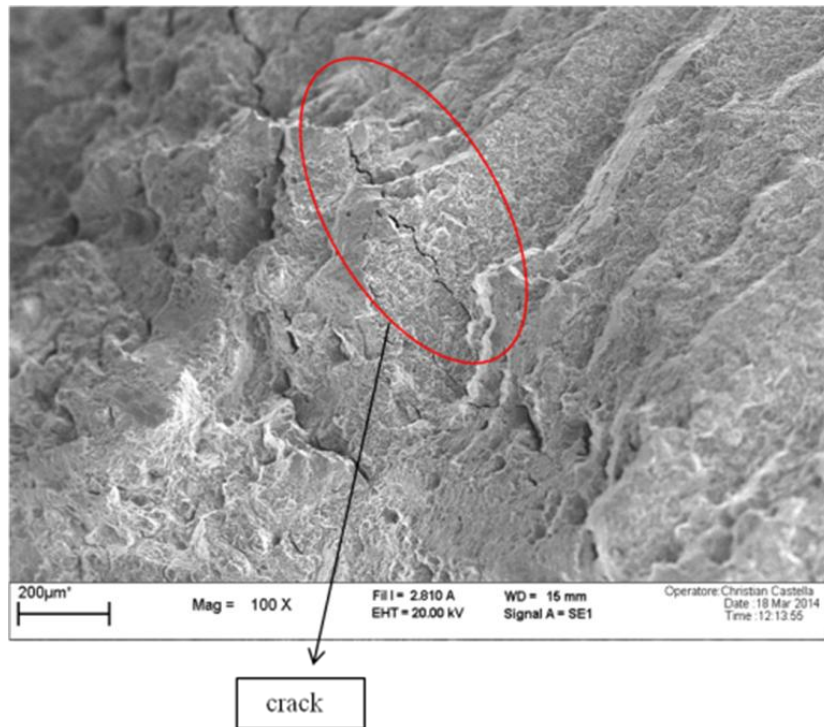


**Figure 19:** Crack individuated in the fractured surface of an aluminum sample (courtesy of Teksid Aluminum).

*Iron Intermetallic*: iron is the principal impurity for aluminum alloys, because form various intermetallic compounds, which are brittle and deleterious for the mechanical properties, acting as stress raisers and for this reason as favourite nucleation site for cracks. Different types of Fe-rich phase exist, such as  $\beta$ -Al<sub>5</sub>FeSi,  $\alpha$ -Al<sub>15</sub>(FeMn)<sub>3</sub>Si<sub>2</sub> and  $\alpha$ ' Al<sub>8</sub>Fe<sub>2</sub>Si, as illustrated in figure 20.

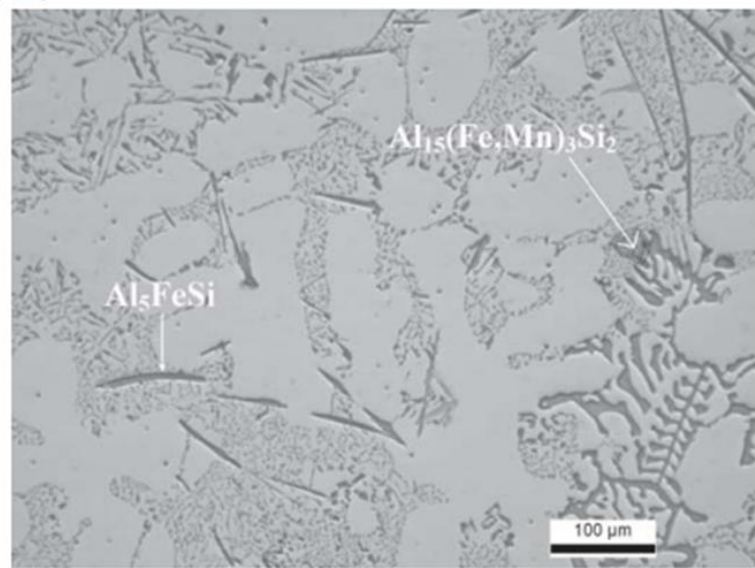


**Figure 20:** Optical microstructure showing  $\beta\text{-Al}_5\text{FeSi}$ ,  $\alpha\text{-Al}_{15}(\text{FeMn})_3\text{Si}_2$  [28].

Iron intermetallic compounds can also be observed in some fractured surface (figures 21 and 22).

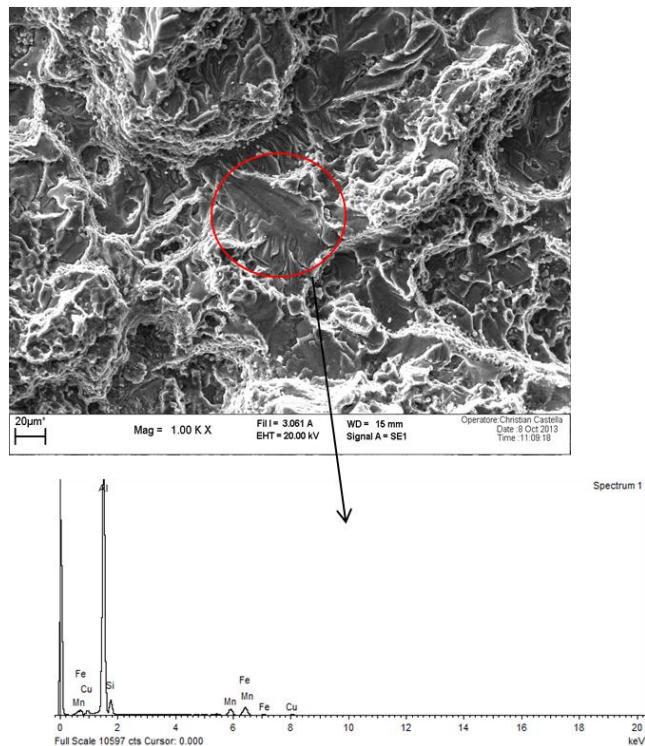


**Figure 21:**  $\alpha\text{-Al}_{15}(\text{FeMn})_3\text{Si}_2$  iron intermetallic compound on the fractured surface of an aluminum sample (courtesy of Teksid Aluminum).

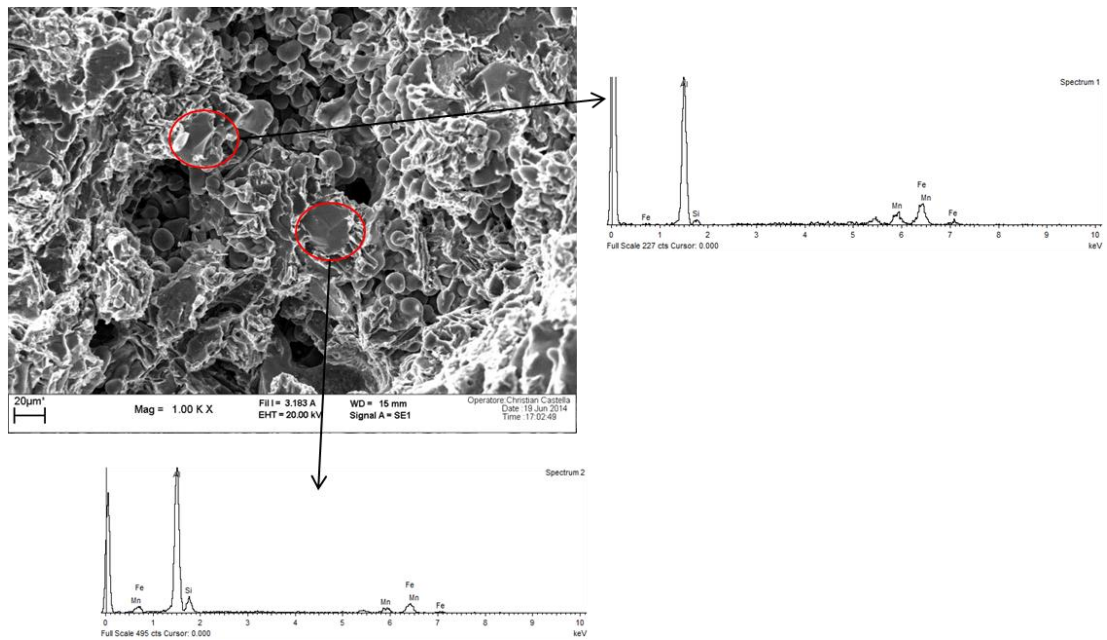


**Figure 22:**  $\alpha\text{-Al}_{15}(\text{FeMn})_3\text{Si}_2$  iron intermetallic compounds on the fractured surface of an aluminum sample, detected close to a shrinkage porosity (courtesy of Teksid Aluminum).

## 1.5 Mechanical components produced with aluminum alloys in the automotive industry

In the last forty years, as can be observed in figure 23, the content of aluminum in cars has had a sharply and continuously increase, because of the increasing demand by the automotive industry of using light materials. This due to the need of reduce car's weight, in order to moderate the fuel consumptions of cars and at the same time also the emission of gas, especially  $\text{CO}_2$ , which is one of the gases responsible of the greenhouse effect. The innovative design strategies are directed toward weight saving, through the substitution of steel ( $\rho \approx 7.8 \text{ g/cm}^3$ ) with light materials manly aluminum ( $\rho \approx 2.7 \text{ g/cm}^3$ ) and magnesium ( $\rho \approx 1.7 \text{ g/cm}^3$ ) alloys [29]. This is very important because in this way is possible reduce the car's mass and to obtain, the decrease of (figure 24): the rolling resistance, the gradient resistance and acceleration resistance; all forces that are directly proportional to the car's mass which compete with car's transfer.

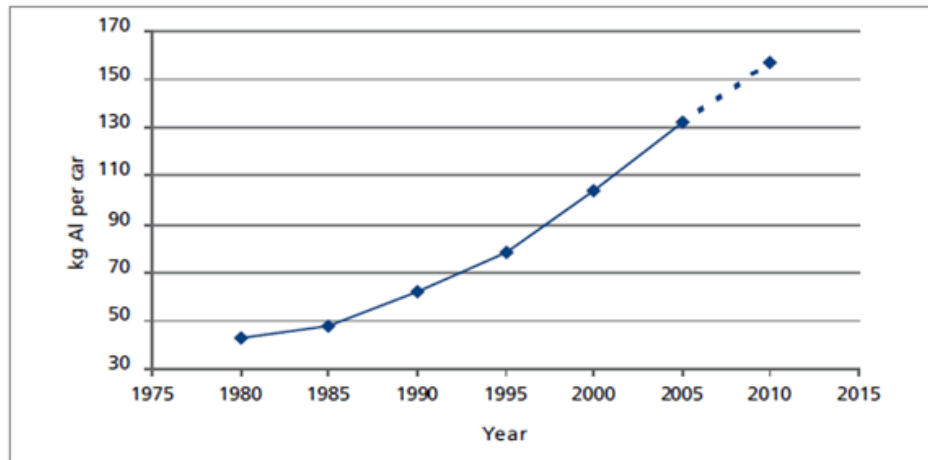


**Figure 23:** Trend of aluminum content in cars in the last 40 years [30].

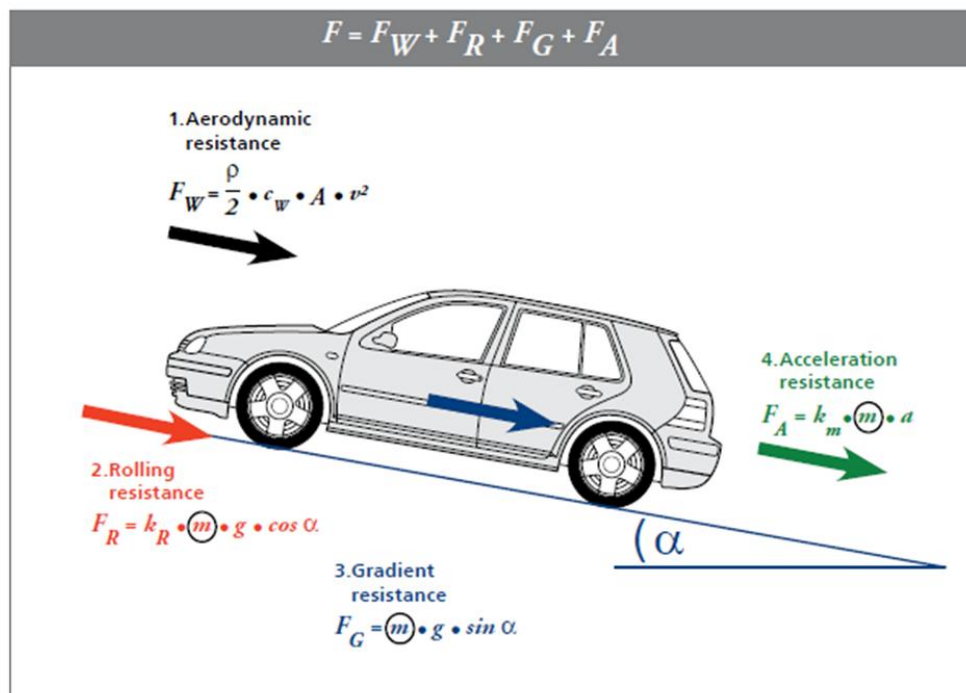


**Figure 24:** Resistance forces to car move [30].

Nowadays, many car's parts and components are produced with aluminum alloys, as reported in figures 25 and 26. In Europe the average aluminum content used for some of the most important car component is [31]:

- 69 kg for the POWETRAIN: engine block and cylinder head, transmission housings, fuel system, liquid lines and radiators;

- 37 kg for CHASSIS and SUSPENSION: cradle, axle, wheels, suspension arms and steering systems;
- 26 kg for CAR BODY: (Body-In-White “BiW”), hoods/bonnets, doors, front structure, wings, crash elements and bumpers and various interiors.

The BIW (body-in-white) is the heaviest car's part, representing up to 30% of the total car's weight. Amplifying the aluminum content it can reach an important and significant weight saving.

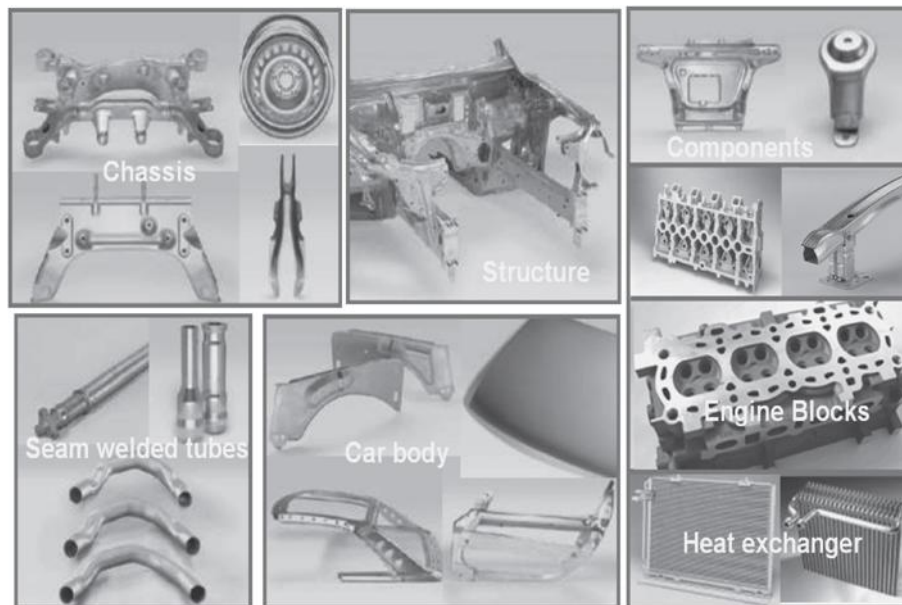


**Figure 25:** Components realized with aluminum in a modern car [31].

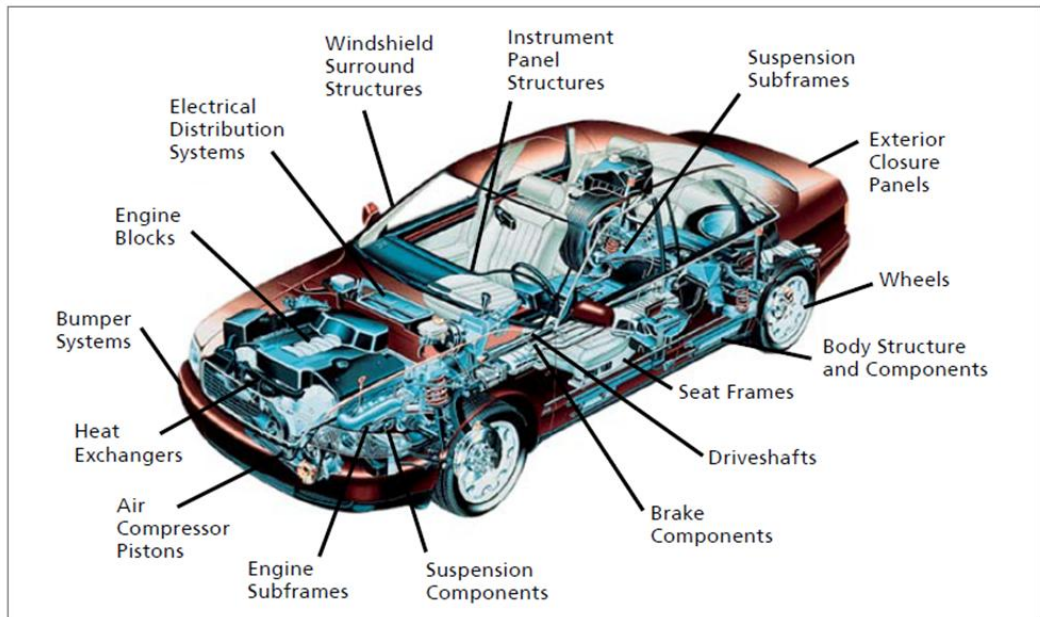


**Figure 26:** Aluminum applications in a car [30].

In figure 27 has been reported the relative and the absolute mass saving, achieved using aluminum alloys for the production of automotive components. Is also reports the market penetration for each components.

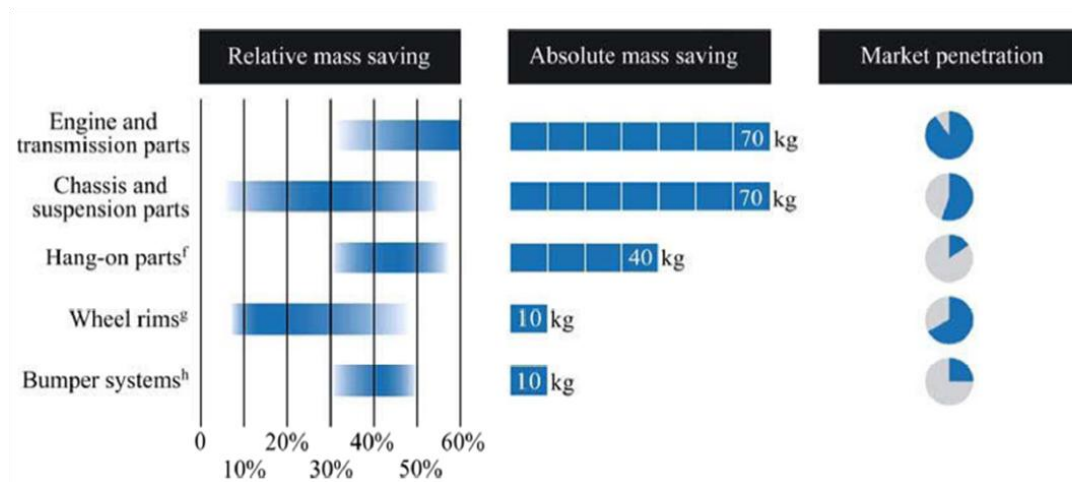


**Figure 27:** Relative mass saving, absolute mass saving and market penetration obtainable with aluminum alloys [32].

Currently, two are the aluminum alloys series principally adopted in the automotive industry, for their good mechanical strength and formability [29,32]:

- the non-heat-treatable Al–Mg–Mn (AA5xxx) alloys;
- the age-hardened Al–Mg–Si (AA6xxx) alloys.

In the case of particular components, such as bumpers and crush-zone, the high-strength Al–Zn–Mg–Cu (AA7xxx) are used. These alloys have been developed and currently are widely used in aerospace area, thanks to their high mechanical performances.

The multi-material design is the innovative car concept, that nowadays is under development by the automobile area. The basic idea of this concept is that to use the “best” material for each car's components, that allows producing emission reduced light-weight car, without losing performance and first of all the car's passenger safety. The adopted materials could be aluminium together with high and ultra-high strength steels, magnesium and plastics or composites. This is the main objective of the “Super Light Car” (SLC) project [32-33-34]. The result reached with this project is shown in figure 28.

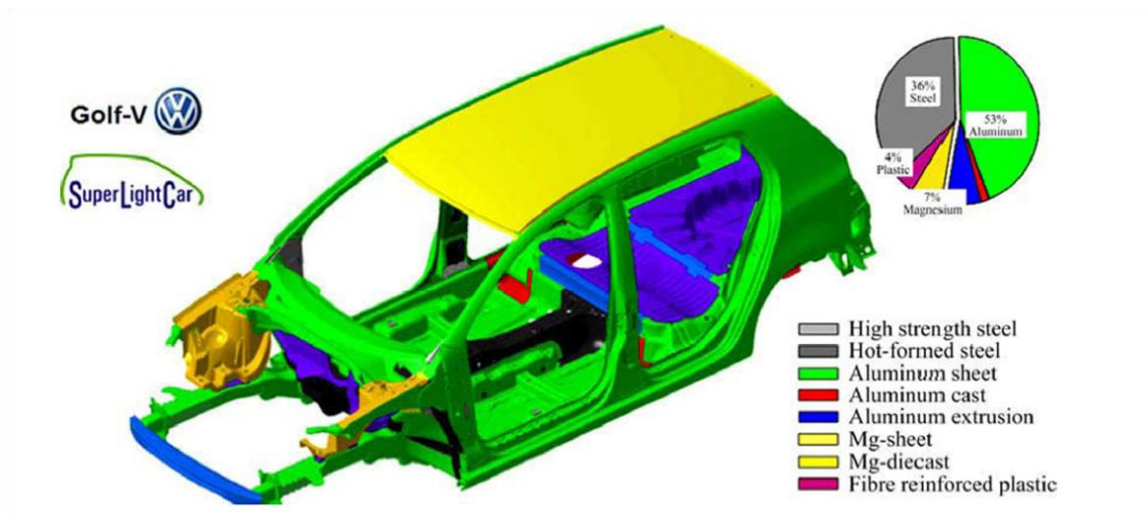


**Figure 28:** Final result of the SLC project based on the "multi-material design" concept [32].

The research of this project led obtained a mass reduction of 95 kg (34%). Due to their excellent properties such as: low density, high mechanical strength, good ductility and formability and finally good corrosion resistance; the aluminum alloys resulted to be, based on the results obtained from the SLC project, as the most suitable materials to produce car's components. They allow to achieve a weight saving and at the same time also to maintain of high performances and more than ever elevate standard for as regard the car's passenger safety.

## 2 CORROSION RESISTANCE OF ALUMINUM ALLOYS

### 2.1 Introduction

Aluminum presents a good corrosion resistance in many corrosive environments thanks to the passive oxide layer formation. Aluminum, as can be observed from the table reported in table 3, is a thermodynamically reactive metal. Only beryllium and magnesium are structural metals more reactive from thermodynamic point of view than aluminum (table 3).

In oxygen containing environment, such as for example air and water, aluminum is quickly covered by an oxide layer, which prevents corrosion. This  $\text{Al}_2\text{O}_3$  layer is chemically bonded to the surface and allows sealing the bulk of aluminum from further corrosion.

The protective oxide layer has a thickness as a function of temperature, environment and alloying elements. This oxide layer in air and at room temperature presents a thickness of about 2-3 nm, which can be increased up to 20 nm by heating at 425°C [35]. As can be observed in figure 29, this protective layer presents a structure made of two different layers:

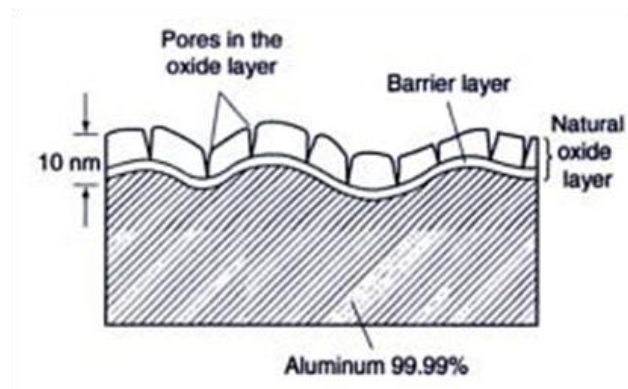
- the first and inner one represents an impermeable barrier, which thickness is influenced only by the environment's temperature;
- the second and outer one is made of hydrate oxide and is more permeable than the inner layer, due to the presence of many pores.

These oxide layers have a different chemical composition as temperature increases. At lower temperature the main form is bayerite  $\text{Al}(\text{OH})_3$  while at high temperature is boehmite  $\text{AlO}(\text{OH})$ .

**Table 3:** Electromotive force series for metals [36].

Electrode reaction	Standard potential at 25 °C (77 °F), V vs. SHE
$\text{Au}^{3+} + 3e^{-} \rightarrow \text{Au}$	1.50
$\text{Pd}^{2+} + 2e^{-} \rightarrow \text{Pd}$	0.987
$\text{Hg}^{2+} + 2e^{-} \rightarrow \text{Hg}$	0.854
$\text{Ag}^{+} + e^{-} \rightarrow \text{Ag}$	0.800
$\text{Hg}_2^{2+} + 2e^{-} \rightarrow 2\text{Hg}$	0.789
$\text{Cu}^{+} + e^{-} \rightarrow \text{Cu}$	0.521
$\text{Cu}^{2+} + 2e^{-} \rightarrow \text{Cu}$	0.337
$2\text{H}^{+} + 2e^{-} \rightarrow \text{H}_2$	(Reference) 0.000
$\text{Pb}^{2+} + 2e^{-} \rightarrow \text{Pb}$	-0.126
$\text{Sn}^{2+} + 2e^{-} \rightarrow \text{Sn}$	-0.136
$\text{Ni}^{2+} + 2e^{-} \rightarrow \text{Ni}$	-0.250
$\text{Co}^{2+} + 2e^{-} \rightarrow \text{Ni}$	-0.277
$\text{Tl}^{+} + e^{-} \rightarrow \text{Tl}$	-0.336
$\text{In}^{3+} + 3e^{-} \rightarrow \text{In}$	-0.342
$\text{Cd}^{2+} + 2e^{-} \rightarrow \text{Cd}$	-0.403
$\text{Fe}^{2+} + 2e^{-} \rightarrow \text{Fe}$	-0.440
$\text{Ga}^{3+} + 3e^{-} \rightarrow \text{Ga}$	-0.53
$\text{Cr}^{3+} + 3e^{-} \rightarrow \text{Cr}$	-0.74
$\text{Cr}^{2+} + 2e^{-} \rightarrow \text{Cr}$	-0.91
$\text{Zn}^{2+} + 2e^{-} \rightarrow \text{Zn}$	-0.763
$\text{Mn}^{2+} + 2e^{-} \rightarrow \text{Mn}$	-1.18
$\text{Zr}^{4+} + 4e^{-} \rightarrow \text{Zr}$	-1.53
$\text{Ti}^{2+} + 2e^{-} \rightarrow \text{Ti}$	-1.63
$\text{Al}^{3+} + 3e^{-} \rightarrow \text{Al}$	-1.66
$\text{Hf}^{4+} + 4e^{-} \rightarrow \text{Hf}$	-1.70
$\text{U}^{3+} + 3e^{-} \rightarrow \text{U}$	-1.80
$\text{Be}^{2+} + 2e^{-} \rightarrow \text{Be}$	-1.85
$\text{Mg}^{2+} + 2e^{-} \rightarrow \text{Mg}$	-2.37
$\text{Na}^{+} + e^{-} \rightarrow \text{Na}$	-2.71
$\text{Ca}^{2+} + 2e^{-} \rightarrow \text{Ca}$	-2.87
$\text{K}^{+} + e^{-} \rightarrow \text{K}$	-2.93
$\text{Li}^{+} + e^{-} \rightarrow \text{Li}$	-3.05

SHE, standard hydrogen electrode

**Figure 29:** Structure of the protective oxide layer forms on aluminum surface [36].

The Pourbaix diagram, represented as a plot of potential vs pH, allows to explain and predict the passivity phenomenon, which control the corrosion behavior of aluminum. As can be observed in figure 30 the  $\text{Al}_2\text{O}_3$  oxide layer presents passivation into the pH range of about 4 to 9, whereas beyond these limits aluminum and aluminum alloys are subjected to corrosion phenomena in aqueous solution. This because the aluminum oxide is soluble in some acids and bases over the passivation limits and so give rise to the formation of  $\text{Al}^{3+}$  ions in acids and on the other hand of  $\text{AlO}_2^-$  ions in bases. The limits of passivation range, for aluminum, can change with temperature and as a consequence of the presence of substances able to react with aluminum and form soluble complexes and/or insoluble salts.

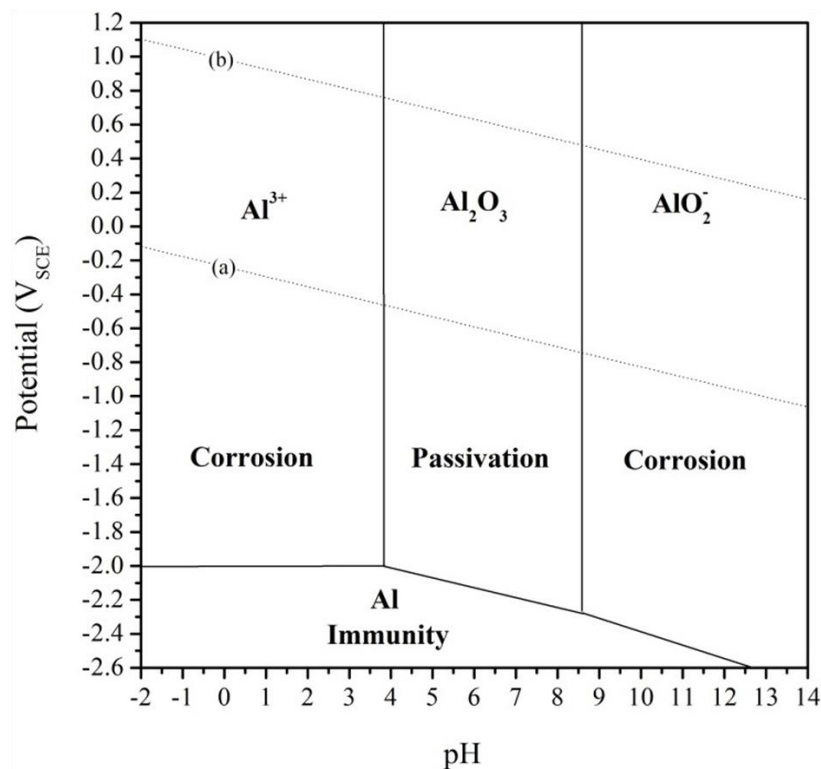


**Figure 30:** Pourbaix diagram of Al-H<sub>2</sub>O system at 25°C [37].

Generally, potentiodynamic polarization test method is adopted to evaluate the corrosion resistance of aluminum alloys.

This test provides information about the kinetics of corrosion phenomenon. The kinetics represent the rate of reaction during corrosion. When a certain metal is insert into an aqueous environment, it stabilize to a precise value of electrochemical potential, which is characteristic of the material and its composition for a given electrolyte. At this potential anodic and cathodic reactions upon the metal surface are equal, and the value of this potential, is significantly influenced, by factors that can modify the relative rates of anodic or cathodic reaction efficiency upon the metal surface, such as alloying elements or precipitates. The kinetics information that can be obtained through the potentiodynamic polarization test concerns current density over a range of potentials, pitting potential (if it exists), corrosion potential, the passive current density. In figure 31 is illustrated a polarization curve for pure aluminum compared to AA2024-T3 (Al-4.3Cu-1.5Mg-0.6Mn) in 0.1M NaCl.

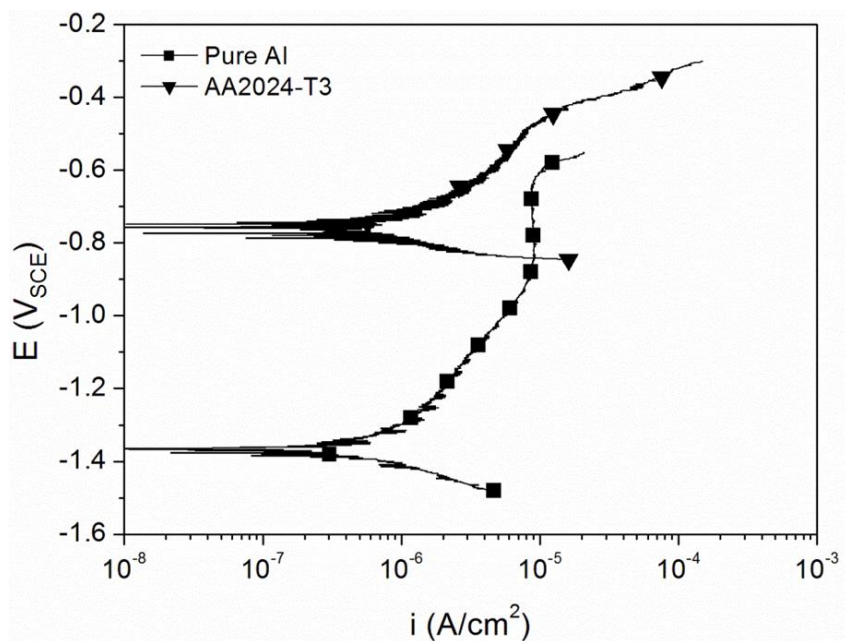


**Figure 31:** Polarization curve of pure Al and AA2024-T3 exposed to 0.1M NaCl for 7 days collected at 1mV/s-1 [37].

Observing this curve information, about the anodic/dissolution reaction, can be obtained from the anodic branch of the curve meanwhile from the cathodic branch of the polarization curve, can get information for as concerns the reduction reaction.

Moreover, from figure 31, can be observe that the addition of noble alloying elements gives rise to an increase of the corrosion potential to more noble values. Since the main corrosion form for aluminum alloys is pitting corrosion, a higher corrosion potential value does not means higher corrosion resistance. The corrosion resistance of aluminum alloys is mostly affected by their chemical composition and microstructure.

## **2.2 Causes of corrosion**

The corrosion phenomenon of aluminum and aluminum alloys is essentially an electrochemical process that can be considered, as a flow of electric current between anode and cathode. As concerns aluminum alloys, that contain several types of intermetallic phases, the corrosion on these alloys is mainly a microgalvanic process between intermetallic phases and the  $\alpha$ -Al matrix. Hence is fundamental to know the electrochemical characteristics of these constituent particle. The chemical composition of intermetallic phases as their spatial distribution and density are all features that affect the level and the morphology of subsequent corrosion.

### **2.2.1 Effect of the alloying elements**

Figure 32 reports the effect of the principal alloying elements, on the electrolytic solution potential of aluminum. One can be noted that Cu, Mn and Si act cathodically towards aluminum, while elements such as Mg and Zn are anodic with respect to the  $\alpha$ -aluminum matrix.

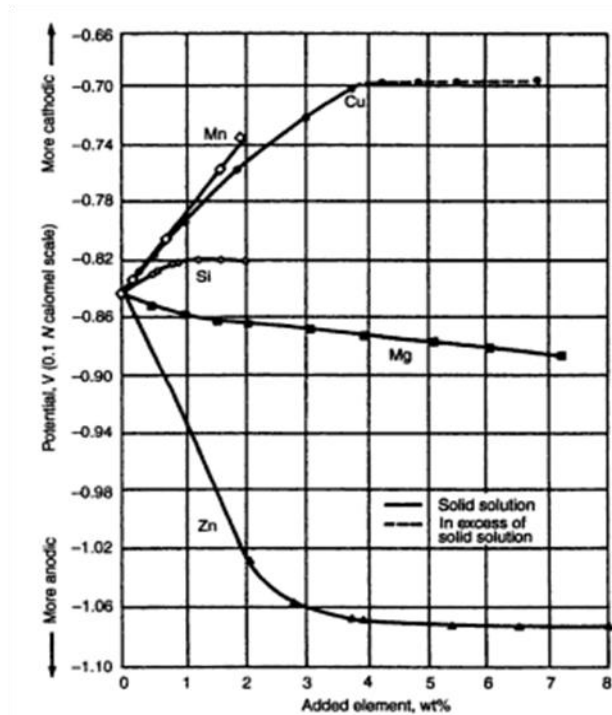


**Figure 32:** Effect of some alloying elements on electrolytic solution potential of aluminum. Potentials are for high-purity binary alloys solution heat treated and quenched. The data are obtained using a solution of 53 g/l NaCl plus 3 g/l H<sub>2</sub>O<sub>2</sub> maintained at 25°C [2].

### 2.2.2 Effect of the microstructure on corrosion

The aluminum alloys microstructure is influenced by the chemical composition, the casting operation and by the thermal treatments adopted. As the corrosion resistance is mainly affected by the grain structure and the presence and the distribution of second phases as constituent particles, precipitates and dispersoids. These particles generally have a different electrochemical characteristics compared to that of the  $\alpha$ -aluminum matrix, certainly they may be anodic or cathodic with respect to the matrix. This leads to the formation of micro-galvanic couples resulting in localized corrosion phenomena. Table 4 reports a summary of the corrosion potential values for intermetallic phases, common to aluminum alloy families mainly in chloride-containing solutions.

**Table 4:** Corrosion potential values for intermetallic phases, common in many aluminum alloys, in NaCl solution [38].

Stoichiometry	Phase	Corrosion potential ( $mV_{SCE}$ )		
		0.01 M	0.1 M	0.6 M
Al <sub>3</sub> Fe	B	-493	-539	-566
Al <sub>2</sub> Cu	θ	-592	-665	-695
Al <sub>3</sub> Zr	β	-752	-776	-801
Al <sub>6</sub> Mn	-	-839	-779	-913
Al <sub>3</sub> Ti	β	-620	-603	-799
Al <sub>32</sub> Zn <sub>49</sub>	T'	-1009	-1004	-1063
Mg <sub>2</sub> Al <sub>3</sub>	β	-1124	-1013	-1162
MgZn <sub>2</sub>	M, η	-1001	-1029	-1095
Mg <sub>2</sub> Si	β	-1355	-1538	-1536
Al <sub>7</sub> Cu <sub>2</sub> Fe	-	-549	-551	-654
Mg(AlCu)	-	-898	-943	-936
Al <sub>2</sub> CuMg	S	-956	-883	-1061
Al <sub>20</sub> Cu <sub>2</sub> Mn <sub>3</sub>	-	-550	-565	-617
Al <sub>12</sub> Mn <sub>3</sub> Si	-	-890	-810	-858
Al-2%Cu	-	-813	-672	-744
Al-4%Cu	-	-750	-602	-642

### 2.2.2.1 Pitting corrosion

Pitting corrosion is the main form of corrosion for aluminum alloys. Some aggressive environments, especially those containing halide ions, such as chlorides, that break down the passive film formed on the surface of aluminum alloys and consequently lead to the formation of pits. Pits generally are formed in correspondence of defects present in the passive layer, for example scratches, mechanical defects or discontinuities. Pitting, as a corrosion phenomenon, takes place only when pH is close to the neutral values, because the oxide layer is unstable in a bulk sense under acidic or alkaline conditions. Chlorides, which are harmful halide ions, through the formation of AlCl<sub>3</sub> give rise to the breakdown of the protective film and when aluminum ions move away from the pits, aluminum oxide precipitates and create a sort of membrane that isolates and intensifies locally the acidity and sustains pitting formation.

Usually pits present a hemispherical shape, as can be observed in figure 33, which is affected largely by the type of alloys and the environment involved into the corrosion phenomenon. Most of the pitting is influenced by the alloy microstructure and by the presence of intermetallic particles, anodic or cathodic with respect to the aluminum matrix. Because of this, two main types of pit morphologies were observed. The first one is the circumferential pit morphology, which appears as a circle of attack around a more or less undamaged particle and in this case the corrosion occurs mainly into the matrix, while the second type of morphology is due to the selective dissolution of particles.

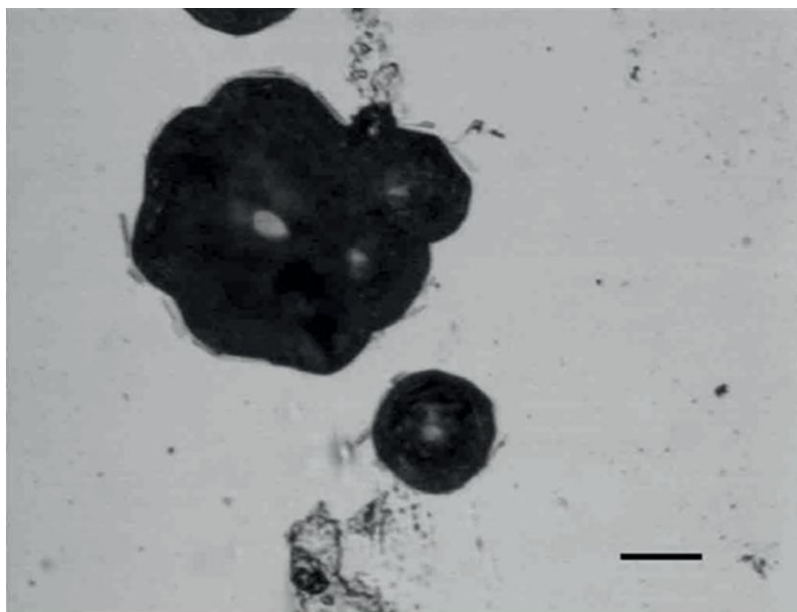


**Figure 33:** Hemispherical pits on aluminum 99.999% in 1.0M NaNO<sub>3</sub> solution at E/1.84 VSHE [39].

As enunciated before the constituent particles and the intermetallic particles play a fundamental role for the pitting corrosion of aluminum alloys. For this reason, recently, many studies have been carried out in order to get a deeper knowledge on the influence of these particles on the corrosion performance [40-44.]. In [40] the authors have demonstrated that silicon can allow to increase the resistance of passive film, formed on the surface of a Al-12%Si aluminum alloy in neutral and slightly alkaline solutions.

This is due to the capacity of silicon to modify the adsorption of chloride ions, delaying it, and in addition because silicon oxide, as illustrated in figure 34, helps to block entry sites and restricts the transport of chloride ions through the passive film.

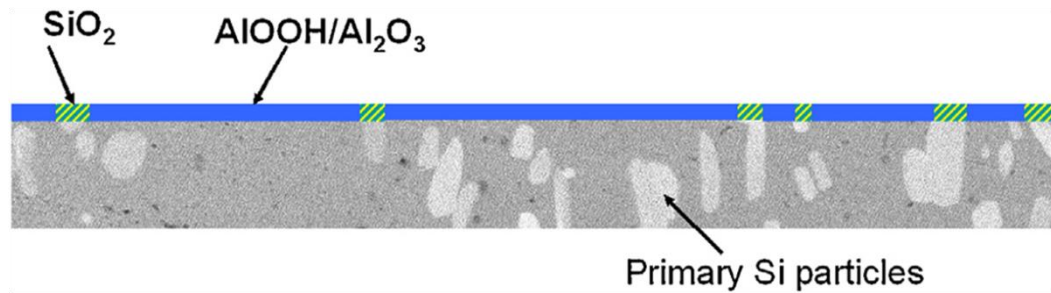


**Figure 34:** Scheme showing the alloy-solution interphase and the presence of  $\text{SiO}_2$  particles within the  $\text{AlOOH}/\text{Al}_2\text{O}_3$  layer [40].

As silicon, also iron-rich intermetallic particles are cathodic with respect to the aluminum matrix. These Al-Fe-Si compounds crystallized in different forms, because of the different amount of silicon in the alloy, in hypoeutectic alloys as  $\beta\text{-AlFeSi}$  and in hypereutectic alloys as  $\alpha\text{-AlFeSi}$  and  $\delta\text{-AlFeSi}$ . The  $\beta\text{-AlFeSi}$  intermetallics are noble than the matrix so makes the alloy susceptible to localized corrosion [41]. Through the addition of Mn the morphology of  $\beta\text{-AlFeSi}$  can be modified into Al-Fe-Si-Mn compounds that, from the electrochemical point of view, are less cathodic with respect to the matrix compared to  $\beta\text{-AlFeSi}$  [42]. Contrary to the iron-rich intermetallics,  $\text{Mg}_2\text{Si}$  hardening precipitates obtained thorough the heat treatment, not only allow to improve the mechanical properties of aluminum alloys but also are anodic with respect to the matrix allowing to increase the localized corrosion [43]. Moreover, magnesium precipitates as Al-Fe-Si-Mg compounds, with a Chinese-script morphology, are cathodic respect to the aluminum matrix, but less detrimental than Al-Fe, Al-Fe-Si and Al-Fe-Si-Mn as a consequence of the presence of magnesium [44]. Finally R.Arrabal et al. [44] have demonstrate that A356 (Al-Si7%-Mg0.3%) aluminum alloy produced by rheocasting route shows a higher corrosion resistance compared to the same alloy produced by gravity casting process.

This is justified by the reduced potential differences between Si/ Fe-intermetallics and the eutectic aluminum phase, due to a higher amount of silicon in the  $\alpha$ -Al matrix.

#### **2.2.2.2 Galvanic corrosion**

The galvanic or bimetallic corrosion is a form of corrosion that takes place when two metals, with a large difference between their corrosion potentials, are in contact in a suitable electrolyte, originating a current flow and therefore a considerable corrosion. An appropriate electrolyte, for the galvanic corrosion, is represented by the seawater due to its low electrical resistance.

Aluminum is an anodic element to many other metals consequently aluminum and its alloys act, as anodes in galvanic cells, with other metals therefore aluminum and its alloy are subjected to corrosion.

Table 5 reports the galvanic series of some metals and of some aluminum alloys exposed to seawater: only magnesium, zinc and galvanized steel are more anodic than aluminum and its alloys.

**Table 5:** Galvanic series of some metals and of some aluminum alloys exposed to seawater [2].

<b>Active end (anodic or least noble)</b>
Magnesium
Magnesium alloys
Zinc
Galvanized steel
Aluminum 1100
Aluminum 6053
Alclad
Cadmium
Aluminum 2024 (4.5 Cu, 1.5 Mg, 0.6 Mn)
Mild steel
Wrought iron
Cast iron
13% chromium stainless steel type 410 (active)
18-8 stainless steel type 304 (active)
18-12-3 stainless steel type 316 (active)
Lead-tin solders
Lead
Tin
Muntz metal
Manganese bronze
Naval brass
Nickel (active)
76Ni-16Cr-7Fe alloy (active)
60Ni-30Mo-6Fe-1Mn
Yellow brass
Admiralty brass
Aluminum brass
Red brass
Copper
Silicon bronze
70:30 Cupro Nickel
G-bronze
M-bronze
Silver solder
Nickel (passive)
76Ni-16Cr-7Fe alloy (passive)
67Ni-33Cu alloy (Monel)
13% chromium stainless steel type 410 (passive)
Titanium
18-8 stainless steel type 410 (passive)
18-12-3 stainless steel type 316 (passive)
Silver
Graphite
Gold
Platinum
<b>Passive end (cathodic or most noble)</b>

One of the possible solutions to reduce the corrosion of aluminum and its alloys, in contact with other metals, is to reduce, as much as possible, the ratio of the exposed area of aluminum to the cathodic metals. Moreover, the use of paints or some type of protective coatings, applied on both the aluminum and on the cathodic metal or only on the cathodic metal, represents another possible and suitable solution to increase the corrosion resistance of aluminum and its alloys.

In some automotive applications aluminum-zinc alloys are frequently used, as sacrificial anodes, to protect the steel structures.

### 2.2.2.3 Intergranular corrosion

The intergranular corrosion resistance (IGC) is caused by the difference between the potential corrosion of precipitates, formed in the grain boundaries, and the matrix that leads to the formation of microgalvanic cell.

Based on their chemical composition precipitates can be anodic or cathodic with respect to the  $\alpha$ -aluminum matrix. For this reason if alloying elements are noble (inactive) can precipitate at the grain boundaries, producing the formation of a exhausted and electrochemically active area, next to the grain boundaries. On the contrary, if the alloying elements are electrochemically active, can precipitate at the grain boundaries and consequently the metal close to the grain boundaries becomes noble.

IGC compared to pitting corrosion is a faster corrosion process, but an inferior depth can be reached, as a consequence of the limited transport of oxygen in the narrow corrosion path. Both IGC and pitting corrosion are deleterious and have a negative effect on the corrosion fatigue of the alloy [2,38].

The intergranular corrosion resistance is mainly influenced by the heat treatments carried out and their effects on the morphology and size of the grain boundary precipitates. The chemical composition of both grain boundary precipitates and aluminum matrix are important too.

Aluminum -copper alloys are particularly sensitive towards the intergranular corrosion, due to the precipitation of  $Al_2Cu$  particles, as a result of the thermal heat treatments, that leaves the adjacent solid solution anodic. As can be observed in Figure 35, the thermal treatments determines the precipitation of very high copper content precipitates, on the grain boundaries, that consequently cause the formation of a copper-depleted area, close to the grain boundaries. A galvanic cell results from the difference of electrochemical potentials of copper rich matrix and copper depleted area. Moreover the anodic copper depleted region has a small area compared to the cathodic matrix and this cause a superior force for intergranular corrosion. The use of a T8 heat treatment can represent a useful solution to increase the 2xxx aluminum alloys IGC resistance thank to a

precipitation, that is not limited to the grain boundaries, but also takes place throughout the grain structure [2].

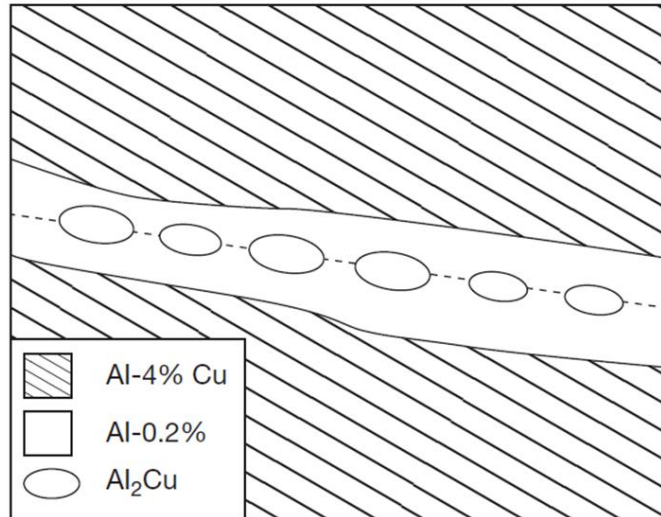


**Figure 35:** Scheme of the grain boundary area in a 2xxx aluminum alloy [38].

Also Al-Zn-Mg-Cu alloys are susceptible to intergranular corrosion because of the precipitation of anodic  $\text{MgZn}_2$  phase [38, 45-46]. Figure 36 highlights the microstructure of the grain boundary of 7055 aluminum alloy. Can be observed that the grain boundary region can contain precipitates  $\eta$  ( $\text{MgZn}_2$ ) and a precipitate-free-zone (PFZ) close to the grain boundary, has a different electrochemical behavior than the inside grain boundary. The formation of a microgalvanic cell can be caused by the electrochemical differences between the anodic  $\eta$  ( $\text{MgZn}_2$ ) grain boundaries precipitates and the adjacent cathodic matrix.



**Figure 36:** Scheme of the grain boundary area in a 7055 aluminum alloy [47].

Recently a study [48] has demonstrated, as shown in Figure 37, that the grain coarsening of the 7075-T6 aluminum alloy determines a decrease of its corrosion resistance.

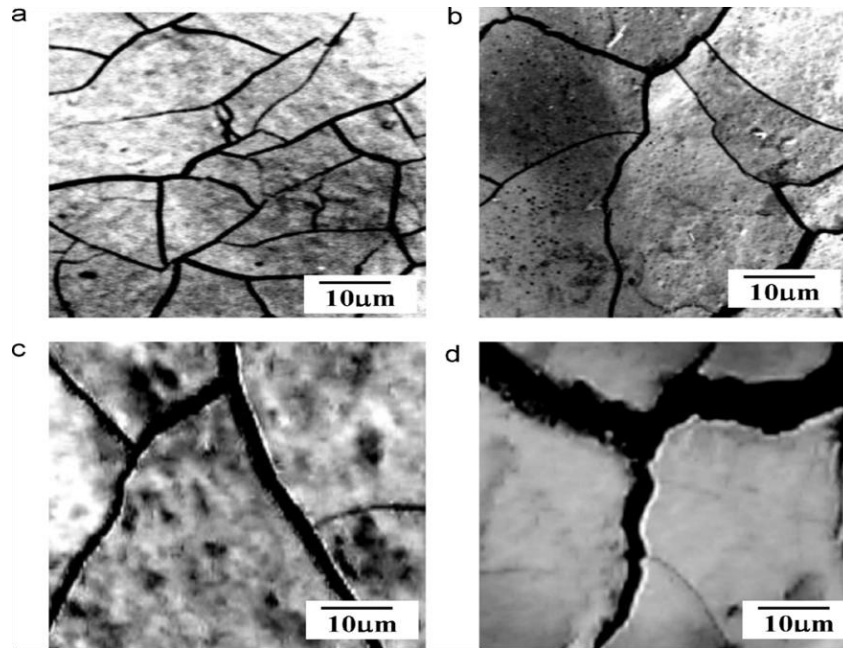


**Figure 37:** Optical micrographs of the surfaces of 7075-T6 aluminum alloy specimens exposed to a deaerated 0.5M NaCl solution at  $-685\text{mVSCE}$ : (a) as-received specimen and (b), (c) and (d) specimens with grain sizes of 40, 130 and 290  $\mu\text{m}$ , respectively [48].

According to another research paper [45] it is possible to enhance the intergranular corrosion resistance of Al-Zn-Mg-Cu-Zr aluminum alloy, through the addition of erbium and chromium, which act as recrystallization inhibitors. This increase in IGC is achieved thanks to an un-recrystallized grain structure together with fine and scattered grain boundary precipitates.

The Al-Mg-Si (6xxx series) alloys have a better corrosion resistance than the high strength 2xxx and 7xxx series aluminum alloys [49].

Alloys of 1xxx series (pure Al) which do not contain any second phases and the alloy of series 3xxx (Al-Mn) which has precipitates ( $\text{MnAl}_6$ ), with a corrosion potential close to the aluminum matrix, are not subjected to intergranular corrosion.

#### 2.2.2.4 Stress-corrosion cracking

Stress corrosion cracking (SCC) is the progressive growth of cracks under the contemporary action of a static stress and a chemically aggressive environment. From electrochemical point of view, for the development of the stress corrosion cracking phenomenon, the susceptibility to intergranular corrosion is a fundamental condition. The failures of many metals, caused by stress corrosion cracking, have been connected with electrochemical activity [2]. Up to now different theories have been developed to describe the mechanism of stress corrosion cracking, summarized in Figure 38.

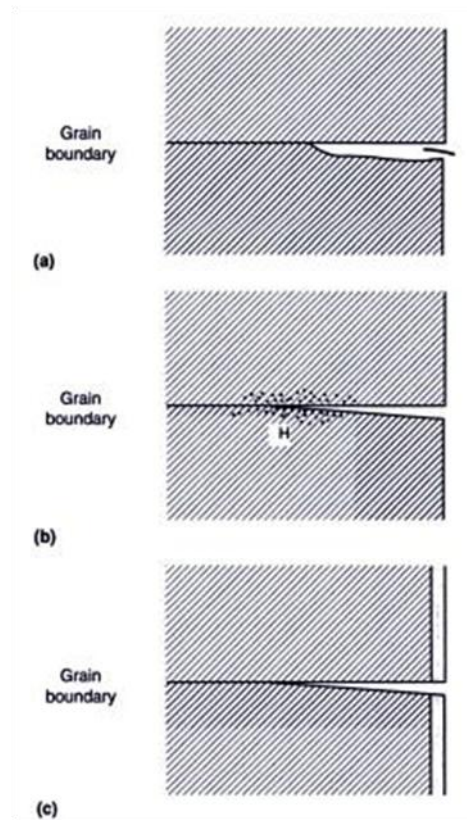


**Figure 38:** Scheme of some theories developed up to now to explain the SCC: a) anodic dissolution; b) hydrogen-induced cracking and c) break of passive film [2].

The first theory, as illustrated in Figure 38a, considers the anodic dissolution of grain boundaries precipitates, as the process that explains the SCC; according to the second theory (Figure 38b) the principal phenomenon that takes place and gives rise to SCC is the hydrogen induced cracking, where the atomic hydrogen adsorbed weakens the grain boundaries; finally the third theory proposed, reported in Figure 38c, assumes that the interruption of the protective passive film, along the grain boundaries, is the principal cause that originates SCC.

The lowest value of tensile stress that can determine SCC is inferior compared to the macroscopic yield strength. The SCC cracks development is influenced by the magnitude and the application time of the tensile stress. Also the residual stress, originated after the quenching of aluminum alloys, plays a crucial role for the SCC. For this reason frequently, aluminum components, after the heat treatment are submitted to a stress relieving process, in order to reduce the intensity of the residual stresses.

The stress corrosion cracks are mainly intergranular, nevertheless under the action of some particular environment can also be transgranular type.

The susceptibility to SCC, of some aluminum alloys, is strongly affected by heat treatments. As a matter of fact, as can be observed in the image reported in Figure 39, the heat treatments, that allow to reach a high stress corrosion resistance are those that make available a microstructure free of precipitates, along the grain boundaries, or a microstructure characterized by a uniform distribution of the precipitates within the grains and not only along the grain boundaries.

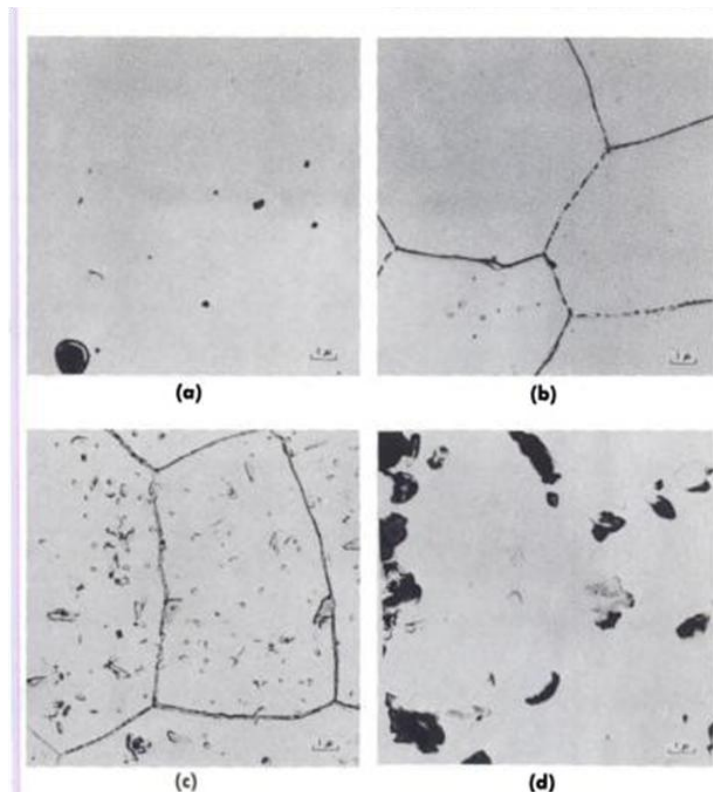


**Figure 39:** Microstructures of 5356-H12 alloy after treatment to produce varying degrees of susceptibility to SCC. a) Cold rolled 20%; highly resistant. b) Cold rolled 20%, then heated 1 year at 100°C; highly susceptible. c) Cold rolled 20%, then heated 1 year at 150°C; slightly susceptible. d) Cold rolled 20%, then heated 1 year at 205°C; highly resistant [2].

As reported in table 6, one can observe that the overaging treatment allows to increase the SCC resistance of some aluminum alloys.

**Table 6:** SCC resistance of some aluminum alloys [38].

<i>Alloy and temper</i>	<i>SCC resistance</i>
2014-T3	Poor
2024-T3, T4	Poor
2024-T8	Good
2124-T851	Good
2219-T3, T4	Poor
2219-T6, T8	Excellent
6061-T6	Excellent
7049-T73	Good
7x75-T6	Poor
7x75-T73	Excellent
7x75-T76	Intermediate

Especially aluminum alloys belong to 2xxx, 5xxx and 7xxx series are susceptible to the stress corrosion cracking. The use of 7xxx series aluminum alloys has been strongly limited by its low SCC resistance, so for this many research have been carried out with the goal to enhance the stress corrosion cracking of Al-Zn-Mg-Cu aluminum alloys. Many studies [50-51] have demonstrated that increase the size and spacing of the grain boundaries precipitates (GBPs), is a suitable way to enhance the SCC resistance of 7xxx high strength aluminum alloys.

Another possible solution studied in [52] has been oriented to increase the Cu content, which contribute to increase the stress corrosion cracking resistance, through the decrease of the electrochemical activity, allowing to enhance the crack initiation resistance.

Moreover, has been demonstrated that Fe-rich and Si-rich phases have a different corrosion potential compared to that of the  $\alpha$ -aluminum matrix [53-54]. Consequently, in an corrosive environment, they are subjected to an anodic dissolution and therefore can act as initiation site for cracks and can promote the production of hydrogen on the cathode [52,55]. Increase the silicon content up to 0.261 % (mass fraction) in a 7050 aluminum alloy, subjected to a T7651 heat treatment, allows to increase its SCC resistance [56]. This because enhance Si content decrease the content of other coarse phase and increase the distance between them.

The addition of erbium and chromium to the Al-Zn-Mg-Cu-Zr, which act as recrystallization inhibitors, allow to improve the stress corrosion resistance significantly [45] as reported in Figure 40.

The crack propagation rate of Al-Zn-Mg-Cu-Zr-Er-Cr alloy is lower than that of Al-Zn-Mg-Cu-Zr alloy and moreover  $K_{ISCC}$  value is increased.  $K_{ISCC}$  is the critical stress intensity factor of stress corrosion cracking, which represents the stress intensity at which the crack velocity achieved a minimum value about  $10^{-10} \text{ m s}^{-1}$ .

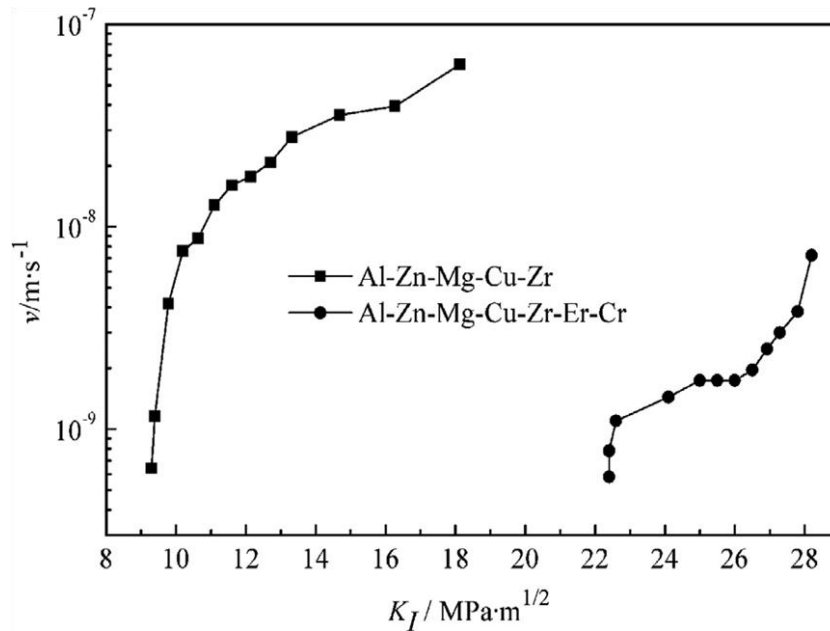


**Figure 40:** Crack propagation rate ( $v$ ) versus crack tip stress intensity factor ( $K_I$ ) in 3.5 wt% NaCl solution of Al-Zn-Mg-Cu-Zr and Al-Zn-Mg-Cu-Zr-Er-Cr alloys [45].

### 2.2.3 Effect of environmental variables on corrosion

More than chemical composition (presence of alloying elements), microstructure and metallurgical variables, for example heat treatments are the main variables which affect significantly the aluminum alloys corrosion resistance.

Other important variables to consider are the environmental variables:

- water;
- pH;
- temperature.

#### *Effect of water*

The presence of water represents a fundamental requirement for aluminum alloys corrosion. Water can be present in different forms, such as: isolated droplets, film of moisture condensed on aluminum surface and finally as aqueous solution. The presence of air, which contains oxygen, in contact with water can increase the corrosion of aluminum alloys while the absence of air can block the corrosion phenomenon. At room temperature aluminum alloys have a good resistance towards high-purity water whereas at high temperatures they do not present a good resistance. The presence of Ni and Fe allow to enhance the corrosion resistance of aluminum alloys to high-purity water [2].

#### *Effect of pH*

The Pourbaix diagram reported in Figure 33, based only on thermodynamics considerations, indicates that aluminum alloys in contact with a aqueous solution, have a good corrosion resistance in the pH range of 4-9. Generally aluminum alloys present a low corrosion resistance when are in contact with both strong acids and alkalis, but as can be observed in Figure 41, there are some exclusion.

Consequently the corrosivity of environments is affected not only by pH.

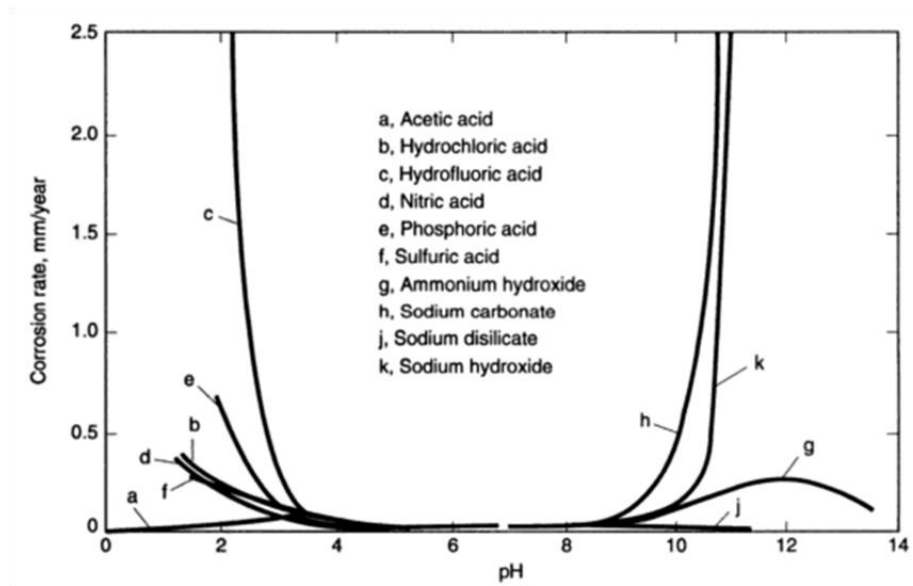


**Figure 41:** Effect of pH on corrosion of 1100-H14 alloy by various chemical solutions [2].

#### *Effect of temperature*

The effect of the temperature on the corrosion of aluminum alloys is influenced by the chemical substances in contact with the Al-alloys. For example in mineral acids, organic acids and alkaline solutions a temperature increase determines a higher corrosion rate, while for example in monoethanolamine a temperature increase decrease the corrosion rate, due to the development of the protective oxide layer. However, the influence of the temperature on the corrosion rate of Al-alloys is enough complex, as reported schematically in Figure 42.

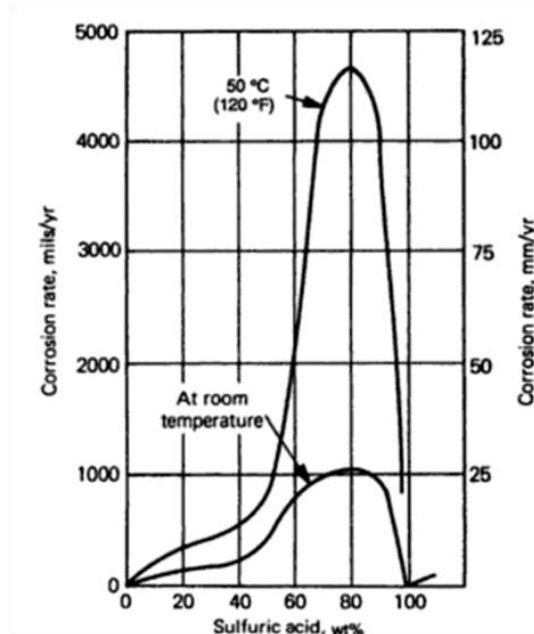


**Figure 42:** Effect of temperature on the corrosion of 1100 aluminum alloy in sulfuric acid [2].

### 2.3 Corrosion prevention methods

Different strategies have been developed to increase the corrosion resistance of aluminum alloys and these, allow to increase the overall number of applications of Al-alloys, in aggressive environment such as marine ambient. The main adopted corrosion prevention methods are:

- inhibitors;
- conversion coatings;
- anodizing;
- organic coatings.

#### *Inhibitors*

Inhibitors are chemical substances, soluble in water, allowing to slow and reduce the corrosion of aluminum alloys.

The soluble corrosion inhibitors are divided into two main categories: "anodic inhibitors" that reduce the anodic reaction and "cathodic inhibitors" which reduce the cathodic reaction. The anodic inhibitors increase the corrosion resistance of Al-alloy through the increment of the pitting potential, whereas cathodic inhibitors act reducing the rate of oxygen reduction reaction on the aluminum alloy surfaces.

Generally inhibitors are ions in solution. Some anions which inhibit corrosion are: chromate, phosphate, nitrate and silicate; while cathodic inhibitors are cations of strontium, cerium and lanthanides. Moreover exist some organic substances that act as inhibitors for aluminum alloys corrosion, such as phosphonates, sulfonates and benzoates.

#### *Conversion coatings*

Conversion coatings are widely used to increase the corrosion resistance of aluminum alloys. In the conversion coating processes the surface that has to be covered by a protective layer, is positioned in contact with the aqueous solutions containing surface activators and coating-forming substances. The principal conversion coatings used are the chromate conversion coatings. In this process is used a sodium dichromate solution, which contain hexavalent chromium, extremely dangerous compound for the human health [57]. For this reason some alternative methods have been studied. The most relevant possibility is: anodizing, rare earth inhibitors and coatings. Especially coatings containing Ce and other rare-earths are currently considered valid possible substitution for chromate-based protective coatings [58].

Another remarkable solution [59], to the chromate coatings involves the use of zinc–magnesium-pigments, produced by atomization, and allows to increase the corrosion resistance of AA 2024 aluminum alloy.

#### *Anodizing*

Anodized coatings are realized through a process involving the immersion of the surface to covered, into a acidic baths, which contain substances able to promote electrochemically the development of a well adherent oxide film. These type of coatings increases the overall aluminum alloys corrosion resistance.

Usually the principal acidic bath used are the chromic acid bath and the sulfuric acid bath. Recently, a research [60] shows that the use of boric acid, helps to increase the corrosion resistance of boric/sulfuric acid anodic film on 7050 aluminum alloy. An example of anodizing coating on a AA6060 aluminum alloy is shown in Figure 43.

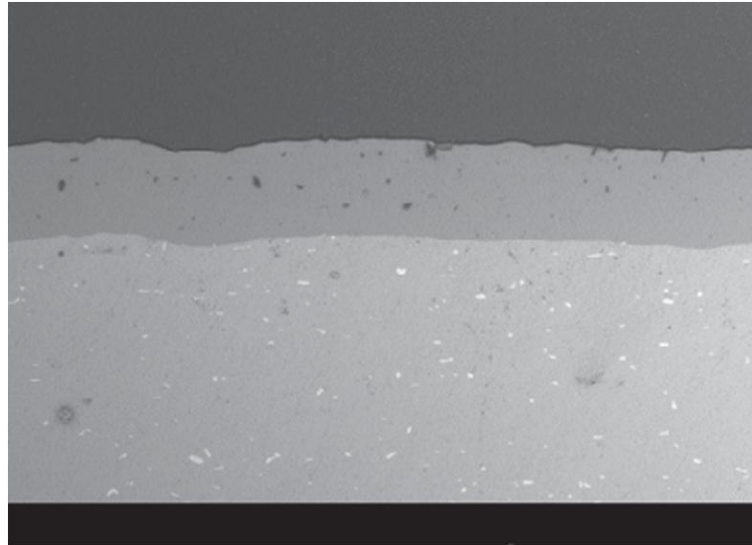


**Figure 43:** SEM image of a anodizing coating on a piece of extruded AA6060 aluminum alloy [38].

### *Organic coatings*

The organic coatings can provide an increase of the aluminum alloys corrosion resistance by two different modes: barrier protection and active corrosion protection.

The previous one is based on the concept to avoid the contact between aluminum substrate and corrosive environment, whereas in the latter one protection is due to the release of corrosion inhibitors. Recently, some studies[61-63] have demonstrated that the use of polymeric coatings containing epoxy ester, polyurea and polymethylhydrosiloxane [61] and the adoption of clay/epoxy ester composite coatings [62], are suitable protective coatings that let to increase the aluminum alloys corrosion resistance.

Moreover a research has revealed that polymer clay nanocomposite coatings (PCN), consisting of polyurea, siloxanes, epoxy ester and montmorillonite clay [63], are useful to enhance the corrosion resistance of the Al 2024-T3 aluminum alloy. The increased corrosion resistance is due to the barrier effect of the protective coating that reduces the diffusivity of reactants, such as for example oxygen, water and salt and consequently increases of the polarization resistance of coated aluminum alloy substrate.

### 3 SELF HARDENING ALUMINUM ALLOYS

#### 3.1 Introduction

Self-hardening aluminum alloys (Al-Zn-Si-Mg alloys) are an innovative class of light aluminum alloys that have high mechanical properties, which make them suitable for many applications in different industrial fields. The most important and relevant feature of the self-hardening alloys is related to their good performance, without the need of any heat treatment: they are subjected to a natural ageing phenomenon at room temperature after a storage period of about 7-10 days [64-69]. The possibility to avoid the heat treatment represents an important benefit, contributing to reduce considerably the production cost of some components and the energy consumption. Moreover, without heat treatment is completely eliminated the risk of component's deformation, that can occur during the different steps of heat treatment, and which are the main reason of most of the component's faults.

Table 7 shows the chemical composition of the self-hardening alloys currently produced.

**Table 7:** Chemical composition of the self-hardening aluminum alloys currently produced [70].

Alloy	Elements wt%							
	Zn	Si	Mg	Fe	Cu	Mn	Ti	Al
AlZn10Si8Mg (UNIFONT-90)	9.0-10.0	8.5-9.5	0.3-0.5	0.15	0.03	0.10	0.15	bal.
AlZn6Si8Mg (UNIFONT-94)	9.0-10.0	8.5-9.5	0.3-0.5	0.4	0.03	0.4	0.10	Bal.

The chemical compositions of these two alloys present some small differences, mainly for as concerns the Fe and Mn content (wt%): UNIFONT-94 alloy contain just a lit bit higher percentage of iron and manganese compared to UNIFONT-90 alloy.

UNIFONT-90 alloy is suitable for sand and permanent mould casting process, while UNIFONT-94 alloy is appropriate for high pressure die casting procedure.

### 3.2 Properties

The mechanical properties of the self-hardening aluminum alloys are reported in table 8.

**Table 8:** Mechanical properties of the self-hardening aluminum alloys currently produced [70].

Alloy	Casting process	$R_m$ [MPa]	$R_{p\ 0.2}$ [MPa]	A [%]	HB
UNIFONT-90	Sand casting	220-250	190-230	1-2	90-100
UNIFONT-90	Permanent moul casting	280-320	220-250	1-4	100-120
UNIFONT-94	High pressure die casting	300-350	230-280	1-4	105-120

These mechanical properties are achieved after a storage period of about 7-10 days at room temperature and no heat treatment is necessary to reach these mechanical performances, according to [64-69]. The self-hardening aluminum alloys reach 50% of the final mechanical properties, one day after the casting; then after three days they achieve 80% of the final mechanical strength and finally after, approximately seven to ten days, their final mechanical properties can be reached [66].

As can be observed in table 8, these aluminum alloys have high mechanical properties and principally show high yield strength values, which is a fundamental mechanical characteristic mainly for all the structural mechanical components production. Especially for UNIFONT-90 alloy, the low iron content has a beneficial effect on the mechanical properties and good fatigue strength.

The main aspect which represents a limitation for the application of these alloys is related to their low value of A%.

According to [64] there are other interesting properties of these aluminum alloys, and in particular:

- good castability;
- light weight;
- good wear resistance;
- low thermal expansion;
- good machining.

### 3.3 Applications

Self-hardening aluminum alloys are employed for the manufacturing of components, which require high mechanical performances. They are suitable in automotive and defense industry and in medical engineering [64,66]. In addition, they are employed for the production of: textile machinery parts, cable car components and mould [64]. Some applications of UNIFONT-90 are illustrated in Figures 44 and 45.

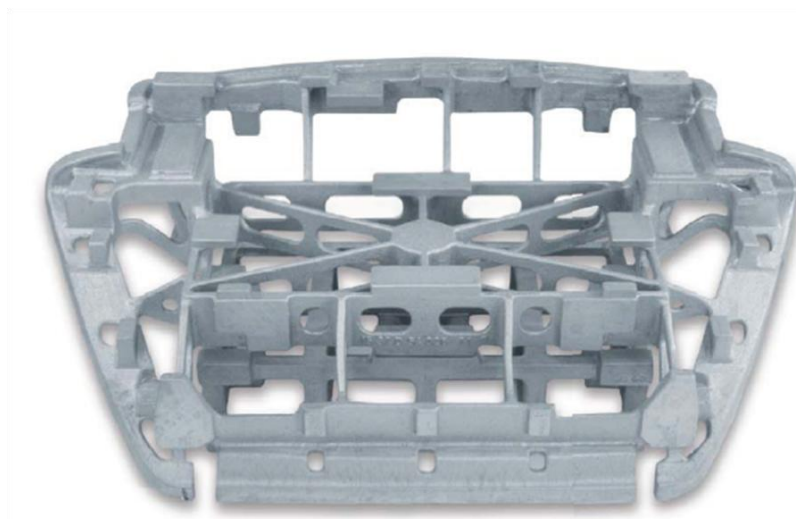


**Figure 44:** Car's door panel produced with UNIFONT-90 self-hardening aluminum alloy [70].



**Figure 45:** Chassis for robot realized with UNIFONT-90 self-hardening aluminum alloy [70].

Components produced with UNIFONT-94 self-hardening aluminum alloys are visualized in Figures 46 and 47.



**Figure 46:** Supports for vibrations dumper fabricated with UNIFONT-94 self-hardening aluminum alloy [70].



**Figure 47:** Supports for the table of plane's seats produced with UNIFONT-94 self-hardening aluminum alloy [70].

## 4 REAL CASE STUDY

### 4.1 Introduction

Self-hardening aluminum alloys (Al-Zn-Si-Mg alloys) represent an innovative class of light aluminum alloys as illustrated in the previous chapter and they present high mechanical properties, which make them suitable for many applications in different industrial fields, especially in transport industry. The most important and relevant feature of the self-hardening alloys is related to their good performance, without the need of any heat treatment: they are subjected to a natural ageing phenomenon at room temperature after a storage period of about 7-10 days. The possibility to avoid the heat treatment represents an important benefit, contributing to considerably reduce both the production cost of some components and the amount of energy. Furthermore, without heat treatment the risk of component's deformation during the production is eliminated. The present PhD thesis is inserted in this context and presents the results of the investigation about the optimization of a recently developed "self-hardening" aluminum alloys [67-69] produced by die-casting. The specific aim of the PhD thesis is the development of the self hardening alloy, starting from a basic composition (AlZn10Si8Mg) and the optimization of the alloy by addition of different amount of Mg. The PhD thesis was focalised on the study of the effect of the Mg content and of the cooling rate on the microstructure of three different self-hardening aluminum alloys, as an alternative to the heat treatable aluminium alloys. The optimal composition will be employed for the production of mechanical components in automotive application and the future target is to substitute the currently used A356 (AlSi7Mg0.3) aluminium alloy (adopted by Teksid), to produce the knuckle component (described in section 4.2). Once the bibliographic data was collected, a consistent part of this thesis was dedicated to study of the microstructural characteristics, the mechanical behaviour and the corrosion resistance of different compositions casted and on the basis of the results obtained it was possible to choose the more appropriate composition for the above mentioned application .

## 4.2 Knuckle component

In Figure 48 is reported the knuckle component that currently Teksid produces using A356 aluminium alloy. The main function of this component is related to attaches the wheel end braking components to the suspension, as illustrated in Figure 49. Additionally, it supports the load and/or torque induced by bumping, braking, and acceleration and also helps in steering the tire connecting tie rod and rotating at the kingpin's axis center.

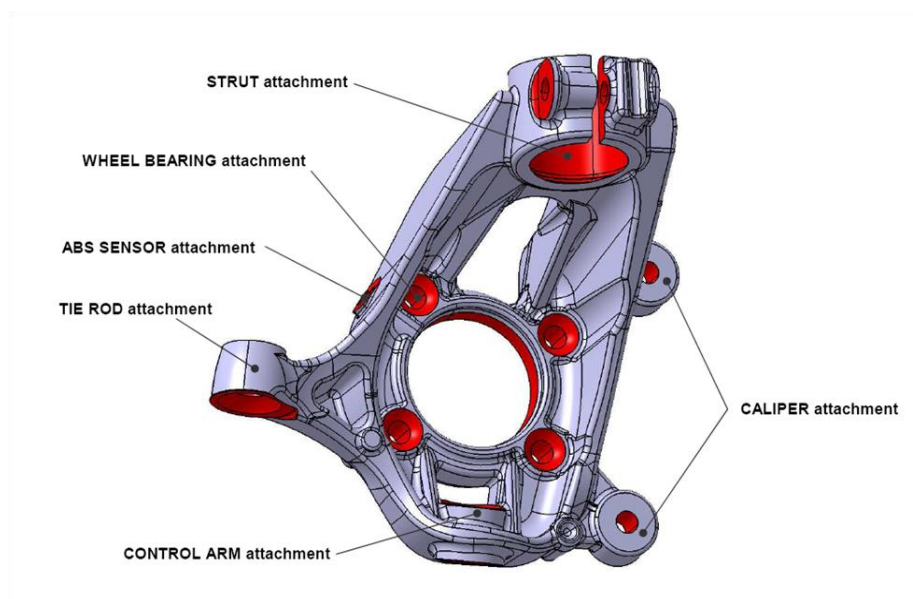


**Figure 48:** Knuckle component produced by Teksid (courtesy of Teksid Aluminum).

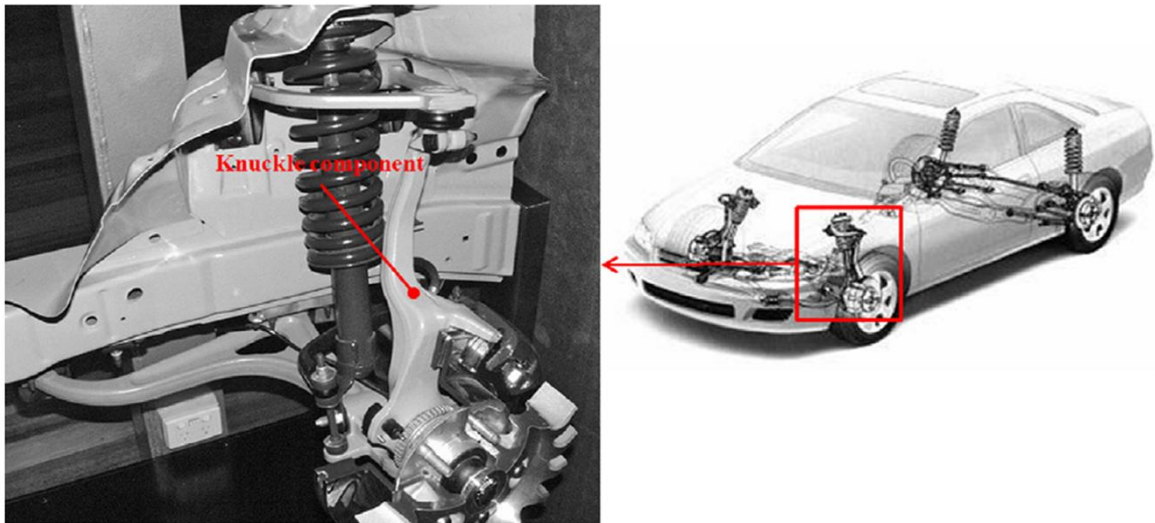


**Figure 49:** Knuckle component [71].

Due to its relatively complex geometry, knuckle component is generally cast and then machined. It has a mass of about 3.5 Kg after casting and more or less of 3 Kg after machining operations. Currently, low pressure die casting has been employed in Teksid for the production of this component using A356 (AlSi7Mg0.3) aluminum alloy. In order to meet the rigorous mechanical requirements after casting the component is subjected to a specific heat treatment, generally T6 heat treatment.

Generally, heat treatment is a time and energy consuming process, which can give rise to many faults. Especially deformations, occurring during the different steps of the heat treatment, are one of the main fault cause. In addition, a considerably increase of the production cost of some components is coming from the heat treatment. For this reason, in the following section of the thesis special attention has been dedicated on how T6 heat treatment affects the final cost of knuckle component reported in Figure 48. Additionally, the feasibility of the substitution of the A356 alloy with the AlZn10Si8Mg alloy, from the economical point of view has been considered and analyzed.

### **4.2.1 Analysis of the heat treatment costs for the production of knuckle component**

There are many parameters which are directly connected to the global production cost of any component.

In particular, for the knuckle component reported in Figure 48, the main elements influencing the whole manufacturing cost is schematically represented in Figure 50. The most important factors are:

- operator machine;
- gas consumption;
- electricity consumption.

These elements influence the cost of the heat treatment and consequently determine how the heat treatment affects the final cost of the production of the knuckle component.

Based on some data coming from Teksid Aluminium, in the present PhD Thesis some economical consideration have been performed. The heat treatment has a cost of about 0.55 € for single component, subjected to the heat treatment. Considering an annual production of about 400'000 knuckle components (Teksid data), through the elimination of the heat treatment one can be achieve a cost saving of about 220'000 €, as can be observed from the detailed data reported in Figure 50.

<b>Costs</b>	<b>[€/pz]</b>
Operator machine	0.20
Gas consumption	0.26
Electricity consumption	0.09
<b>Cost for single component [€]</b>	<b>0.55</b>

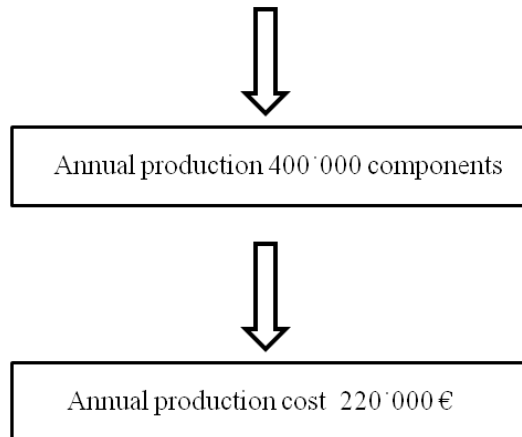


**Figure 50:** Elements of cost of the heat treatment used for the knuckle component of figure 48 and annual production cost of the heat treatment, used for 400'000 knuckle components.

Other costs that can be abolished through the removal of the heat treatment are indicated in table 9 .

**Table 9:** Costs that can be eliminated without the realization of a heat treatment plant.

Heat treatment's plant realization cost [€]	2'000'000
Annual maintenance cost of heat treatment plant [€]	170'000
<b>Cost saving realized without the realization of a heat treatment plant [€]</b>	<b>2'170'000</b>

As a consequence, the total cost saving, excluding any heat treatment, generally adopted for the knuckle component is about 2'390'000 €.

This results from the sum of: 220'000 € that is the total cost of the heat treatment, for an annual production of 400'000 knuckle components and 2'170'000 € which is the sum of the cost of realization and the cost of annual maintenance of a heat treatment plant.

Table 10 reports a comparison between the cost analysis for the annual production of knuckle component, using A356 aluminium alloy and AlZn10Si8Mg self-hardening aluminium alloy. This analysis has been realized considering the knuckle component, reported in Figure 48, which has a mass of 3.5 Kg and usually there are an annual production of 400'000 components. Based on these considerations one can conclude that the production of 400'000 knuckle components, with the AlZn10Si8Mg alloy as an alternative of A356 alloy, determines a considerable increase of the production cost, about 1'260'000 €.

**Table 10:** Comparison of the cost analysis of an annual production of 400'000 knuckle components, with the A356 aluminium alloy and with the AlZn10Si8Mg self-hardening aluminium alloy.

<b>Alloy</b>	<b>A356</b>	<b>AlZn10Si8Mg</b>
Purchase cost [€/Kg]	2	2.9
Production cost for single component [€]	7	10.15
Annual production cost [€]	2'800'000	4'060'000
<b>Difference between production costs [€]</b>	<b>1'260'000</b>	

The substitution of the A356 alloy with the AlZn10Si8Mg self-hardening alloy, for the annual production of 400'000 knuckle components, gives rise to:

1. a total cost saving of 2'390'000 €, achieved with the elimination of the heat treatment;
2. and to a considerable increase of the production cost 1'260'000 €, mainly due to the actual high purchase cost of the self-hardening aluminium alloy.

Currently, the self-hardening alloy has a price of about 50% higher than that of the A356 alloy, but is important to consider that the alloy's price can be subjected, during the time, to relevant oscillations. At the beginning of the production, the use of this

alloy is non a convenient choice from economical point of view, but there are other comforting parameters which encourage this option:

the studied self-hardening alloy represent an interesting alternative to the heat treatable aluminium alloys, because consent to achieve an important energy saving, especially in terms of gas and electricity consumption, as can be observed by the data reported in Figure 50.

In the next section of this thesis will be presented and discussed the results obtained about the microstructure, the mechanical properties and the corrosion resistance of the self-hardening aluminum alloy investigated.

### **4.3 AlZn10Si8Mg self hardening alloy as a possible alternative to A356 alloy to produce the knuckle component**

#### **4.3.1 Microstructural analysis**

Samples for the microstructural analysis have been prepared by standard metallographic technique by mounting and polishing procedure, then the samples have been investigated, through an optical microscope (OM, MeF4 Reichart-Jung) and a scanning electron microscope (SEM, Leo 1450VP) equipped with energy X-rays dispersive spectroscopy unit (EDS, Oxford microprobe) for the compositional analysis.

The microstructure has been evaluated immediately after the casting and after seven days, during which the alloy has been subjected to a natural ageing. The comparison, as microstructural features concerns has been realized, in order to evaluate the modification and the microstructural evolution during the time. Figure 51 reports the microstructure of the AlZn10Si8Mg self-hardening aluminum alloy in these two condition. In both cases, the microstructure consists of a primary  $\alpha$ -aluminum matrix phase, an eutectic mixture of Al-Si and some intermetallic phases. The  $\alpha$ -aluminum matrix precipitates from the liquid as the primary phase. Zinc is present in the  $\alpha$  solid solution [64], due to the high solubility of zinc into aluminum, as can be observed in the Al-Zn phase diagram reported in Figure 52.

The main difference revealed between the microstructure in the as cast condition and after seven days of natural ageing regard the secondary dendritic arm space (SDAS) value, as can be observed by the data of Table 11. After seven days of natural ageing the microstructure appears finer than in the as cast condition.

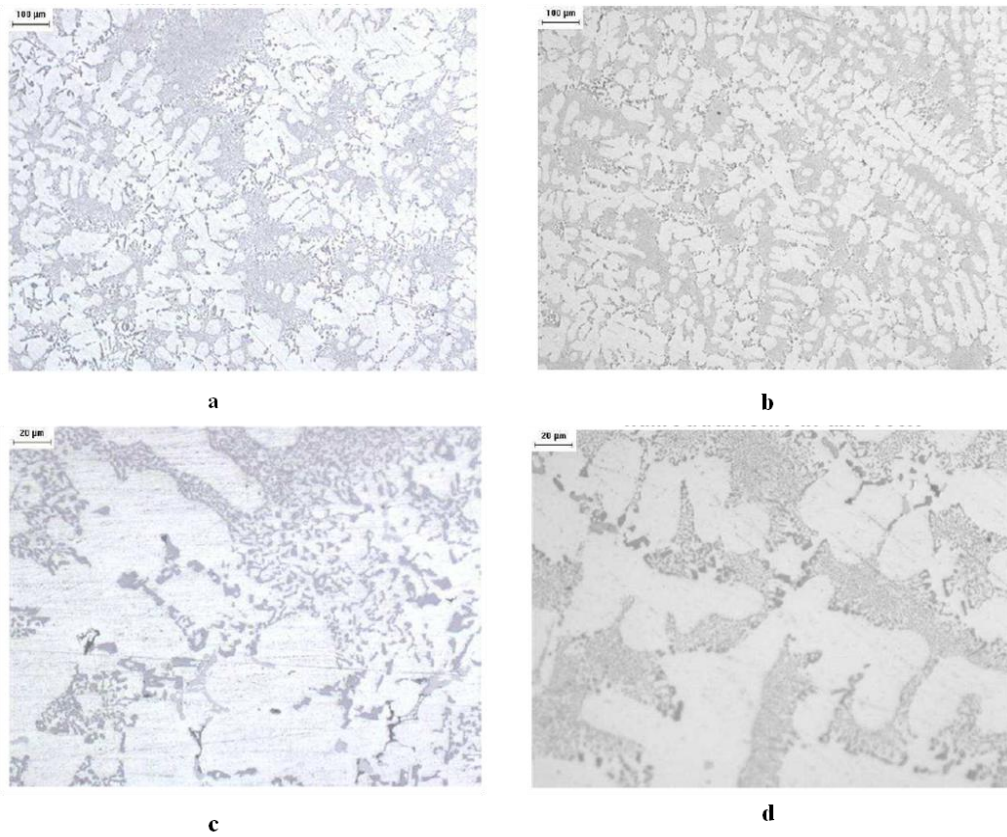


**Figure 51:** Microstructure of the AlZn10Si8Mg self-hardening aluminum alloy: a) in the as cast condition (100X); b) after seven days of natural ageing (100X); c) in the as cast condition (500X); d) after seven days of natural ageing (500X).

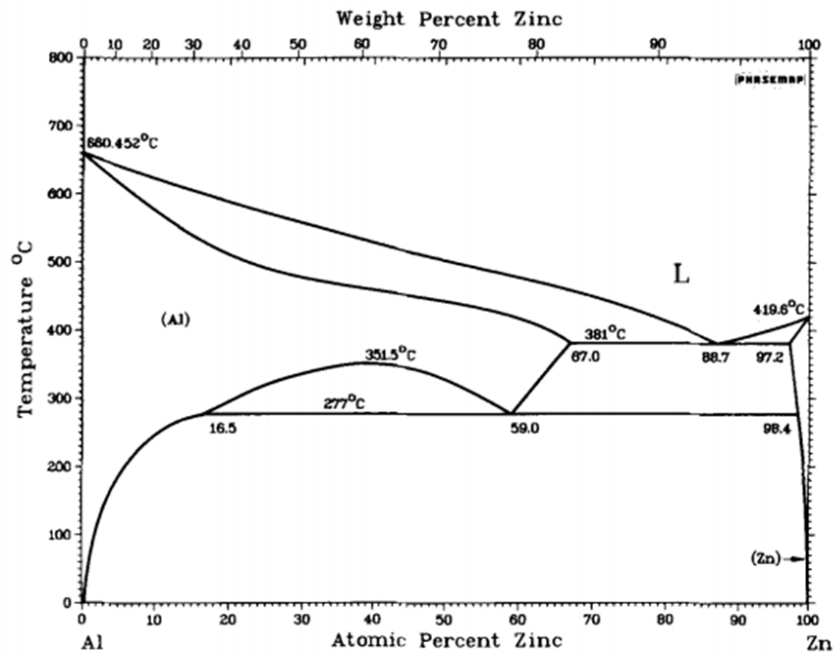


**Figure 52:** Aluminum-zinc phase diagram [72].

**Table 11:** Secondary dendritic arm space of the AlZn10Si8Mg aluminum alloy: a) in the as cast condition; b) after seven days of natural ageing.

SDAS value [ $\mu\text{m}$ ]	
As cast condition	After 7 days of natural ageing
30	25

The presence of Mg-Zn, Mg-Si, Fe-Mn intermetallic particles and of some Zn-rich areas into the Al matrix, have been detected in both condition, as reported in the SEM images of Figures 53 and 54.

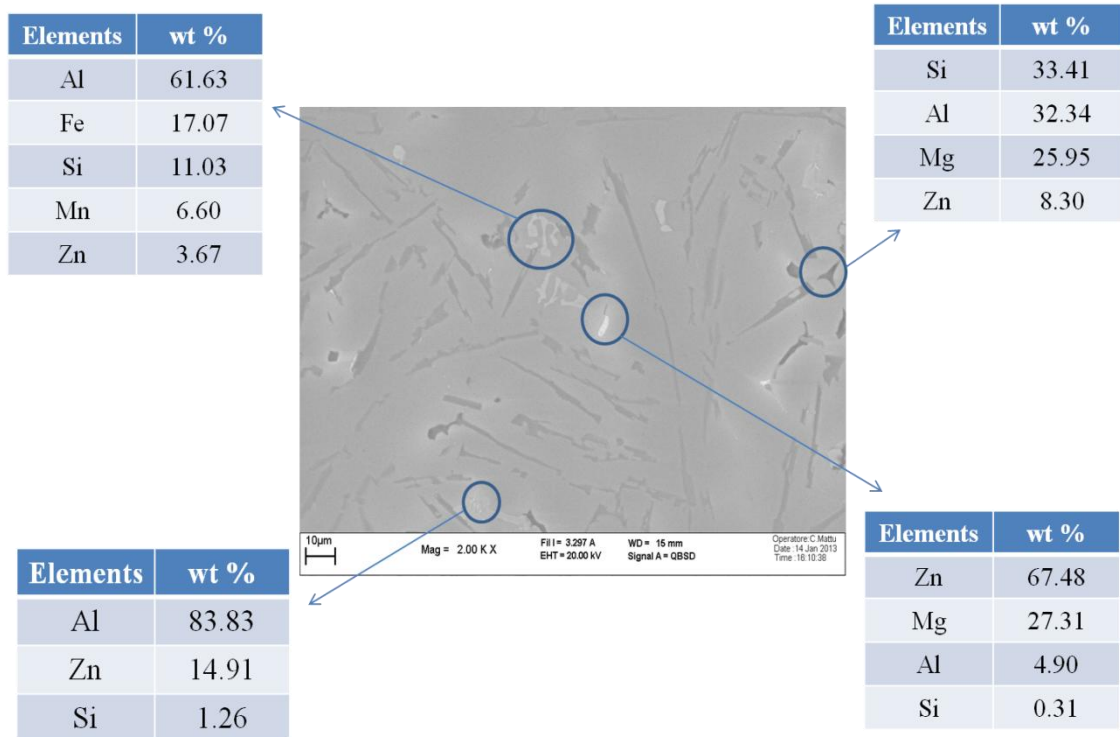


**Figure 53:** SEM micrographs and EDS analysis results of the AlZn10Si8Mg self-hardening aluminum alloy in the as cast condition.

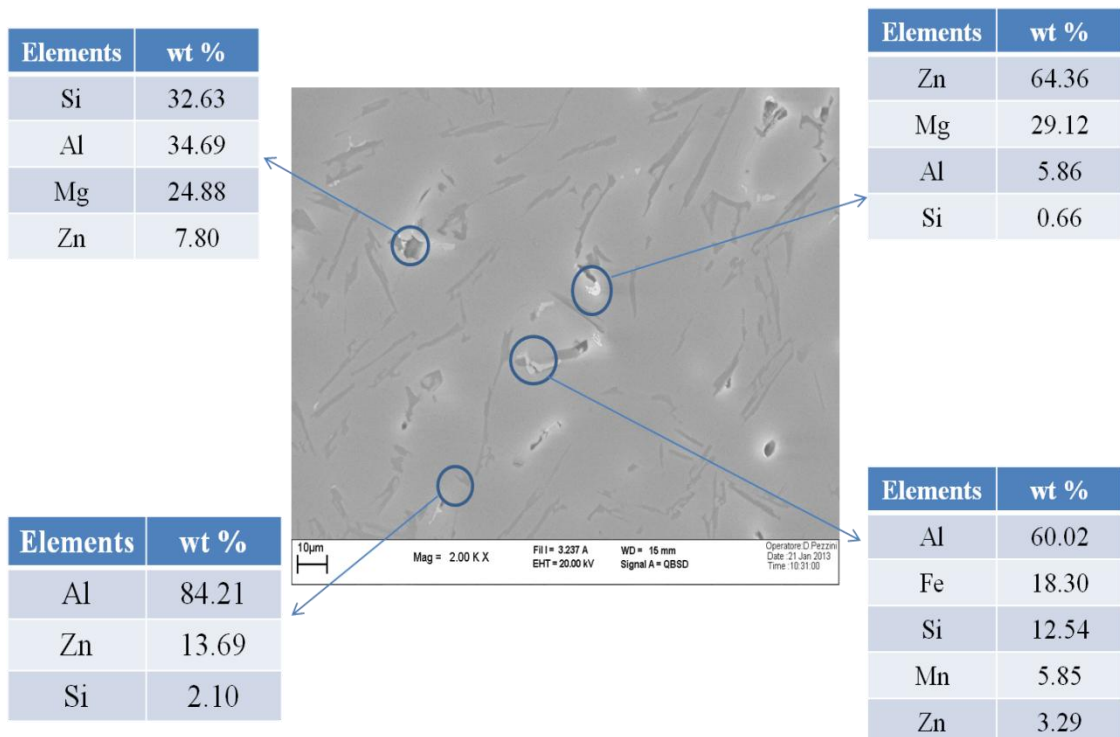


**Figure 54:** SEM micrographs and EDS analysis results of the AlZn10Si8Mg self-hardening aluminum alloy after seven days of natural ageing.

The Fe-rich intermetallics are hard and brittle particles and affect negatively the mechanical strength of aluminium alloys, because induces an effect of stress concentration. The intermetallics detected into the AlZn10Si8Mg alloy are the  $\alpha$ - $\text{Al}_{15}(\text{Fe,Mn})_3\text{Si}_2$  particles, which are more compact than the  $\beta$ - $\text{Al}_5\text{FeSi}$  ones and show a Chinese script, star-like or polyhedral morphology. According to [73] for this reason they present a lower effect of fragility. The  $\beta$ -intermetallics are converted into the  $\alpha$ -ones thanks to the presence of Mn. In Figure 55 are reported the partial phase diagrams of Al-Si-Fe system with different amount of Mn. It can be observed that increasing the Mn wt%, from 0% up to 0.3%, the area of  $\alpha$ - $\text{Al}_{15}(\text{Fe,Mn})_3\text{Si}_2$  in the phase diagram increases, this guarantees the precipitation of  $\alpha$ -intermetallics also with high wt% of iron [73]. Furthermore exists a formula which allows to calculate the % of Mn, necessary to neutralize the  $\beta$ - $\text{Al}_5\text{FeSi}$  intermetallics particles [74]. This formula have been developed by Mascrè and is reported in Eq.nr 1:

$$\% \text{ pond Mn} = ( 2 \times \% \text{ pond Fe} ) - 0.5$$

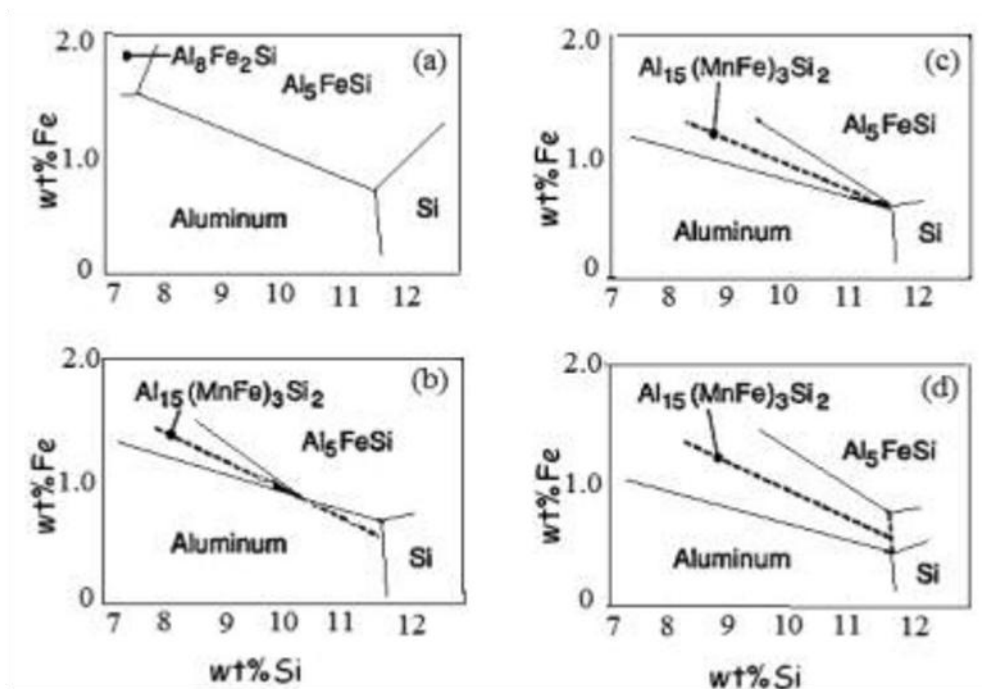


**Figure 55:** Partial phase diagrams of Al-Si-Fe system with different amount of Mn: a) 0 wt%; b) 0.1 wt%; c) 0.2 wt% and d) 0.3 wt% [73].

Mg-Zn intermetallics particles as well as Zn-rich areas into the  $\alpha$ -Al matrix, allow to obtain high mechanical properties, by the precipitation hardening and the solid solution strengthening mechanism, respectively. The hardening precipitates that have been individuated, in the AlZn10Si8Mg alloy, are both the  $\text{MgZn}_2$  and the  $\text{Mg}_2\text{Si}$ , as can be observed in the spectrum obtained by X-Ray analysis, reported in Figure 56. This spectrum also evidenced the diffraction signals related to the presence of  $\alpha$ -Al matrix and to the presence of Si.

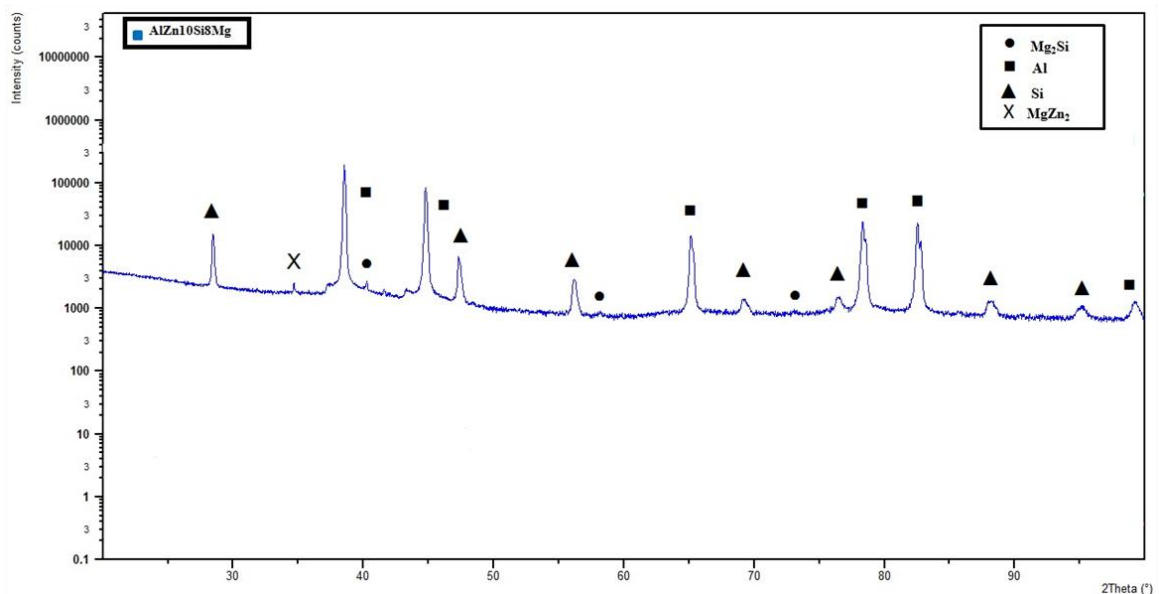


**Figure 56:** X-Ray diffractograms for the AlZn10Si8Mg self-hardening alloy.

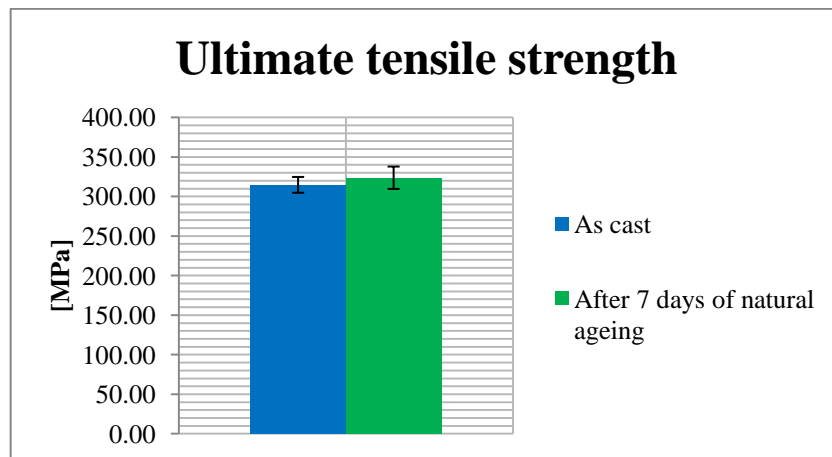
### 4.3.2 Mechanical properties

The mechanical performance have been investigated by tensile tests and Brinell hardness tests. The obtained properties have been compared to those of the A356 heat treated alloy, currently used by Teksid, and to those required at the knuckle component reported in Figure 48. Among the vehicle structural components, the knuckle is one of the most important parts in the suspension system, to which are required stringent mechanical requirements.

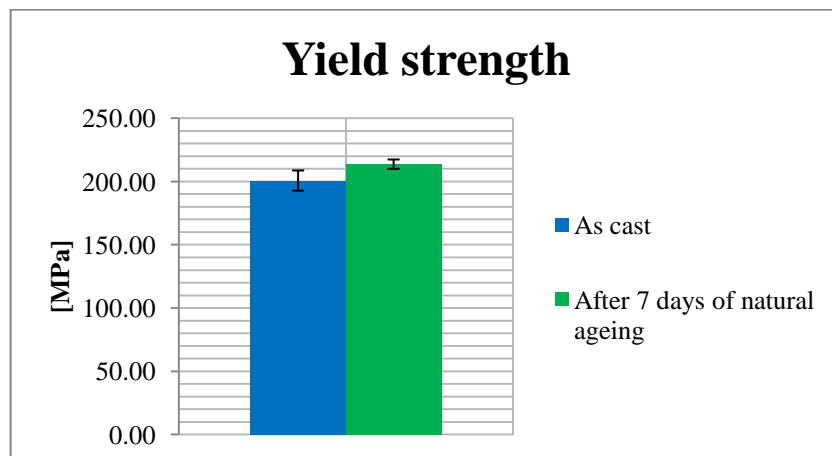
### 4.3.2.1 Tensile test

The tensile tests have been performed with a Dynamometer Zwick Z100 tool, using a load cell of 100 KN and applying a strain rate equal to 10 mm/min. The obtained results are reported in Figure 57: one can observe that after seven days of natural ageing the alloy shows a high mechanical strength and a reduced percentage of elongation (A%), mainly due to the precipitation of hardening precipitates that appear during the natural ageing. Therefore seven days of natural ageing represents the time necessary for the AlZn10Si8Mg self-hardening aluminium alloy, to reach the highest mechanical properties.

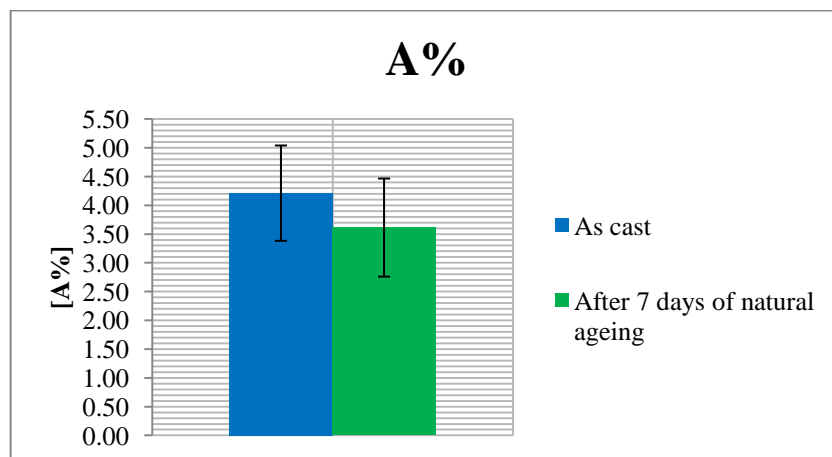
The mechanical properties, obtained for the AlZn10Si8Mg self-hardening alloy, are summarized in Table 12 and have been compared to those obtained for A356 heat treated alloy and to those required, by Teksid, for the knuckle component. Comparing the results obtained it can be concluded that the AlZn10Si8Mg self-hardening alloy mechanical properties are comparable to those of the A356 (AlSi7Mg0.3) aluminum alloy, subjected to a T6 heat treatment. The self-hardening alloy allows to reach such a properties which are adequate to satisfy the requirements for the knuckle component. The elongation to fracture A%, of the AlZn10Si8Mg alloy, shows a value which is a little bit different and it is not acceptable for such component.



a



b



c

**Figure 57:** Tensile test results: a) ultimate tensile strength; b) yield strength; c) elongation to fracture (A%).

**Table 12:** Mechanical properties of: AlZn10Si8Mg , A356 aluminum alloy subjected to T6 heat treatment and those required by Teksid for the knuckle component.

Alloy	UTS [MPa]	YTS [MPa]	A%	HB
AlZn10Si8Mg	323.72	213.69	3.61	104.54
A356 + T6	289.16	222.38	6.71	95
Properties require by Teksid for the knuckle component	$\geq 250$	$\geq 200$	$\geq 6$	$\geq 84$

#### 4.3.2.2 Brinell hardness test

The hardness measurements have been performed on the polished samples and have been carried using a Volpert DU01 tester. A force of 50 N has been applied for 15 s for each measurement and a minimum of 5 indentations were performed on each samples. The obtained results are reported in Figure 58. As well as for the mechanical strength, also the hardness of the AlZn10Si8Mg aluminum alloy, after seven days of natural ageing, increases slightly with respect to the value obtained in the as cast condition.

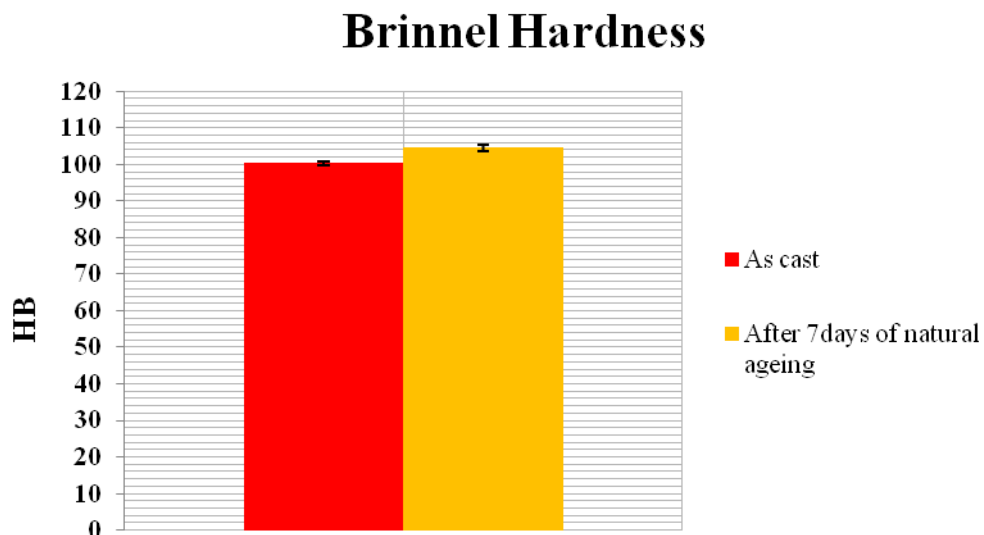


**Figure 58:** Brinell hardness test results.

### 4.3.3 Corrosion resistance evaluation

The corrosion resistance of the AlZn10Si8Mg self-hardening aluminum alloy has been evaluate through a salt spray corrosion test, performed according to the ISO 9227 Standard. In these tests, samples have been positioned inside a spray cabinet, as illustrated in Figure 59, where a solution, with a sodium chloride concentration of 50 g/l, was sprayed through a series of nozzle. The temperature inside the spray cabinet has been maintained at  $35 \pm 2$  °C while the exposure time was 480 hours. During the test the samples have been monitored at a prefixed time: every 24 hours the samples were extracted from the cabinet and they have been subjected to a visual inspection, in order to evaluate the evolution of the corrosion phenomenon. Finally, at the end of the corrosion test, the external surface of the samples have been observed by SEM analysis



**Figure 59:** Position of the samples inside the batch during salt spray corrosion test.

Figure 60 reports the images of the samples, subjected to the salt spray corrosion test, after 24,168 and 480 hours: it can be observed that, just after 24 hours, some signs related to the corrosion appear, on the external surface of the samples. At the end of the test the samples are completely covered by an oxide layer, as reveals the EDS results reported in Figure 61. This layer can act as a total barrier to further oxidation and corrosion.

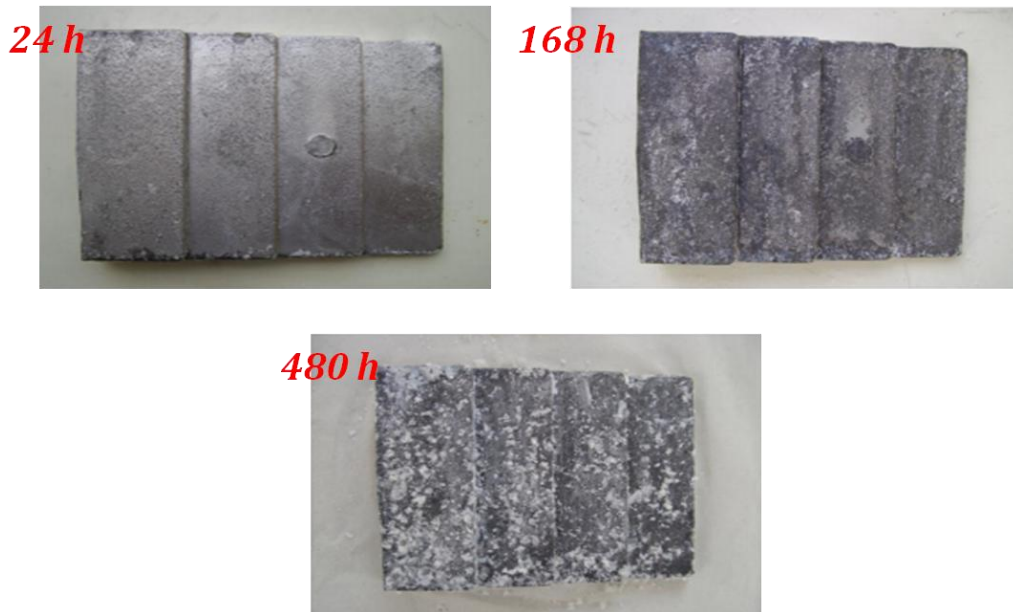


**Figure 60:** Photograph of the samples investigated following the salt spray corrosion test.

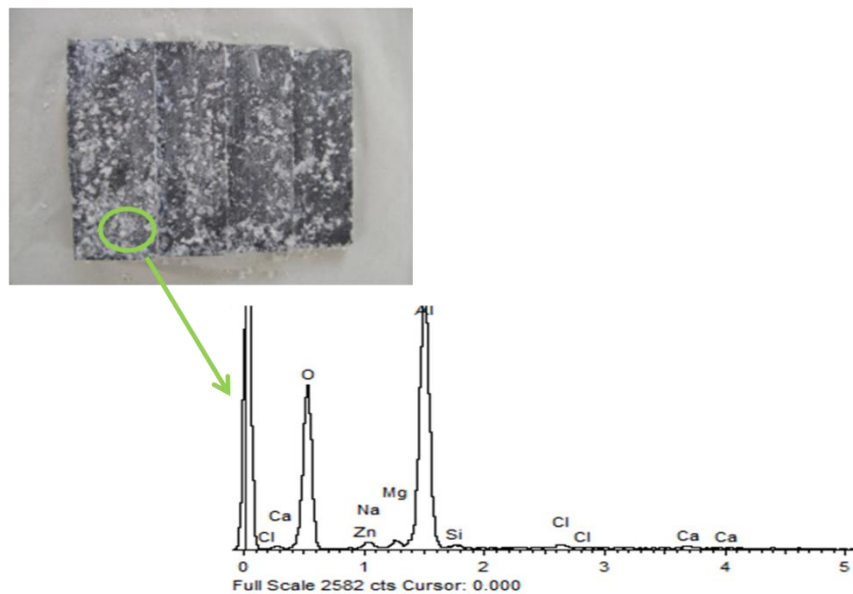


**Figure 61:** Photograph of the samples subjected to the salt spray corrosion test and the composition of the altered layer, obtained by EDS analysis.

These results demonstrate that, even if the studied alloy seems to be a promising candidate, from mechanical point of view, to substitute A356 alloy, do not has an adequate corrosion resistance. The investigation has been continued, by modifying the basic alloy composition in order to improve its corrosion resistance.

#### 4.4 Modification of AlZn10Si8Mg chemical composition through the addition of Mg up to 3%wt

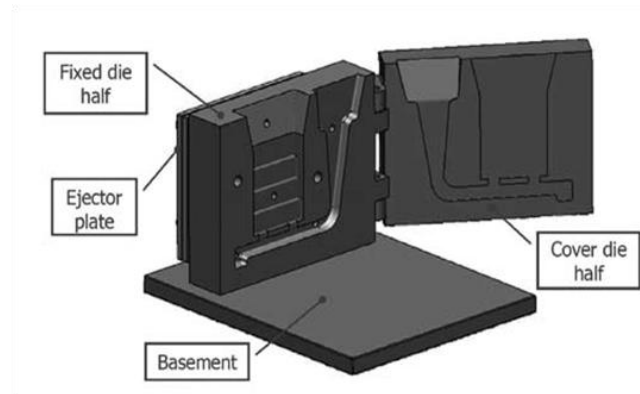
Firstly, the composition of the basic alloy has been modified by Mg addition in order to favor the precipitation of  $Mg_2Si$  precipitates, that are anodic with respect to the  $\alpha$ -aluminum matrix and that allow to enhance the corrosion resistance [75-76].

The modification of the chemical composition has been realized through the increase of the Mg content from 0.3-0.5 wt% up to 3 wt%. In this way two modified alloys have been casted and investigated: one with 1wt% of Mg and the second one with 3wt% of Mg. The alloys produced, with an increasing Mg content, have been labelled as AlZn10Si8Mg, AlZn10Si8Mg1 and AlZn10Si8Mg3, as reported in Table 13. Structural and mechanical properties, as well as corrosion resistance, as a function of Mg content have been investigated.

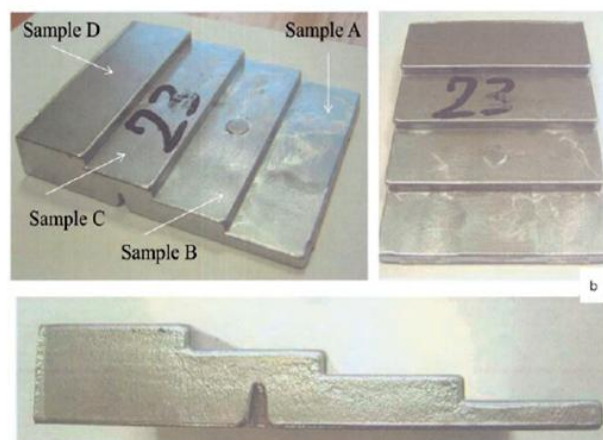
**Table 13:** Chemical composition of the three self-hardening aluminum alloys produced and studied.

Alloy	Zn wt %	Si wt %	Mg wt %	Fe wt %	Cu wt %	Mn wt %	Ti wt %	Al wt %
AlZn10Si8Mg	9.0-10	8.5-9.5	0.3-0.5	0.15	0.03	0.10	0.15	Bal.
AlZn10Si8Mg1	9.0-10	8.5-9.5	1.0	0.15	0.03	0.10	0.15	Bal.
AlZn10Si8Mg3	9.0-10	8.5-9.5	3.0	0.15	0.03	0.10	0.15	Bal.

The samples used for the microstructural, mechanical and corrosion tests, have been obtained from the step geometry sample. A scheme of the die is reported in Fig.62 a, while in Fig.62 b the obtained samples were represented. This type of sample allow to evaluate the effect of the cooling rate (CR) on the microstructure. Since in the casting the solidification is a key element for the evolution of the microstructure and governs its development having a strong impact on the mechanical properties. During the process a cooling rate has been measured by thermocouples and the average values obtained have been reported in the Table (Fig.62 c).



a



b

Average cooling rate [ $^{\circ}\text{C}/\text{s}$ ]			
Sample A	Sample B	Sample C	Sample D
~ 14	~ 8	~ 6	~ 3

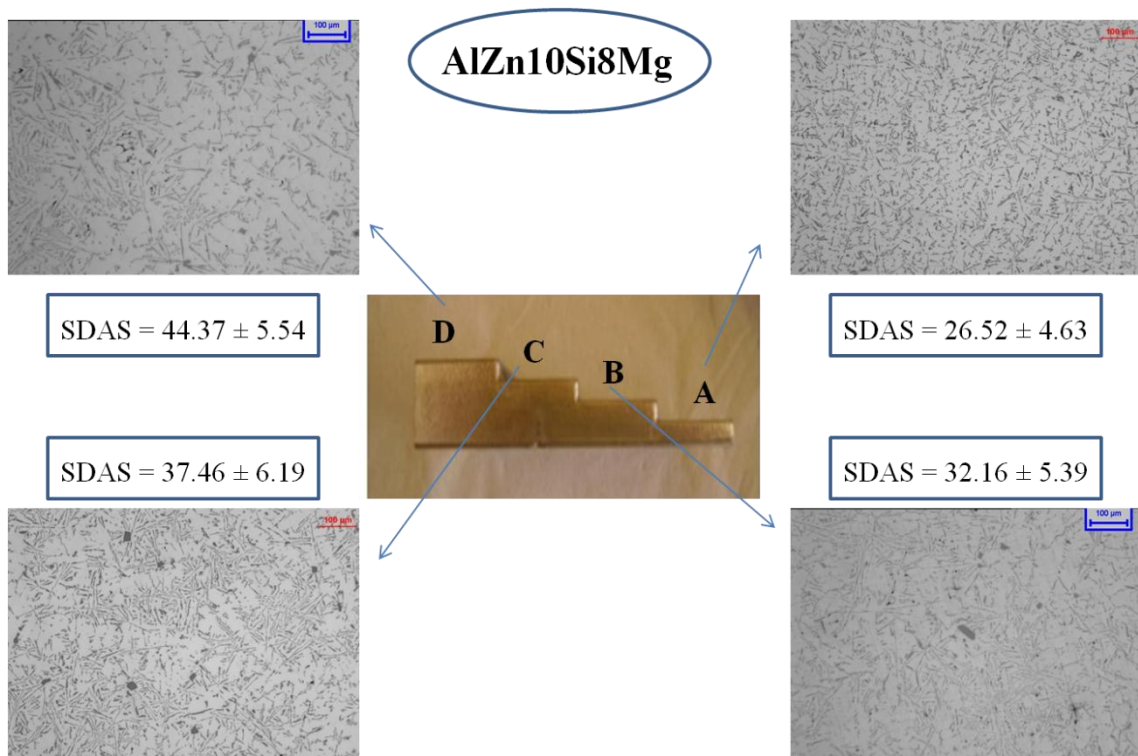
c

**Figure 62:** Step casting geometry: a) general view; b) used geometry for the analysis with side views; c) average cooling rate measured by thermocouples.

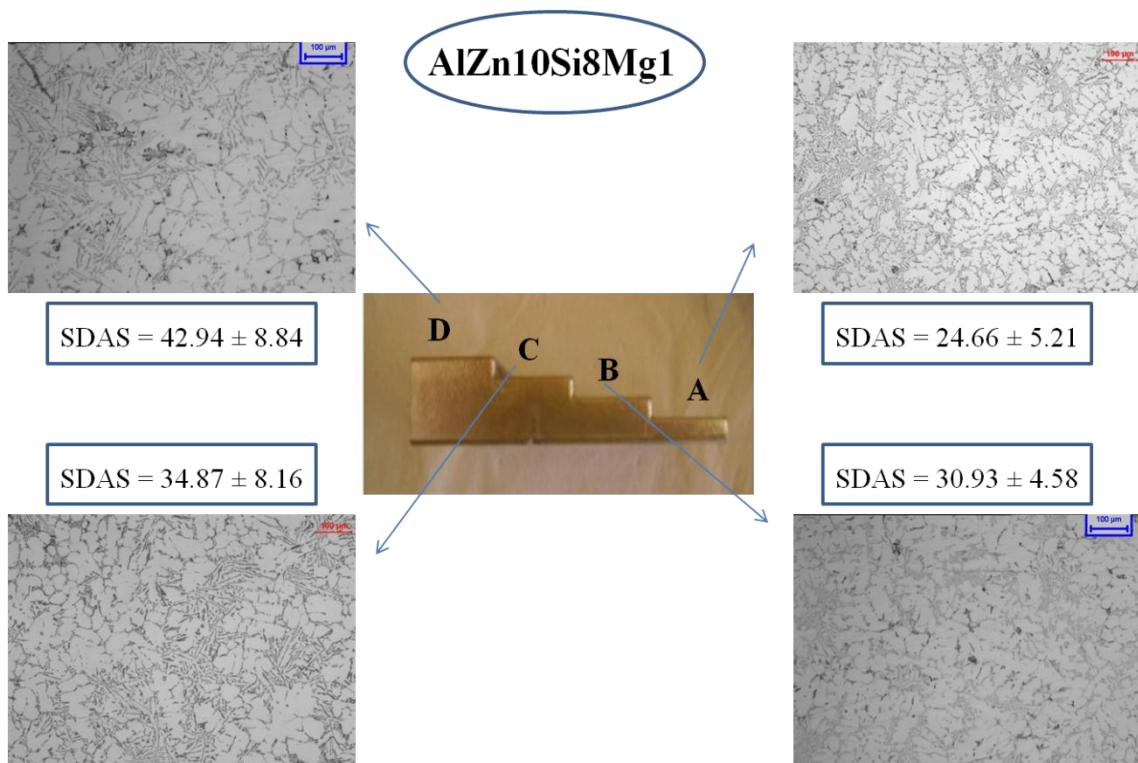
#### 4.4.1 Microstructural analysis

The three self-hardening aluminum alloys, with different cooling rates and different Mg content, have been submitted to morphological observation. The microstructure of the

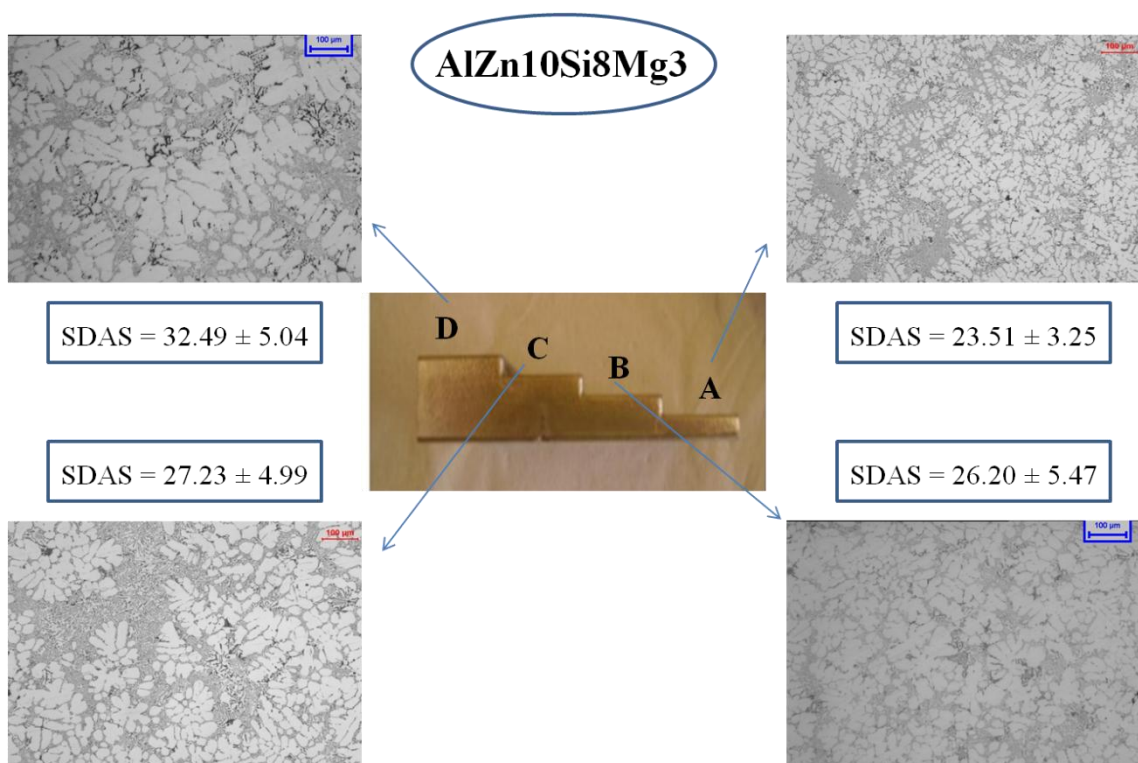
considered alloys consists in  $\alpha$ -Al matrix, originated from the liquid metal as primary phase, and in Al-Si eutectic mixture. Figures 63-64-65 report the microstructure of the alloys as a function of Mg content and of the cooling rate. Independently from the Mg wt%, high cooling rate promotes the rapid nucleation and the growth of the particles and the development of a finer particles/microstructure in all cases. Especially, for the samples coming from zone A, with the highest cooling rate, a finer microstructure has been observed compared to zone D, with the lowest cooling rate. As expected, SDAS values are inversely proportional to the cooling rate.



**Figure 63:** OM micrographs and SDAS values [ $\mu\text{m}$ ] of the AlZn10Si8Mg self-hardening aluminum alloy, as a function of the cooling rate.

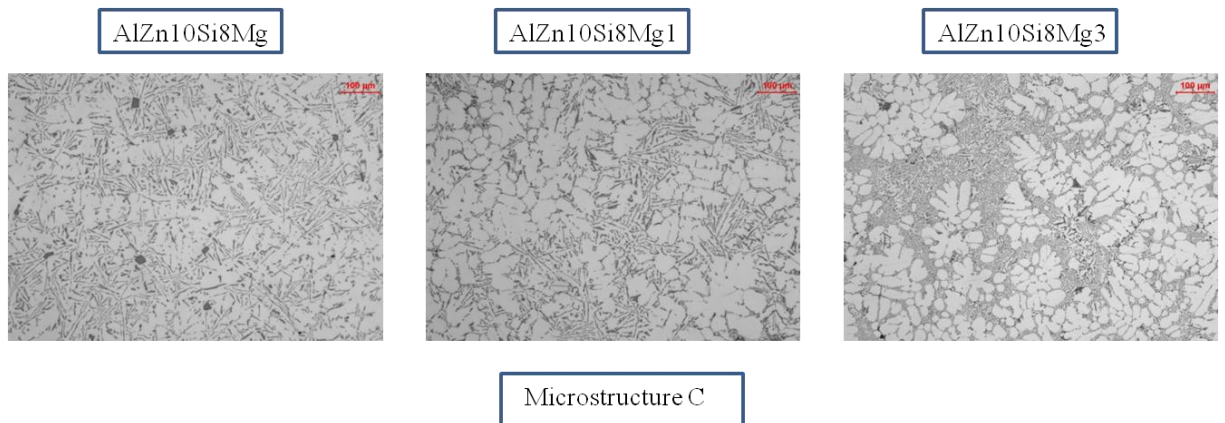


**Figure 64:** OM micrographs and SDAS values [ $\mu\text{m}$ ] of the AlZn10Si8Mg1 self-hardening aluminum alloy, as a function of the cooling rate.



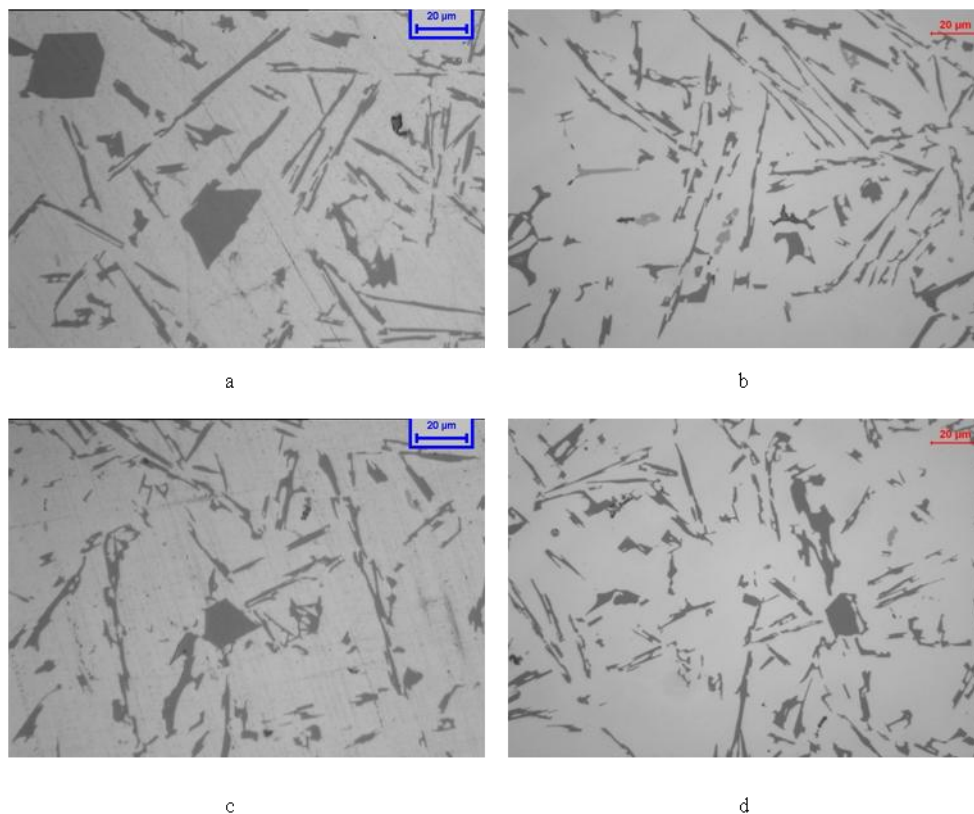
**Figure 65:** OM micrographs and SDAS values [ $\mu\text{m}$ ] of the AlZn10Si8Mg3 self-hardening aluminum alloy, as a function of the cooling rate.

As highlighted in the images reported in Figure 66, the morphology of the alloys results to be governed by the Mg wt%. As Mg content increases, the development of a more accentuated dendritic morphology can be observed, the microstructure grows into the formation of a  $\alpha$ -Al matrix in form of dendrites associated to some segregation of the eutectic regions. With low Mg content the microstructure shows an acicular features.



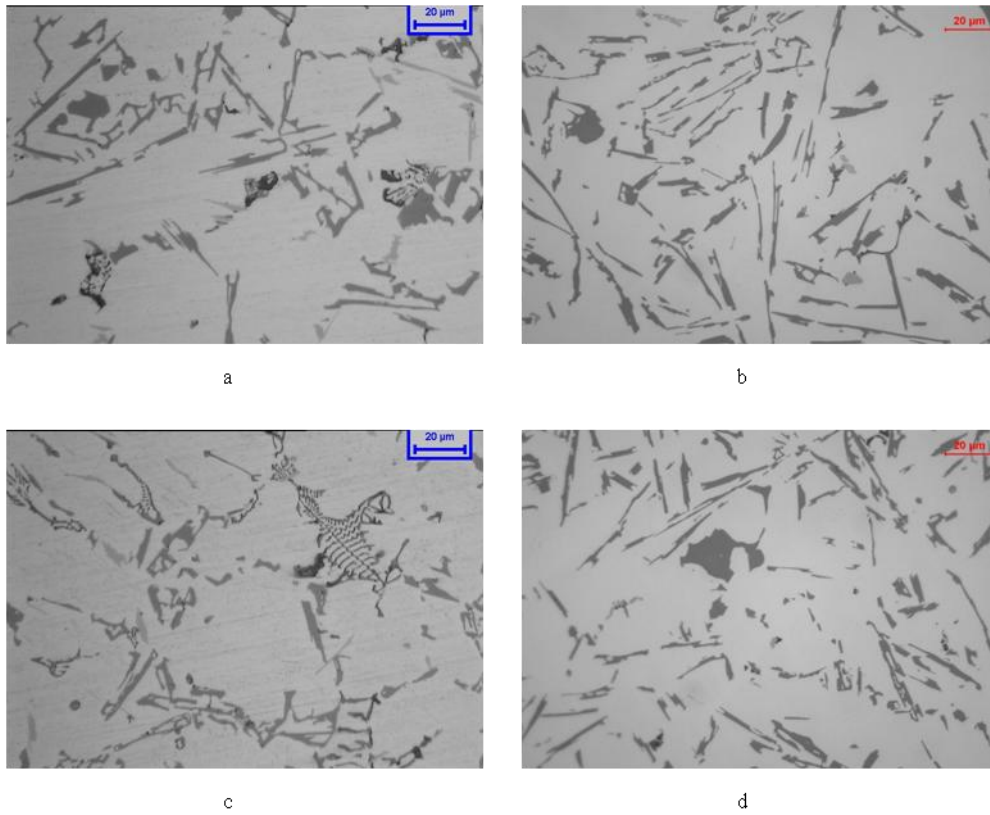
**Figure 66:** OM micrographs comparing the microstructure of zone C for all considered alloys.

Figure 67 reports the microstructures of the AlZn10Si8Mg alloy at different cooling rate. It can be observed that an increased cooling rate has an effect on both the dimensions and the morphology of the eutectic silicon particles. Silicon particles became smaller and their morphology has been changed from acicular to fine lamellar, as a consequence of the higher cooling rate.



**Figure 67:** OM micrographs of AlZn10Si8Mg self-hardening alloy at different cooling rate: a) Sample D (3 °C/s), b) Sample C (6°C/s), c) Sample B (8°C/s) and d) Sample A (14°C/s) (500x).

The microstructure of AlZn10Si8Mg1 and AlZn10Si8Mg3 alloys, at different cooling rate, are reported in Figures 68 and 69 respectively. Mg appears to act as a modifier of the silicon particles, when its wt% is increased up to 3%. Additionally higher cooling rate seems to amplify the modification effect, due to the Mg addition. In the AlZn10Si8Mg 3 alloy, silicon particles appear finer with a partial fibrous structure, while in the AlZn10Si8Mg1 alloy, these particles, even if result finer compared to those of the AlZn10Si8Mg alloy, still show a fine lamellar morphology.



**Figure 68:** OM micrographs of AlZn10Si8Mg1 self-hardening alloy at different cooling rate: a) Sample D (3 °C/s), b) Sample C (6°C/s), c) Sample B (8°C/s) and d) Sample A (14°C/s) (500x).

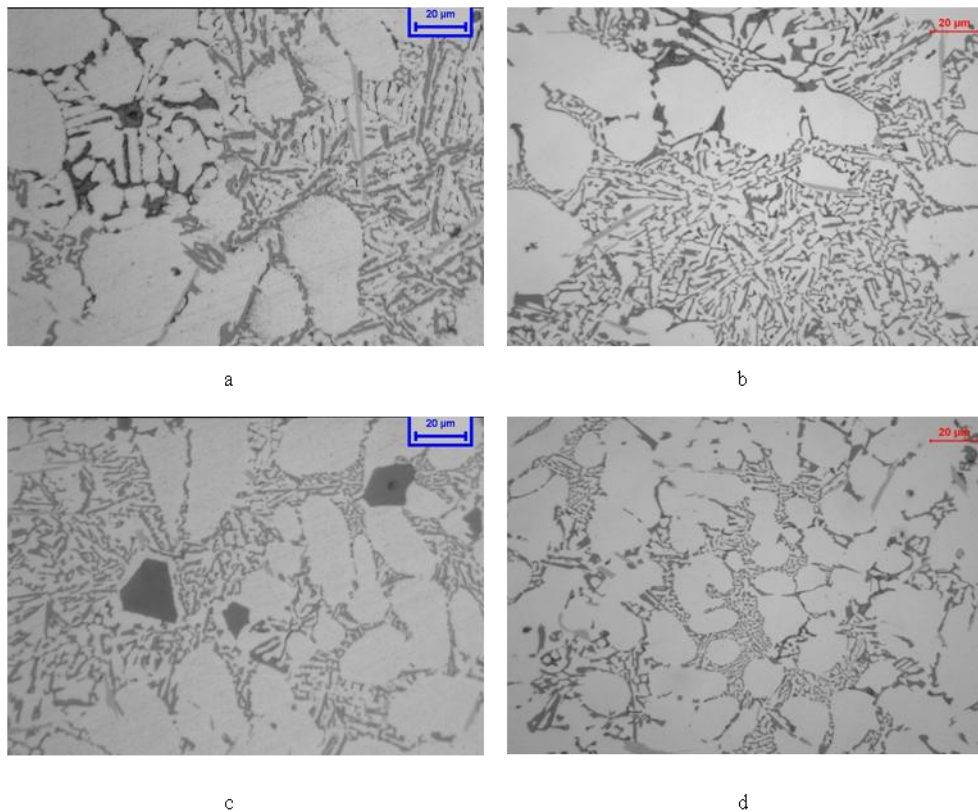


**Figure 69:** OM micrographs of AlZn10Si8Mg3 self-hardening alloy at different cooling rate: a) Sample D (3 °C/s), b) Sample C (6°C/s), c) Sample B (8°C/s) and d) Sample A (14°C/s) (500x).

Addition of Mg has determined an expansion in the modification of the silicon eutectic particles as illustrated in the microstructures reported in Figures 67, 68 and 69. In addition, the increase of cooling rate has allowed reaching a modification of the silicon eutectic particles. In order to evaluate the modification of silicon particles, some silicon particles' morphological characteristics have been investigated. Particularly the area ( $A$ ), the roundness ( $R$ ) and the equivalent diameter ( $D_{eq.}$ ) of those particles have been considered.

The effect of both cooling rate and Mg content on the modification of silicon particles is reported in Figure 70.

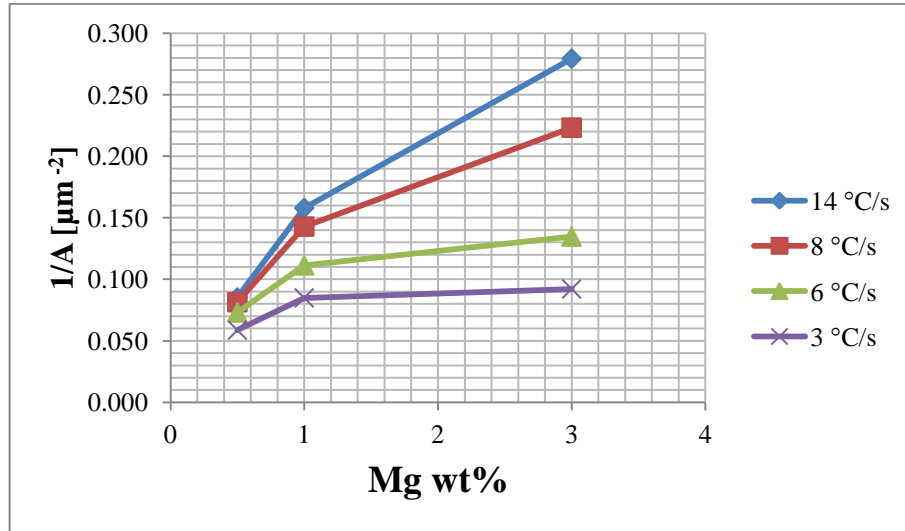


**Figure 70:** Inverse area of silicon particles for different Mg wt% and cooling rate.

For all the four cooling rates considered a higher Mg wt% allows to reach finer silicon particles, but when the Mg content is increased up to 3% the silicon particles show a fibrous structure. Increasing the Mg wt%, up to 1%, allows to reduce the silicon particles size, but the particles still have a lamellar morphology. For all the three Mg wt% considered, as cooling rate increases silicon particles dimensions a reduces.

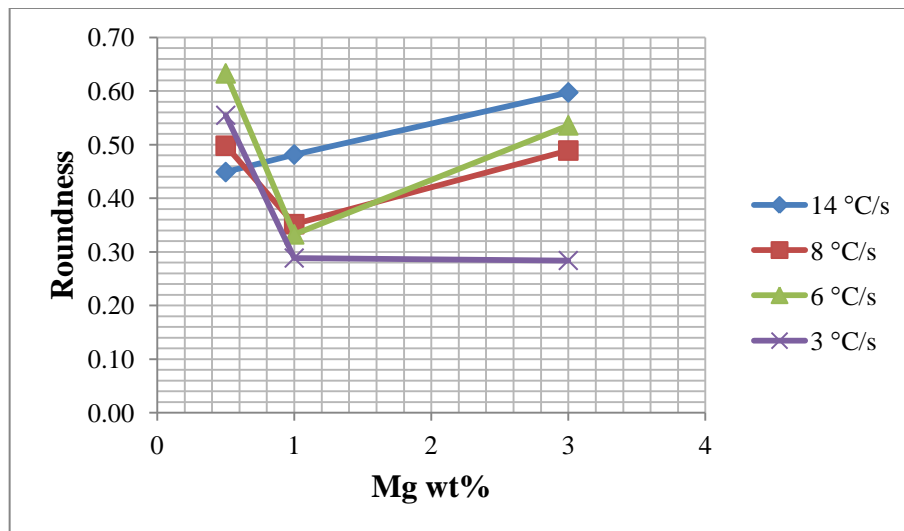
Considering the micrographs reported in Figures 67-68-69 and according to the graph reported in Figure 70 the best modification of eutectic silicon particles and the lowest silicon particles area, has been obtained with a cooling rate of about 14 °C/s and with 3 wt% of Mg.

In addition, the roundness (R) of silicon particles as important morphological characteristic has been evaluated, by the following formula:

$$R = p^2 / 4 \pi A$$

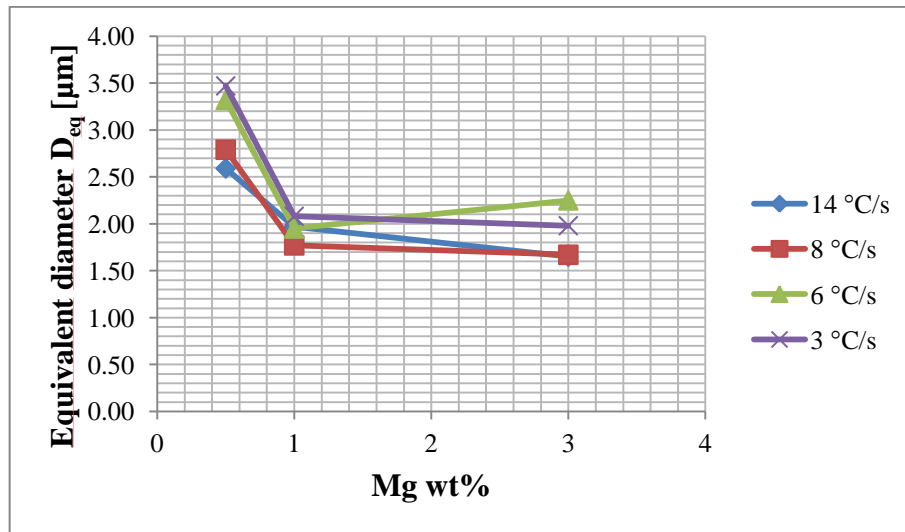
where p is the perimeter silicon particles and A is the area of silicon particles.

Figure 71 reports the plot of the roundness of silicon particles as a function of both the Mg wt% and the cooling rate. When the Mg content increased up to 1% the roundness has the tendency to decrease, only for the CR equal to 14°C/s has a different trend. While with a Mg content of 3 wt%, R increased with the exception of CR equal to 3°C/s. Consequently, to obtain R values, as close as possible to 1 (spherical particle), high CR and high Mg wt% are required. The spheroidization of the silicon particles is very important, since spherical silicon particles have lower probability to act as stress raisers and consequently as cracks initiation sites.



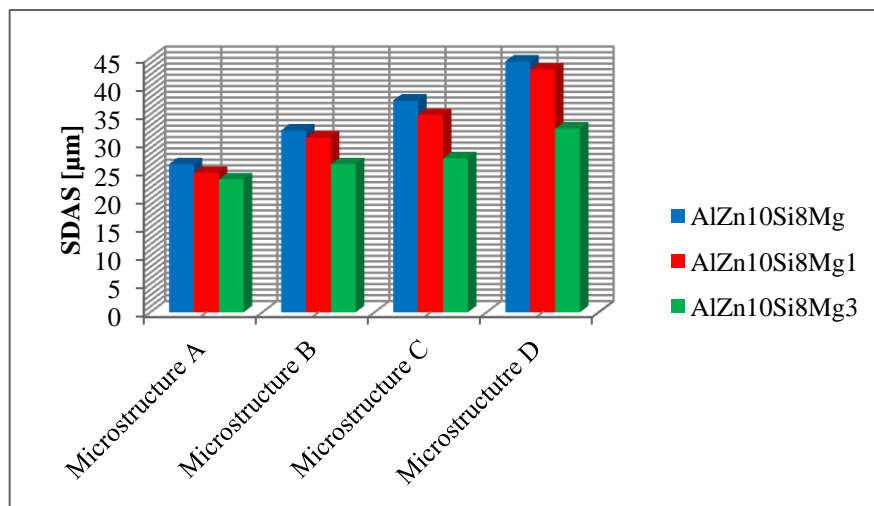
**Figure 71:** Roundness of eutectic silicon particles for different Mg wt% and cooling rate.

Figure 72 reports the  $D_{eq}$  of Si particles as a function of Mg content and of cooling rate.  $D_{eq}$  has the tendency to decrease when CR is increases, for all the three Mg content investigated. According to [77], this is due, mainly, to the amplified nucleation rate and to the lower diffusion rate. The lowest  $D_{eq}$  values are reached with both high CR and Mg content.



**Figure 72:** Equivalent diameter of silicon particles for different Mg wt% and cooling rate.

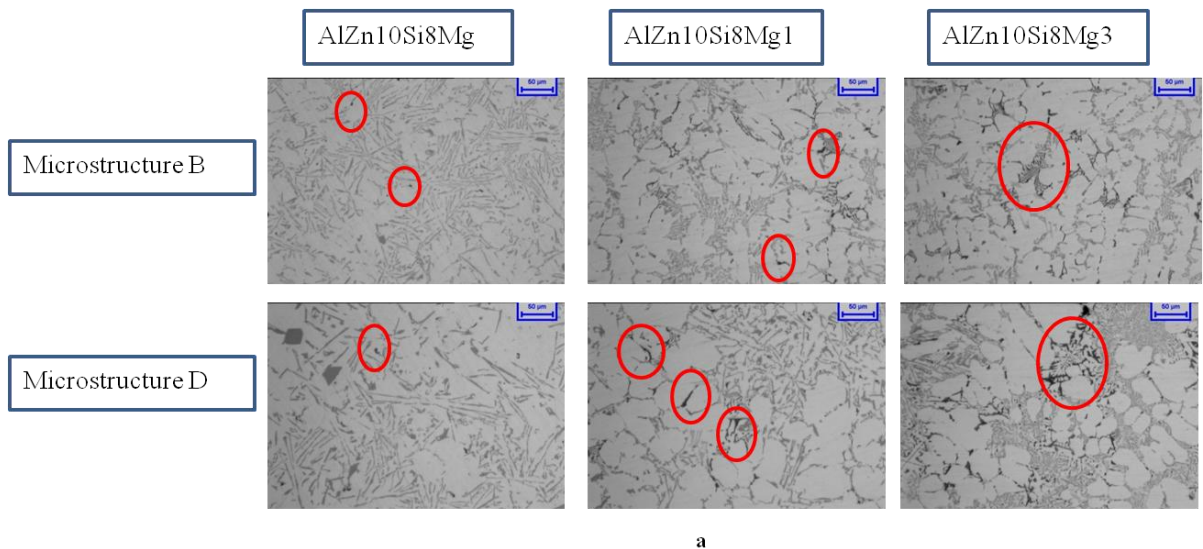
From the SDAS values, summarized in Figure 73, it can be concluded that SDAS values are inversely proportional to the cooling rate and, as Mg content (wt %) increases a reduction of SDAS values was obtained.



**Figure 73:** SDAS valued of the alloys.

In all alloys investigated Mg-based intermetallics, with a Chinese - script morphology (areas highlighted in Figure 74 a) have been detected . The dimensions of the Mg

compounds can be directly correlated to the Mg content of the alloys, in fact as expected, higher percentage of Mg leads to the enlargement of Mg intermetallics. At the same time, the cooling rate controls the growth of these intermetallic particles. In the case of samples extracted from zone D, with the lower cooling rate, largest Mg-based precipitates have been developed, while samples from zone B, with a cooling rate higher than that of zone D, shows smaller Mg intermetallics. A relatively equivalent condition has been obtained with high Mg content and low cooling rate. The EDS analysis, as can be observed in Figure 74 b, have demonstrated that these Mg intermetallics are Mg-Si precipitates, precipitated during the natural ageing of the alloy.



a

Elements	wt %
Mg	35.36
Si	33.65
Al	28.58
Zn	2.41

b

**Figure 74:** a) OM micrographs showing the microstructure of samples of AlZn10Si8Mg, AlZn10Si8Mg1 and AlZn10Si8Mg3 alloys, extracted from zone B and zone D and b) EDS analysis results.

Figure 75 reports the X-Ray spectra. In all alloys considered, the presence of  $\alpha$ -Al and Si has been detected. Moreover some differences have been evidenced, the diffraction signals related to the presence of  $Mg_2Si$  precipitates, are more accentuated in the case of AlZn10Si8Mg1 and AlZn10Si8Mg3 alloys compared to the AlZn10Si8Mg alloy. In addition, the presence of  $MgZn_2$  intermetallic phases has been detected. Both the  $Mg_2Si$  that the  $MgZn_2$  are the hardening precipitates allowing to increase the mechanical properties of the alloys.

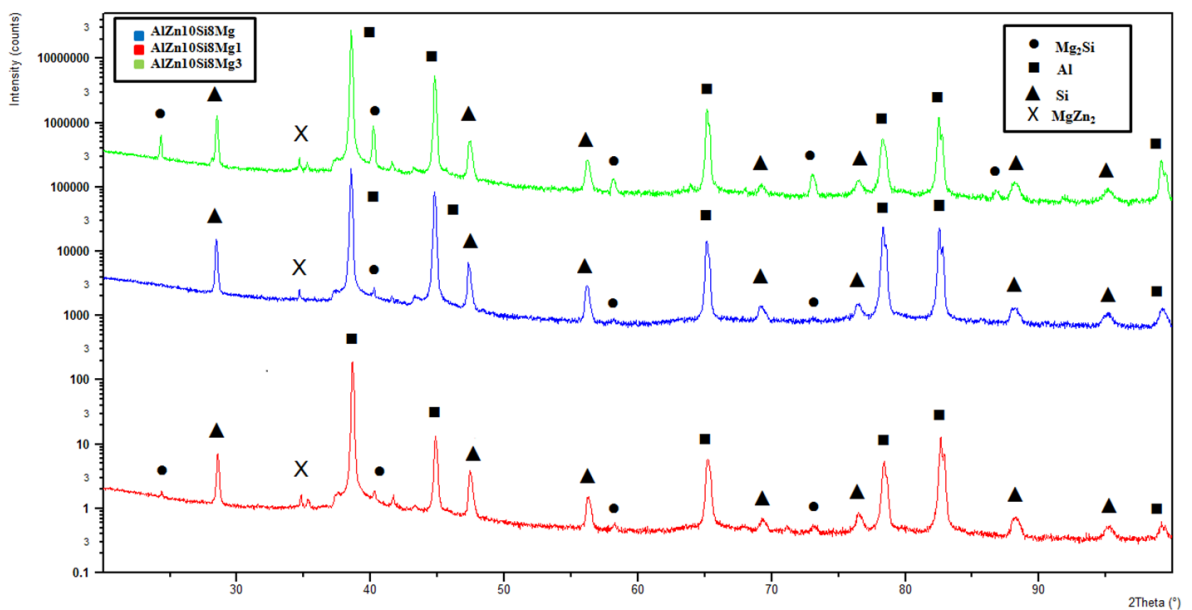


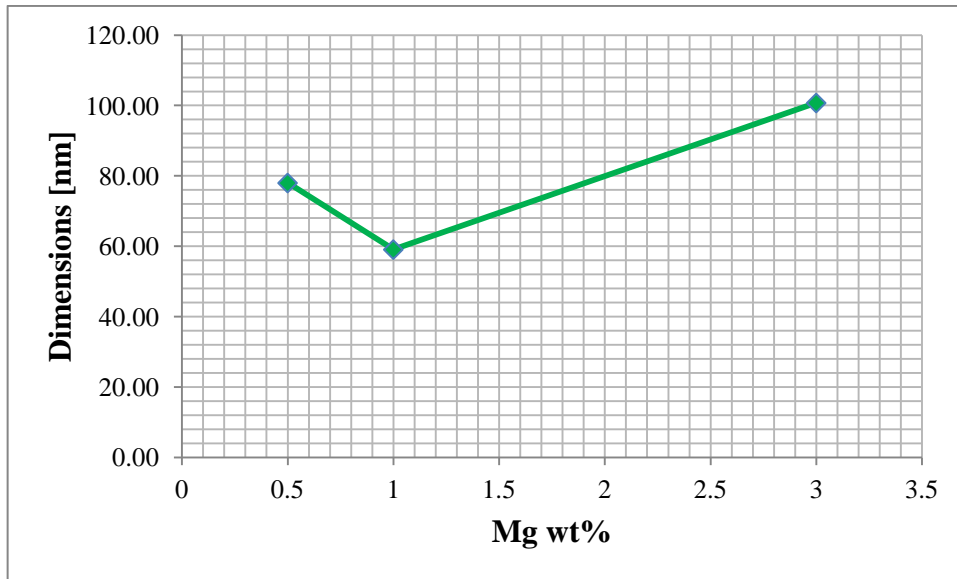
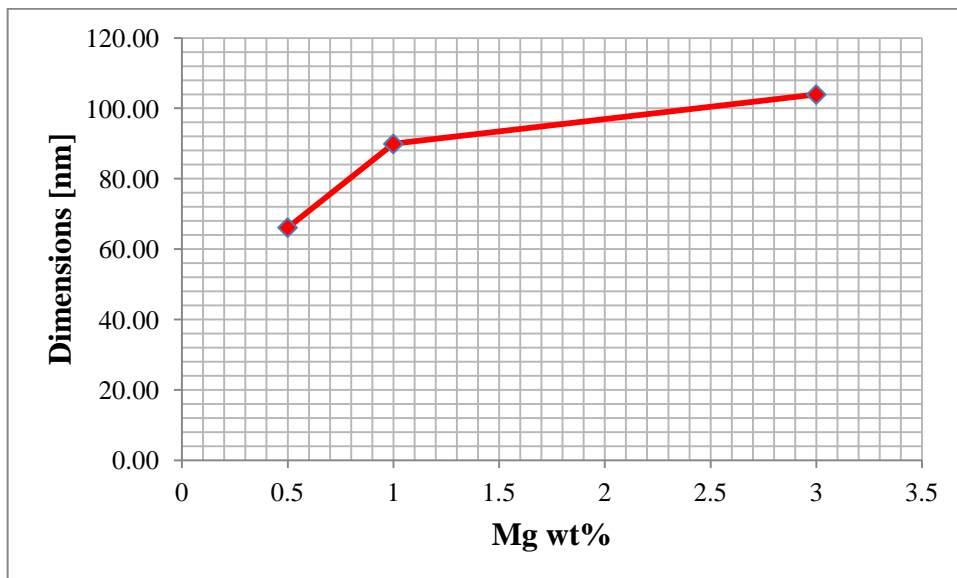
**Figure 75:** X-Ray spectra of the studied alloys.

By the use of the Scherrer formula [78], have been calculated the dimensions of the hardening precipitates:

$$B = 0.9 * \lambda / t \cos\theta$$

where  $t$  is the diameter of crystal particle,  $B$  (FWHM) is the broadening of diffraction line measured at half its maximum intensity (radians),  $\lambda$  wavelength of X-ray and finally  $\theta$  is the Bragg angle. The  $B$  values have been obtained by the XRD data.

The obtained results for both the  $Mg_2Si$  than the  $MgZn_2$  hardening precipitates are reported in Figure 76. For alloys investigated, both the hardening precipitates present an average dimension between 60-100 nm. The  $Mg_2Si$  as well as the  $MgZn_2$  precipitates show the higher dimensions when the Mg content is equal to 3 wt%.

**a****b**

**Figure 76:** Dimensions of : a)  $Mg_2Si$  and b)  $MgZn_2$  hardening precipitates, calculated according to the Scherrer formula.

## 4.4.2 Mechanical properties evolution

Mechanical properties, have been investigated using samples extracted directly from the step sample, reported in Figure 62. In particular, the mechanical performance have been evaluated by three point bending test, Charpy test and Vickers hardness test. The tests have been conducted on samples subjected to seven days of natural ageing and to ten months of natural ageing, in order to evaluate the evolution of the mechanical properties as a function of the natural ageing time.

### 4.4.2.1 Three point bending test

The samples for the three point bending test, with the following dimensions (50 mm x 10 mm x 5mm), have been obtained from zone A and C. The three point bending test has been employed for the determination of the flexural stress and the flexural strain at break, through three point bending test machine (Dynamometer Zwick Z100 tool). The applied load corresponds to 5 KN.

Figure 77 shows the results of the flexural stress at break. First of all it can be observed that the properties of all samples, after seven days of natural ageing, for the three self-hardening alloys investigated, are comparable to those obtained after ten months of natural ageing. As discussed in Section 4.3.2, 7 days is the necessary time to reach the highest mechanical properties.

Secondly, the mechanical performance of the samples extracted from zone A are higher with respect to those of the samples obtained from zone C, for all the three self-hardening alloys investigated, because of the higher cooling rate of samples extracted from zone A, with respect to the sample removed from zone C. The highest cooling rate determines a finer microstructure, which allows reaching higher mechanical properties.

The AlZn10Si8Mg1 alloy has the highest values of flexural stress at break, thanks to the presence of Mg<sub>2</sub>Si and MgZn<sub>2</sub> hardening precipitates. Increasing the Mg wt%, the Mg-Si based intermetallics shown in Figure 74, become larger, and consequently have contributed to the crack growths followed by the failure of the alloys. This is the reason why AlZn10Si8Mg3 alloy presents lower flexural stress at break values than those of the AlZn10Si8Mg and AlZn10Si8Mg1 alloys.

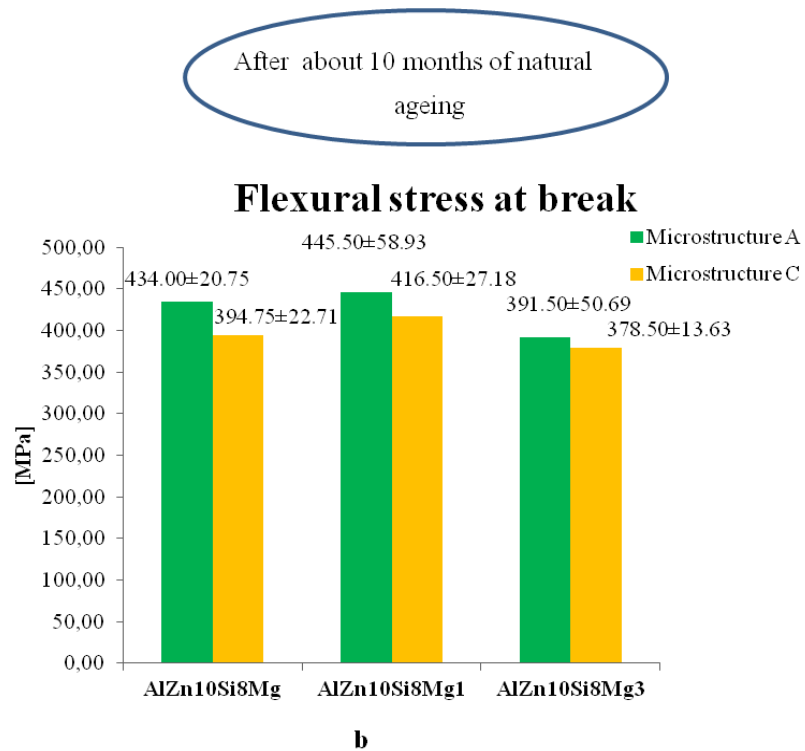
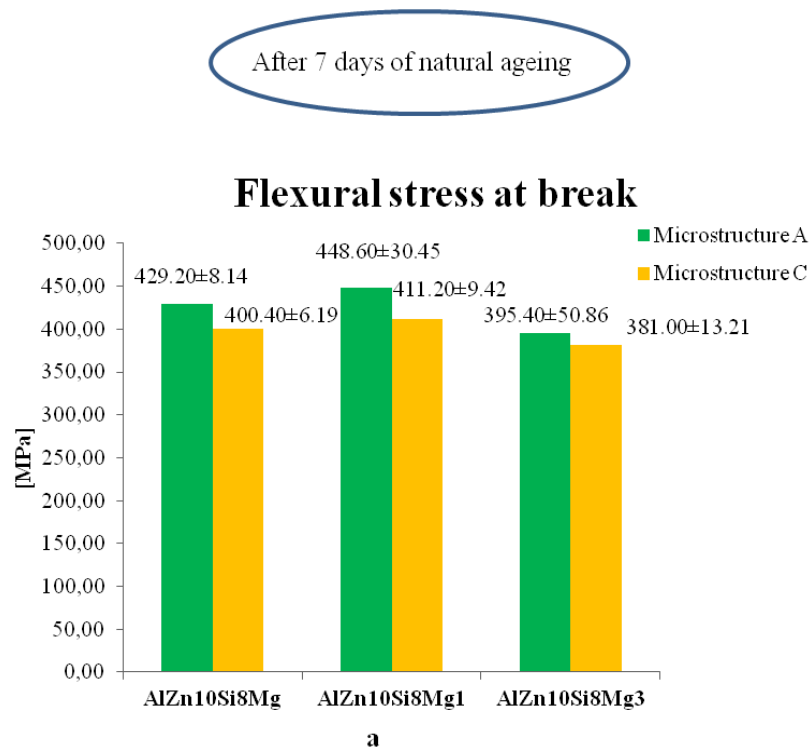


**Figure 77:** Flexural stress at break for the alloys investigated: a) after 7 days of natural ageing and b) after 10 months of natural ageing.

As can be observed by the graphs of figure 78, the increase of Mg wt% have determined a drastic reduction of the flexural strain at break.

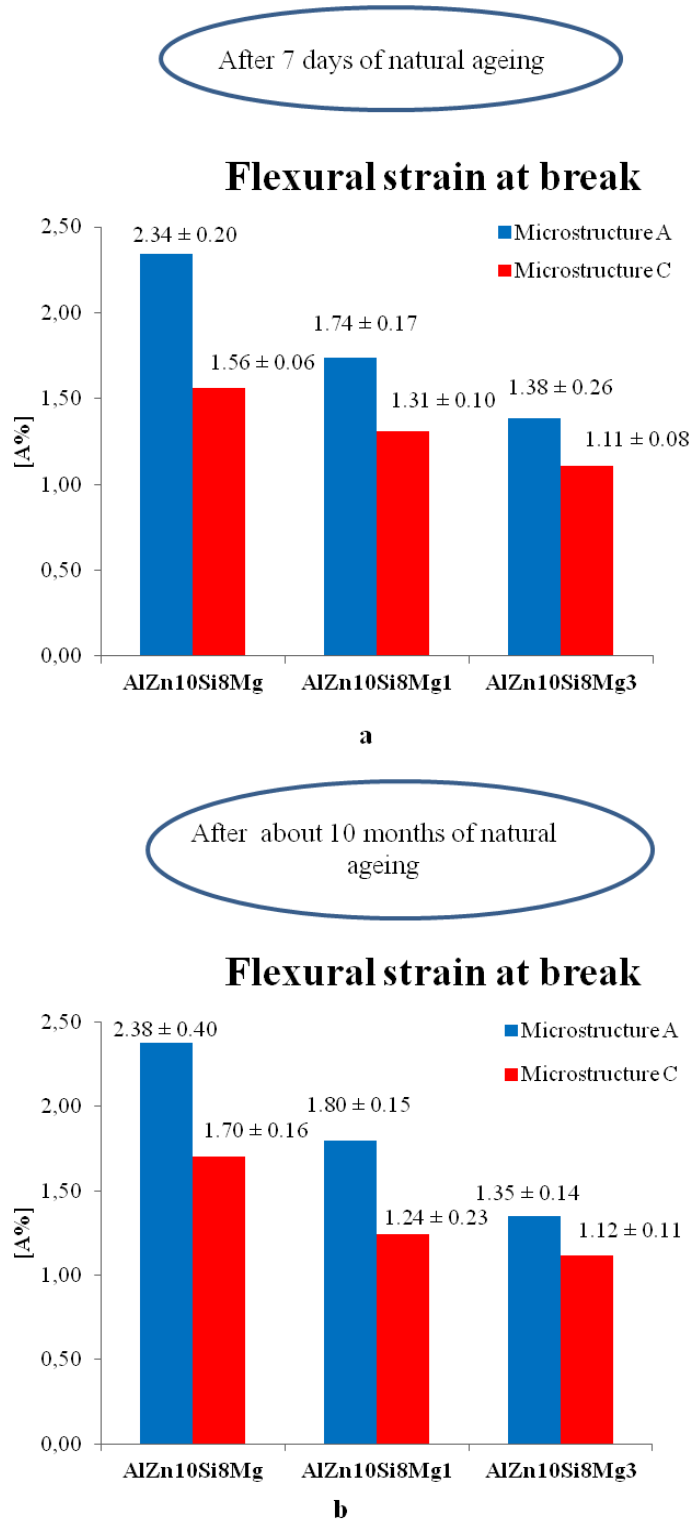


**Figure 78:** Flexural strain at break for the alloys investigated : a) after 7 days of natural ageing and b) after 10 months of natural ageing.

#### **4.4.2.2 Charpy Impact test**

The energy adsorbed by the samples during fracture has been evaluated by Charpy Impact test. For this purpose the samples have been extracted from zone B and D. Charpy pendulum, 50 J at room temperature, and un-notched samples with standard dimension (10 mm x 10 mm x 55 mm) have been used for the test. Figure 79 reports the obtained results.

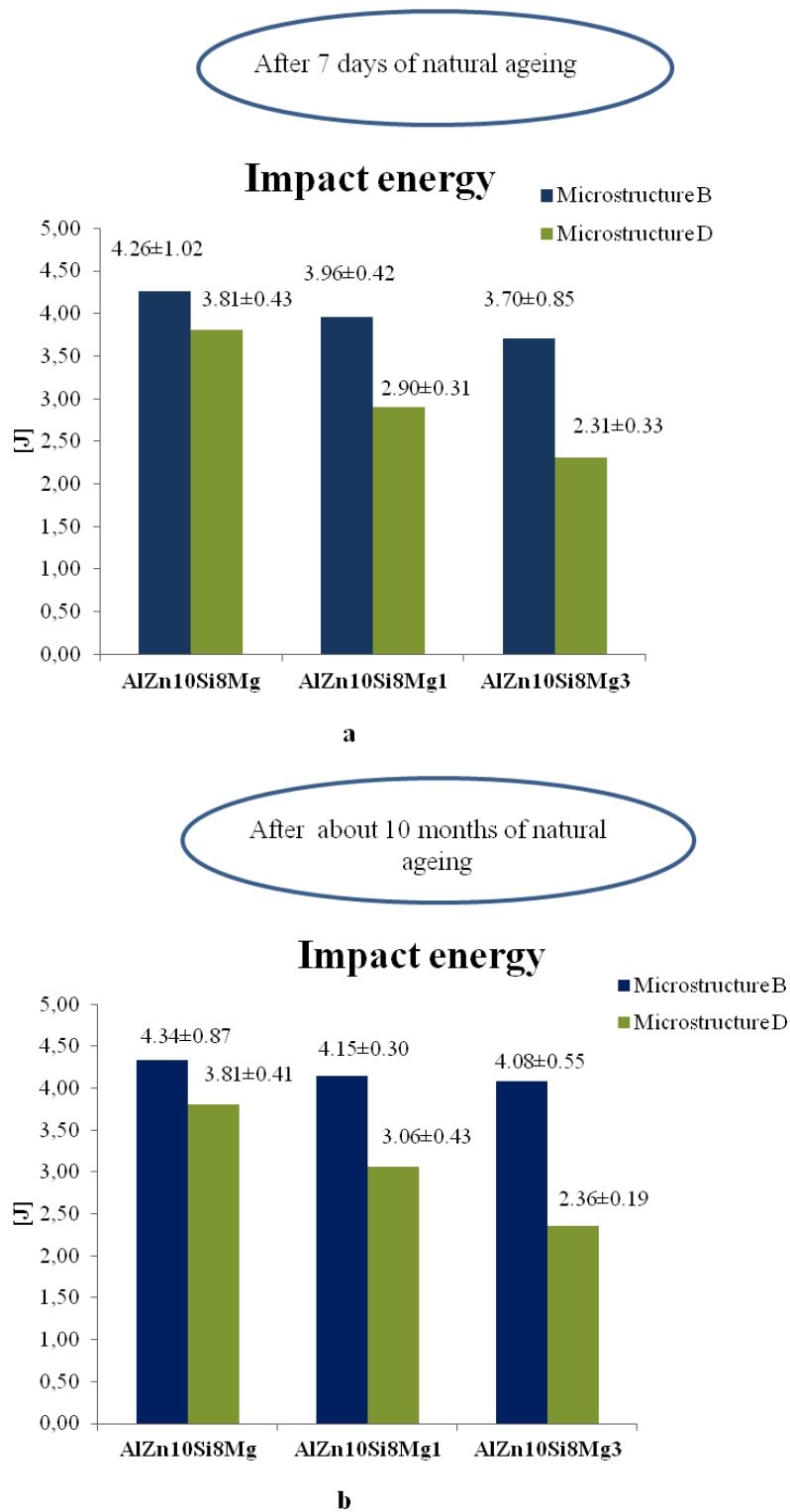


**Figure 79:** Charpy test results: a) after 7 days of natural ageing and b) after 10 months of natural ageing.

For all the three investigated alloys, samples coming from zone B have higher impact energy with respect to the impact energy of sample coming from of zone D. When the cooling rate decreases and Mg content increases, due to the development of a coarser microstructure with larger intermetallic particles, the impact energy of the samples considerably decreases. Therefore, as for the flexural stress and strain at break regards for the impact energy, large Mg-based intermetallics reported in Figure 74, are resulted to be detrimental.

#### **4.4.2.3 Vickers hardness test**

On the polished samples hardness measurements have been performed using a Volpert DU01 tester. A force of 50 N has been applied for 15 s for each measurement and a minimum of 5 indentations were performed on each samples. Figure 80 reports the comparison between the results obtained after seven days of natural ageing and those achieved after ten months of natural ageing.

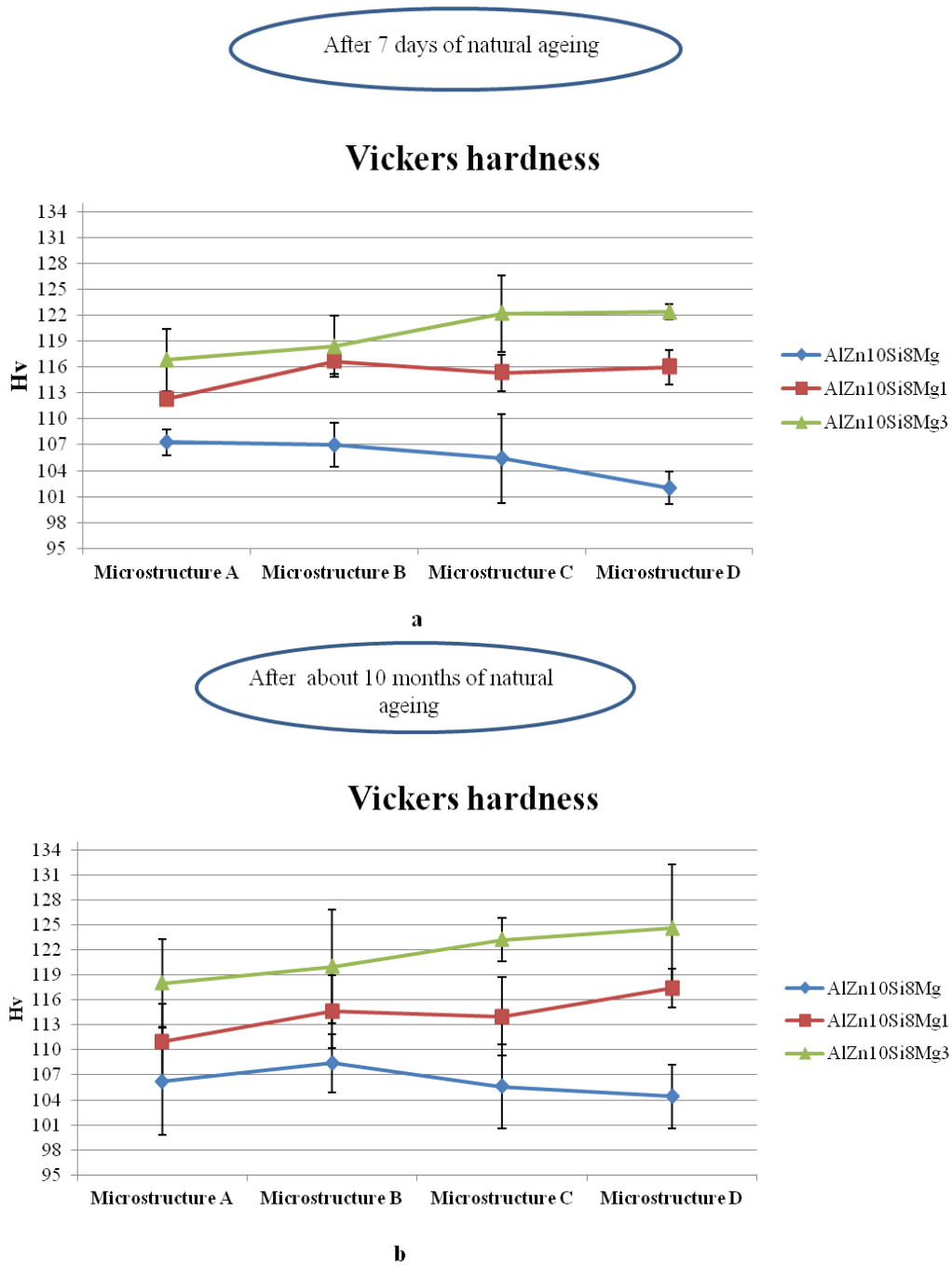


**Figure 80:** Vickers Hardness values obtained: a) after 7 days of natural ageing and b) after 10 months of natural ageing.

The increase of Mg content has gave rise to the growth of hard intermetallic particles and consequently to higher hardness values, as reported in Figure 80. In the case of the highest Mg content, as cooling rate decrease, a locally amplification of this property has been obtained.

#### 4.4.3 Fracture surfaces analysis

Fracture surface analysis were carried out on the fractured surfaces, by SEM, on the samples following mechanical tests, in order to determine, if possible, the causes related to the samples failure. Fig.81 reports the micrographs of the fractures surfaces showing a mixed type of fracture. Shrinkage porosities (Fig.82 a) and the presence of oxide particles (Fig.82 b) are the main defects, which have a detrimental effect on the mechanical strength of all samples, as can be observed in Figure 82 a-b.

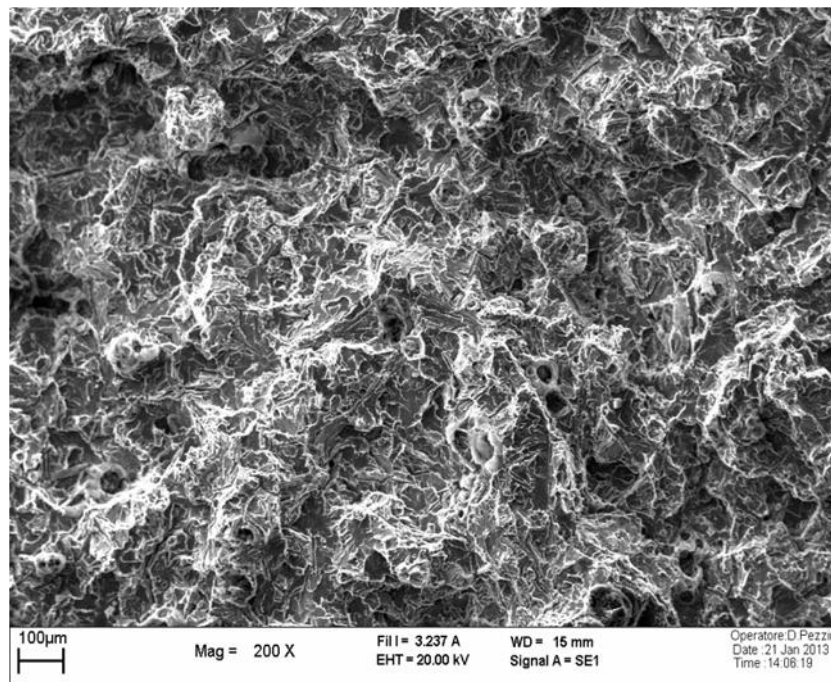
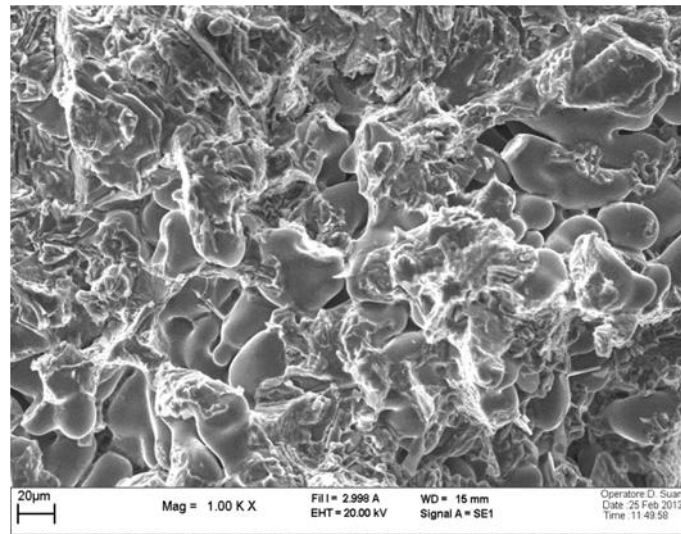
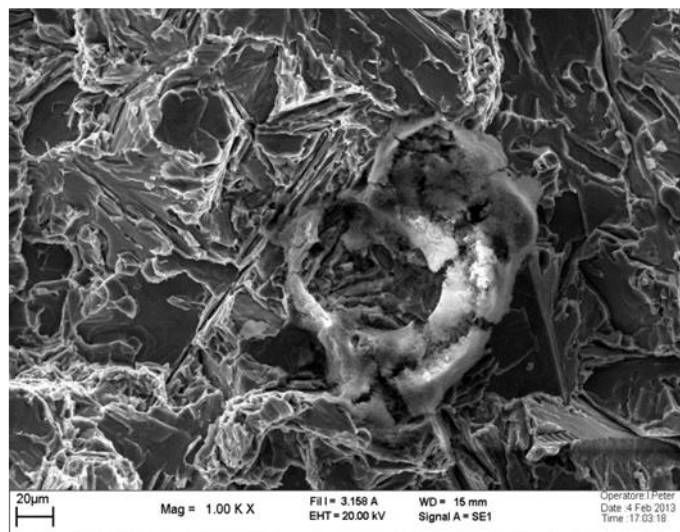


**Figure 81:** SEM micrographs of the fractured surface.



a



b

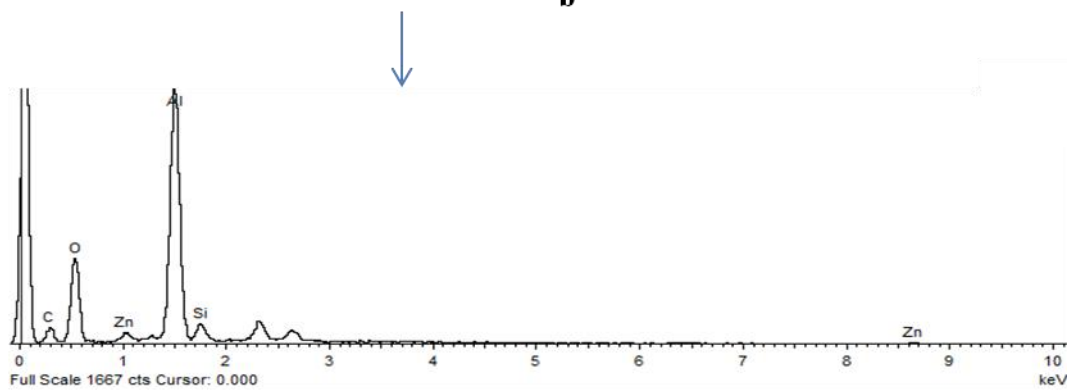


**Figure 82:** SEM images showing some details of the fractured surface: a) shrinkage porosity and b) oxide particle.

These defects have been originated probably from the manual production step, during the solidification of the alloys or during the feeding operations of the dies and, most of them, can be removed through some small correction of the different steps during the manufacturing.

#### **4.4.4 Corrosion properties**

The corrosion resistance of alloys produced has been evaluated through two different test:

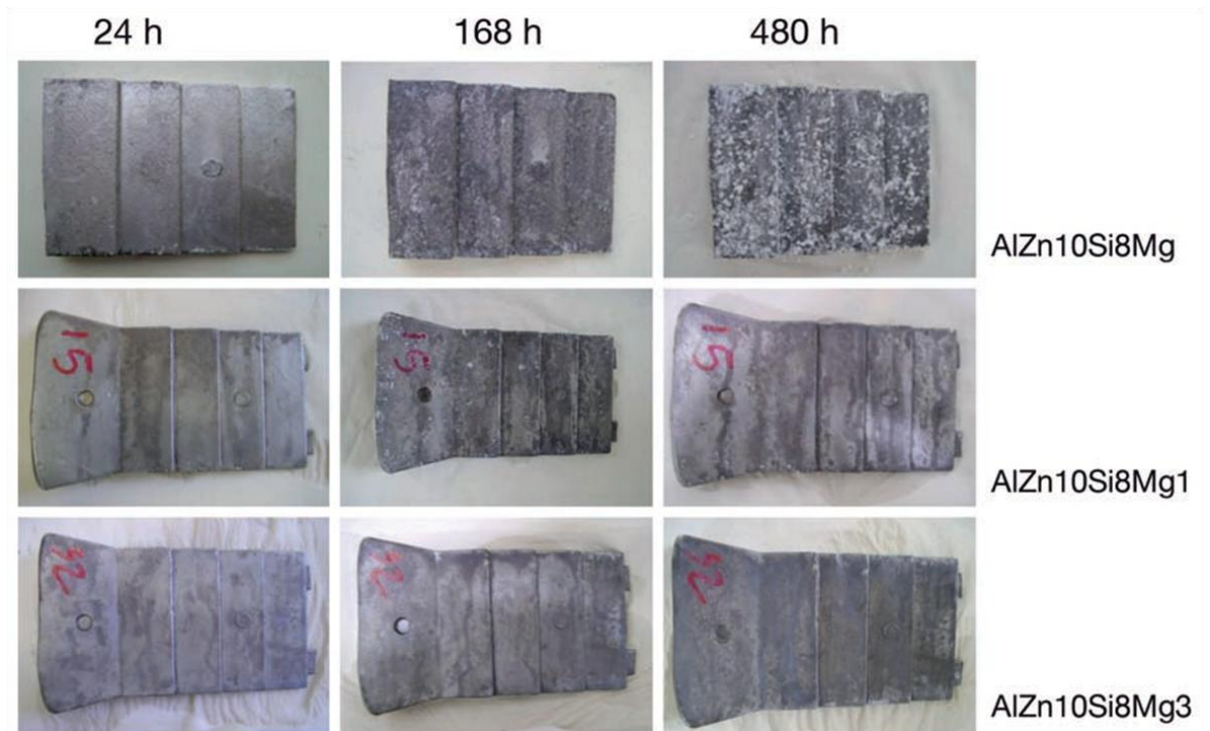
- salt spray corrosion test
- intergranular corrosion test

The effect of the Mg content on the corrosion properties of the alloys have been evaluated. To complete the study some mechanical tests have been carried out, before and after both the two corrosion tests, in order to investigate the effect of corrosion phenomena on the mechanical properties.

##### **4.4.4.1 Salt spray corrosion test**

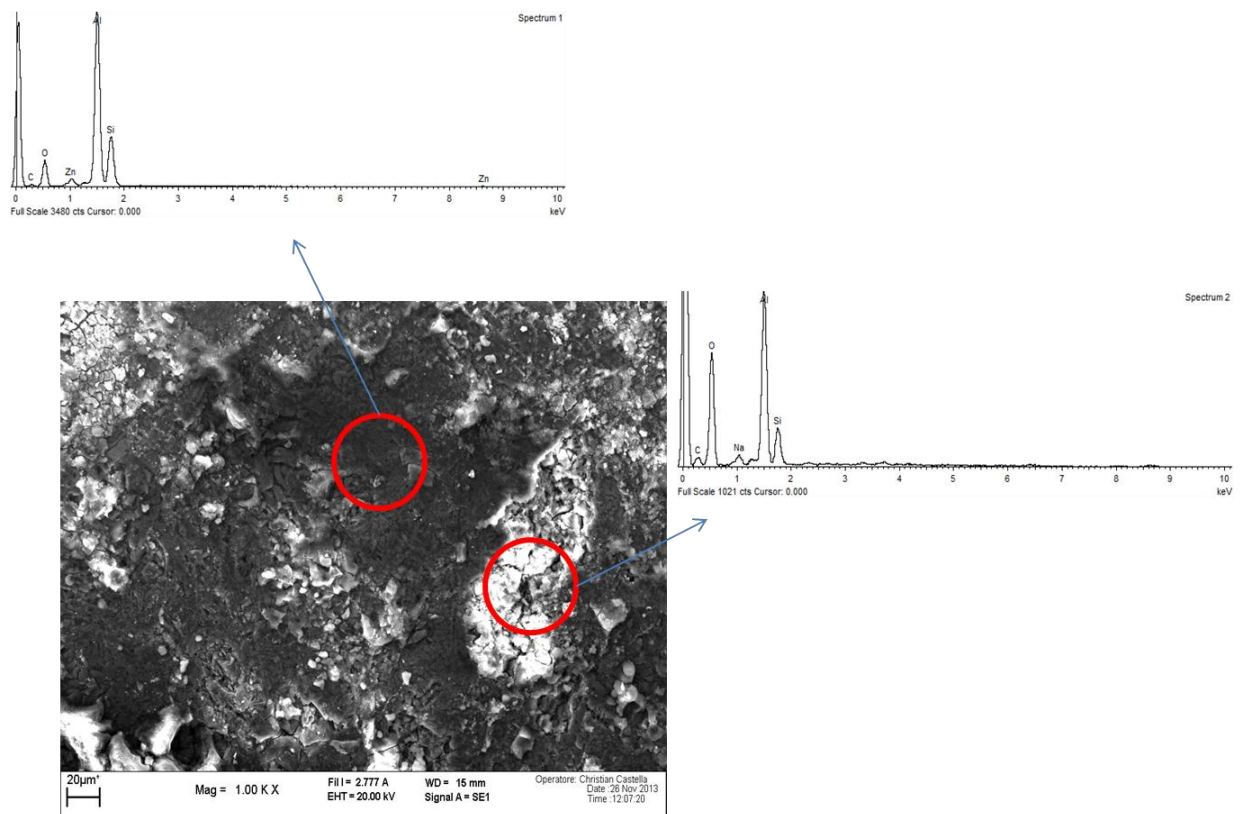
This test has been carried out according to the Standard ISO 9227, as described previously in section 4.3.3.

Figure 83 reports the photographs acquired after the maintenance for 24, 168 and 480 hours into the corrosive media. Some signs related to the corrosion appear on the surface of the AlZn10Si8Mg alloy, just after 24 hours of exposure. While the AlZn10Si8Mg1 and AlZn10Si8Mg3 alloys seem to be more resistant to the corrosion environment: at the end of the corrosion test the exposed surface is more or less identical to the original one.



**Figure 83:** Samples investigated following the salt spray corrosion test.

At the end of the test some chemical analysis have been carried out, through EDS analysis, on the external surface of samples. The results are reported in Figure 84, highlighting that the AlZn10Si8Mg alloy sample, is covered by an aluminum oxide layer.



**Figure 84:** Chemical composition of the altered layer individuated on the external surface of AlZn10Si8Mg samples, obtained by EDS analysis.

Charpy test results reported in Figure 85 demonstrate that the corrosion does not affect the mechanical properties of the alloys, the mechanical resistance of the alloys in both condition is comparable. The corrosive media determines only an aesthetic problem, which can be easily solved in the future by an adequate surface treatment.

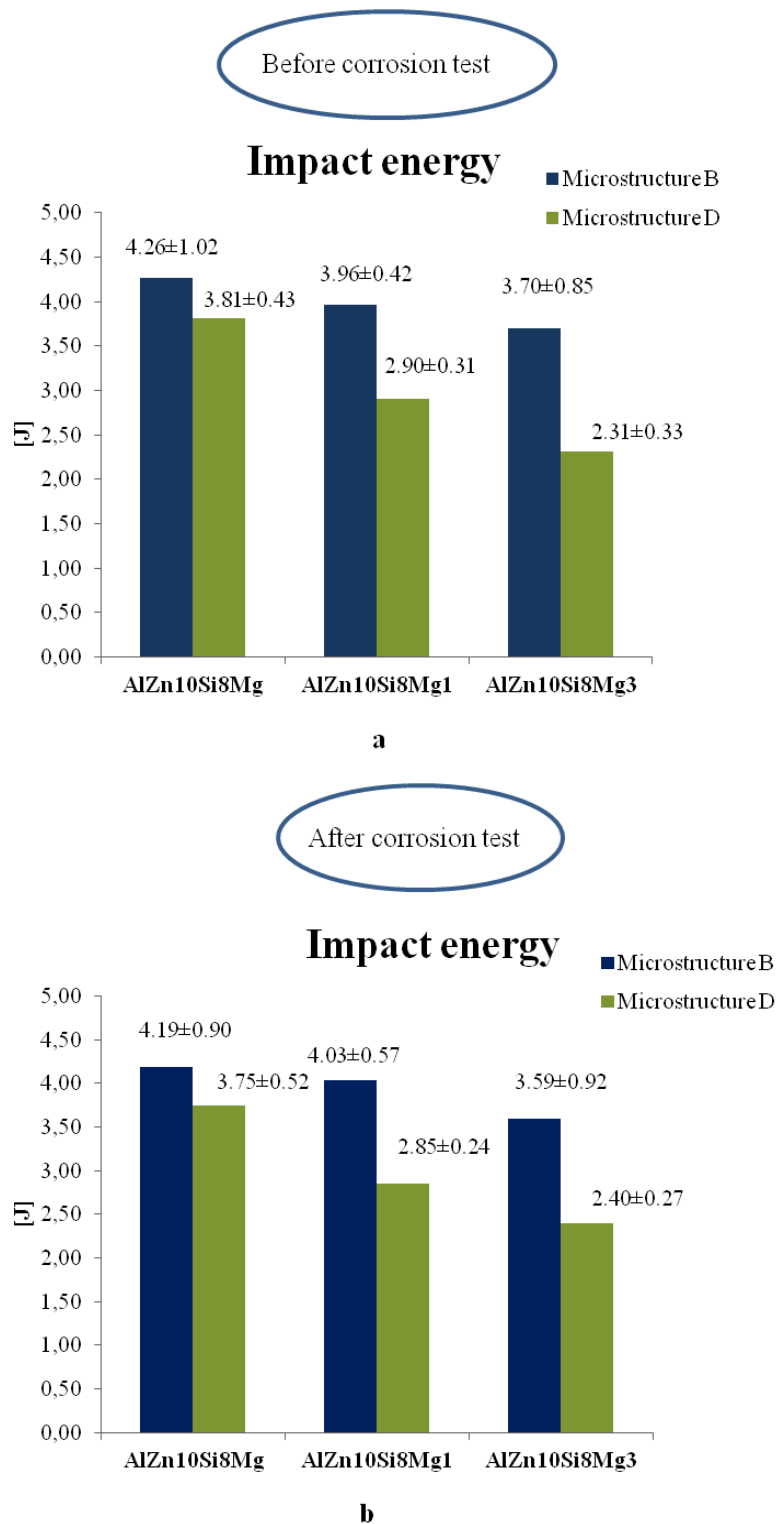


**Figure 85:** Charpy Impact test results: a) before the salt spray corrosion test and b) after the salt spray corrosion test.

#### 4.4.4.2 Intergranular corrosion test

The second type of corrosion test has been carried out according to the BS 11846, method B [79]. In this test various steps are included: degreasing in acetone and ethanol, alkaline etching (5 min in 7.5 wt% NaOH at 55–60 °C) followed by 24 h immersion in an acidified salt solution (30 g NaCl and 10 ml concentrated HCl per liter). After immersion, specific treatments have been performed on the samples, including cleaning by washing in water and ethanol and drying procedure to eliminate any components which can have alter the further analysis. The susceptibility to intergranular corrosion (IGC) has been estimated through the evaluation of corrosion depth and the weight loss following corrosion. The corrosion depth has been measured by optical microscopy using the transverse section of the corroded samples. After corrosion test, the mechanical performances of the alloys have been investigated by three point bending test and the Charpy test, using samples extracted directly from those subjected to the corrosion test.

The corrosion for all aluminum alloys principally occurs through the eutectic areas, as illustrated in Figure 86, due to the presence of Si particles, which, according to literature data [75], act as local cathodes with respect to the eutectic Al phase. In addition, also iron-containing intermetallics are cathodic with respect to the aluminium-rich matrix. Through the addition of Mn the iron-intermetallics are modified from Al-Fe-Si to Al-Fe-Si-Mn compounds, which have a less detrimental effect on the mechanical properties of aluminum alloys . Furthermore thorough the addition of Mn is possible to reduce the cathodic effect of iron-compounds [75]. Figures 86 and 87 show the OM and the SEM microstructures of the transverse cross sections on the corroded samples. These figures revealed localized corrosion at the interface between silicon particles and the  $\alpha$ -Al (Figure 86) and between Fe-intermetallics (Al-Fe-Mn) and the  $\alpha$ -Al (Figure 87). No corrosion attack have been observed on the primary  $\alpha$ -Al phase.

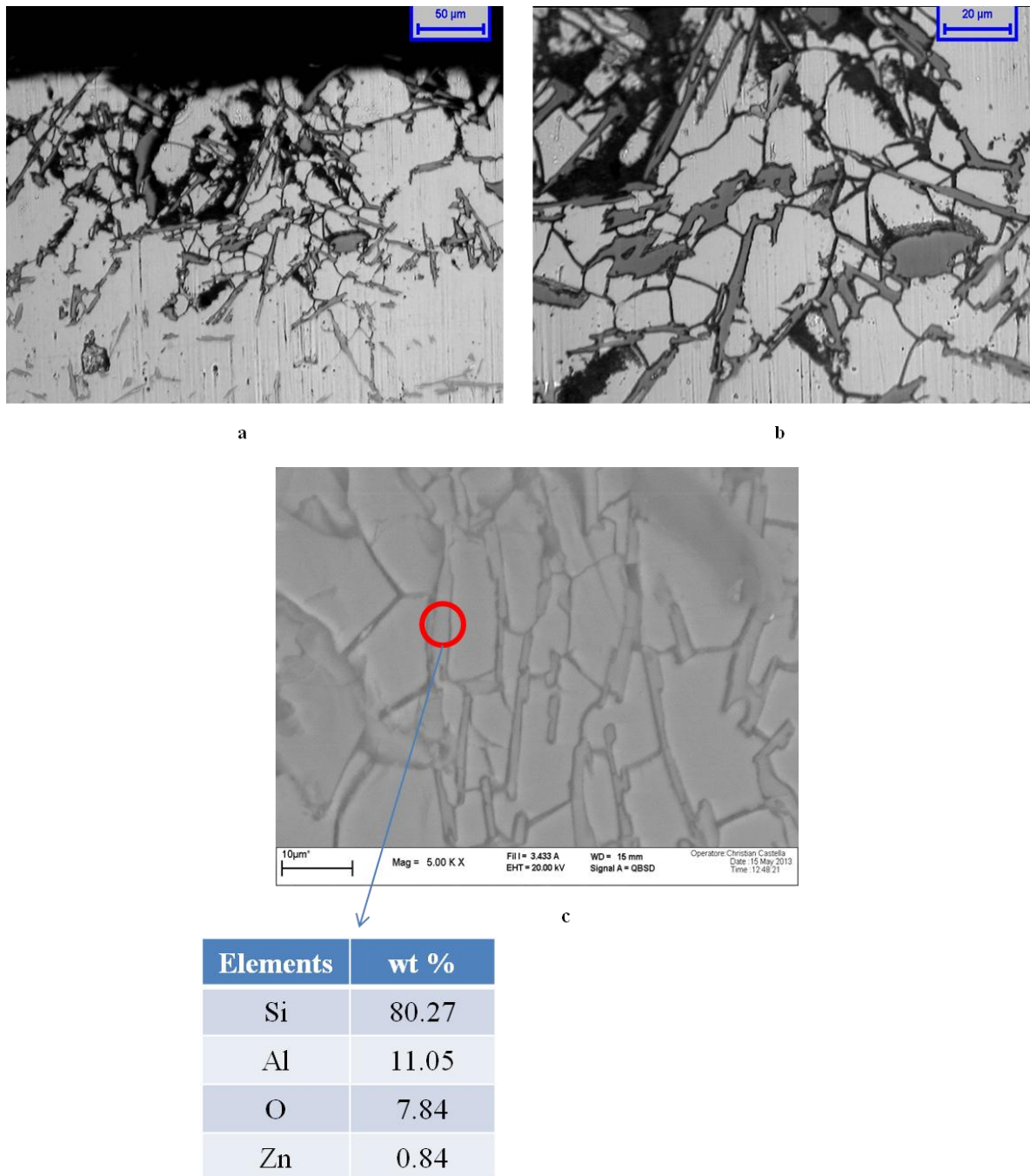
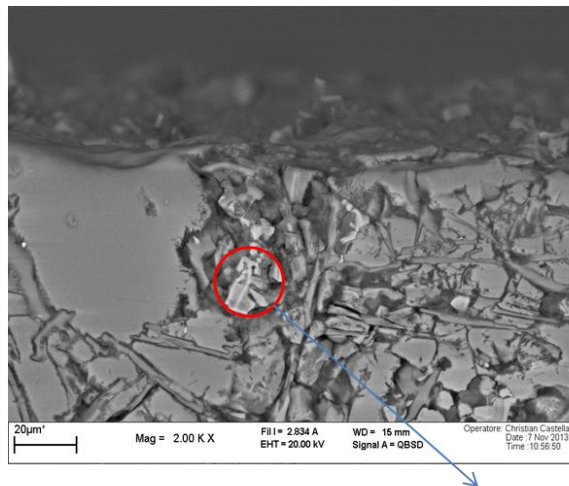


**Figure 86:** Optical microstructure a), b) and SEM microstructure with EDS analysis results c) of the transverse cross sections of the corroded samples, showing Si particles that act as local cathodes with respect to the eutectic Al matrix.



Elements	wt %
Al	57.50
Fe	16.40
Si	15.15
Mn	7.96
Zn	2.99

**Figure 87:** SEM microstructure and EDS analysis results of the transverse cross sections of the corroded samples, showing Fe-intermetallic which act as local cathodes with respect to the eutectic Al matrix.

Through the addition of Mg, up to 3 wt%, magnesium precipitates as Al–Fe–Si–Mg compounds, which behave cathodically with respect to the  $\alpha$ -Al phase, but they are expected to be less detrimental than Al–Fe, Al–Fe–Si and Al–Fe–Si–Mn and Si particles due to the presence of magnesium [75]. As can be observed by the SEM and the FESEM image of figure 88 these Al–Fe–Si–Mg compounds act as sacrificial anode with respect to the Al-matrix.

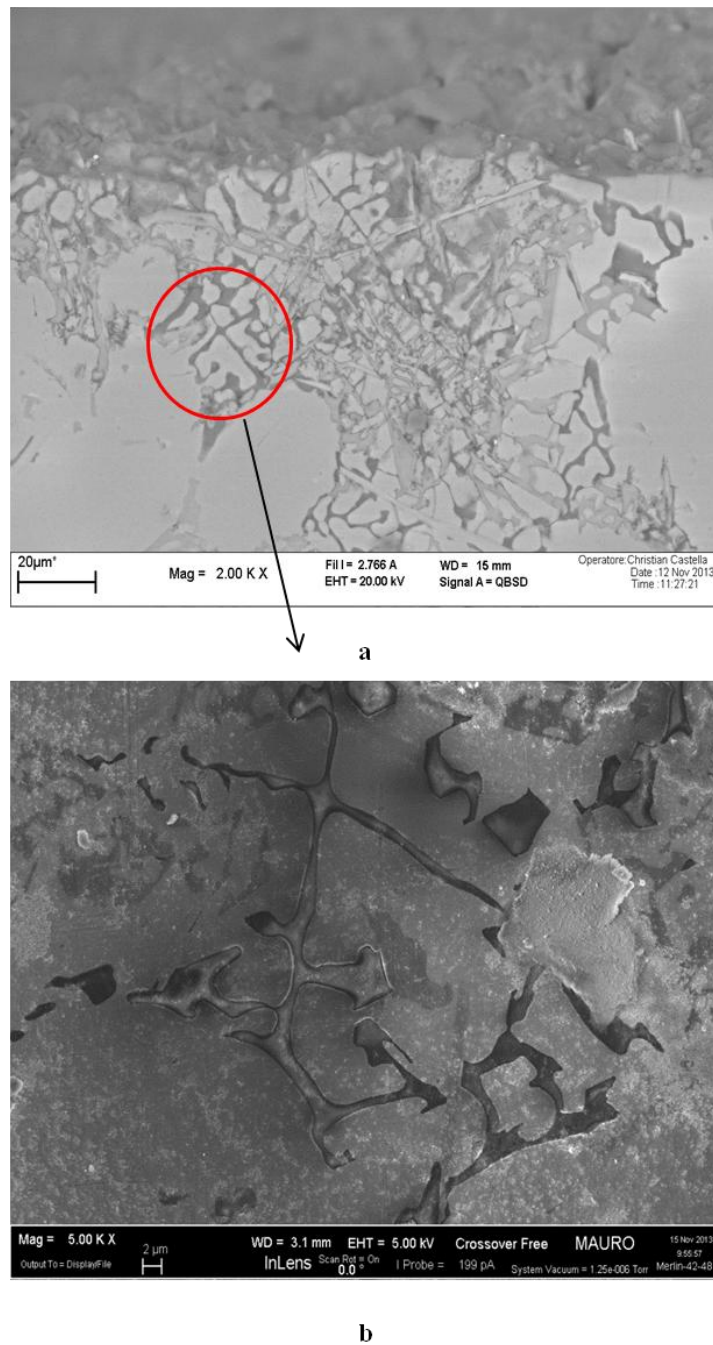


**Figure 88:** SEM image a) and FESEM image b) of Al-Fe-Si-Mg compounds.

Moreover, as can be observed by the X-Rays spectra of Figure 75, increasing the Mg content is increased the total amount of  $Mg_2Si$  hardening precipitates, that are anodic with respect to the aluminium matrix and thus may improve the localised corrosion phenomenon [75-76]. Some investigators [76] have been demonstrated that when a

AA5083 aluminum alloy is immersed in 0.005 M NaCl, during the first period of immersion, the  $Mg_2Si$  precipitates are covered by an hydroxide layer, that acts as a diffusion barrier, consequently impedes the dissolution of the intermetallics. The chemical reactions involved are the following:

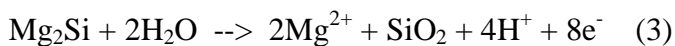
first of all the  $Mg_2Si$  precipitates are subjected to the hydrolyzation by water and as a results there is the development of silanes according to the reaction (1):



at the same time silanes are hydrolized, giving rise to the release of hydrogen and the formation of silicon hydroxides, on the  $Mg_2Si$  precipitates according to the reaction (2):



simultaneously the electrochemical dissolution of Mg from  $Mg_2Si$  precipitates takes place as reported in the reaction (3):



Therefore, the precipitation of Al–Fe–Si–Mg compounds and the increased amount of  $Mg_2Si$  precipitates, due the increase of Mg wt%, allow to reach a high corrosion resistance. In fact, as shown by the results reported in Figure 89, AlZn10Si8Mg3 self-hardening alloy presents the lowest values of both the weight loss and of the penetration depth.

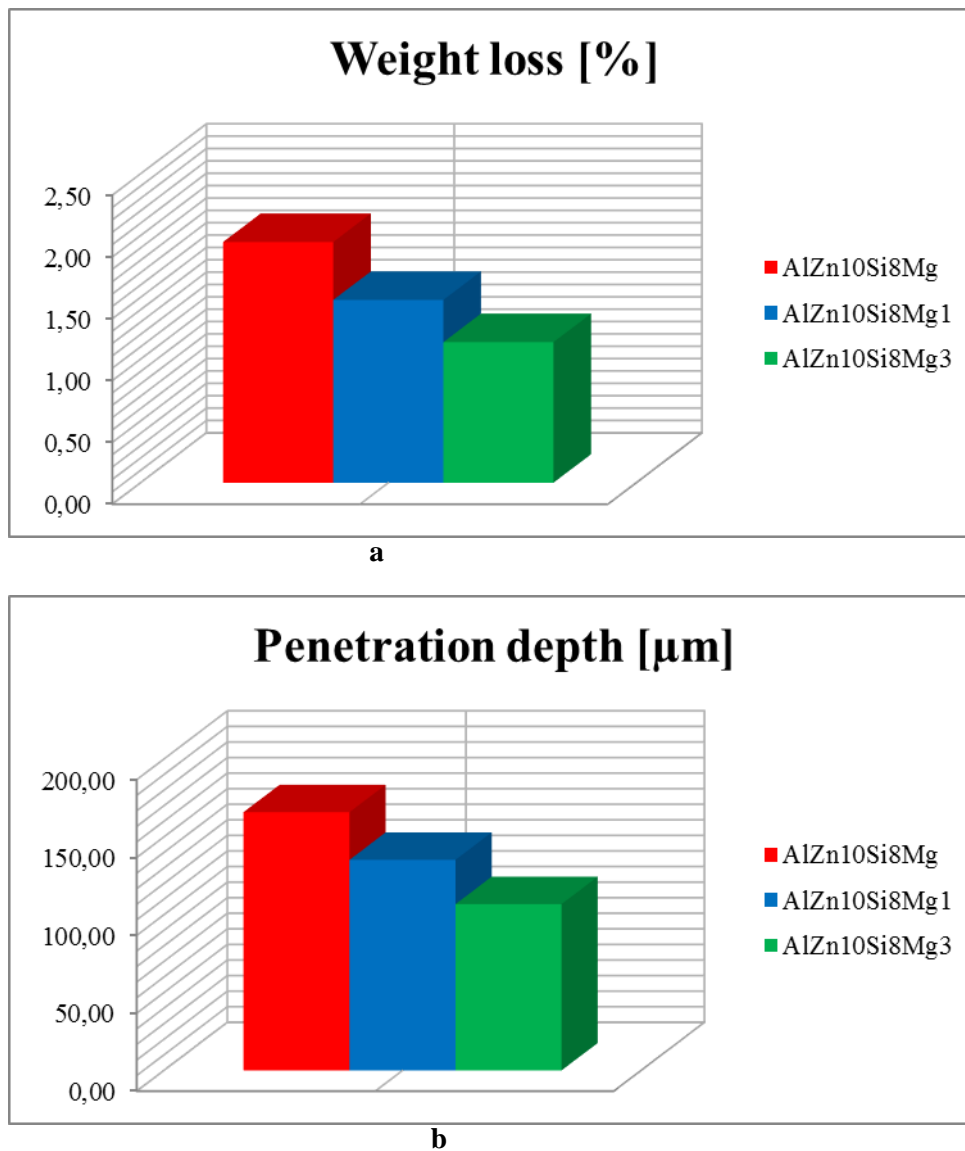


**Figure 89:** a) Weight loss and b) penetration depth, measured after the intergranular corrosion test.

The EDS analysis, reported in Figure 90, carried out on the external surface of the samples subjected to the intergranular corrosion test, have highlighted the presence of the mixed layer of aluminum and silicon oxide.

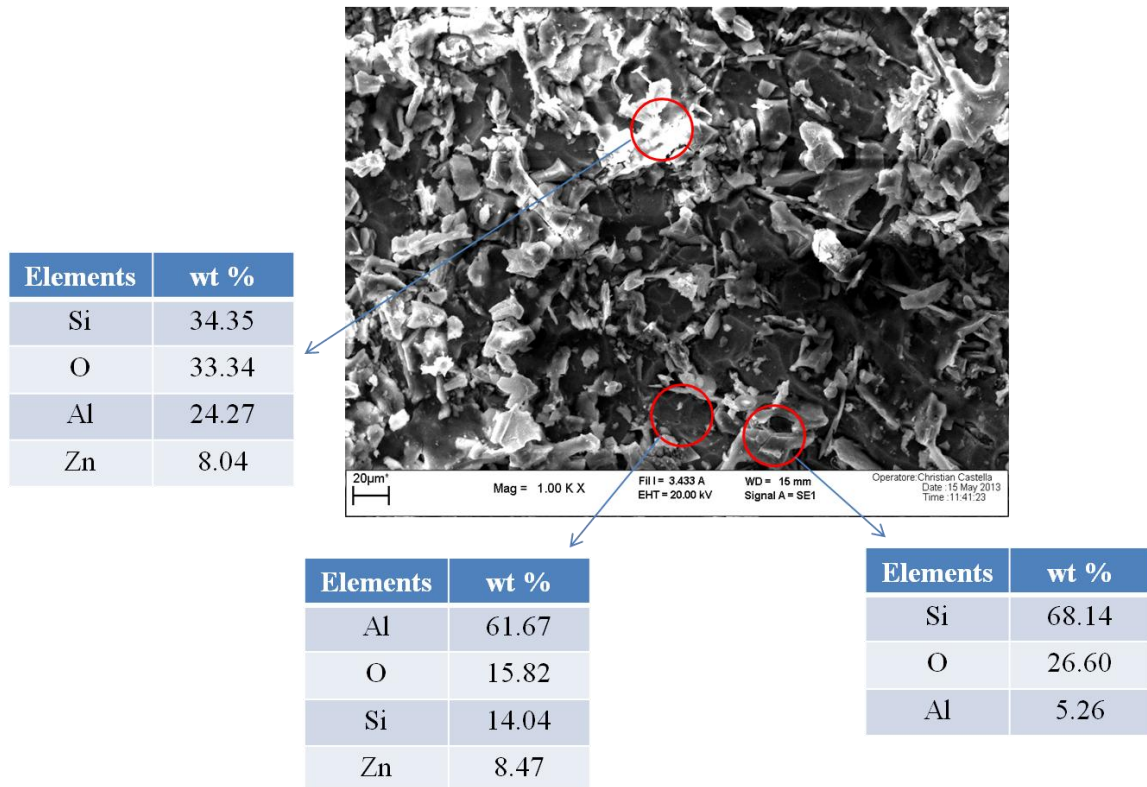


**Figure 90:** EDS results of the analysis conducted on the external surface of samples subjected to the intragranular corrosion test.

The mechanical properties of the alloys have been investigated prior to corrosion test and after the corrosion test, with the aim to assess how the corrosion phenomena affect the alloy's mechanical performances. Figures 91,92 and 93 show the results of the flexural tests and of the Charpy Impact test , performed on the samples. As can be observed the results reported in Figure 91, the corrosion causes a decrease of about 20% of the flexural stress at break for the AlZn10Si8Mg and AlZn10Si8Mg1 alloy, while the AlZn10Si8Mg3 alloy presents values of flexural stress at break similar before and after the corrosion test. The same behavior has been individuated for the flexural strain at break, as illustrated in Figure 92.

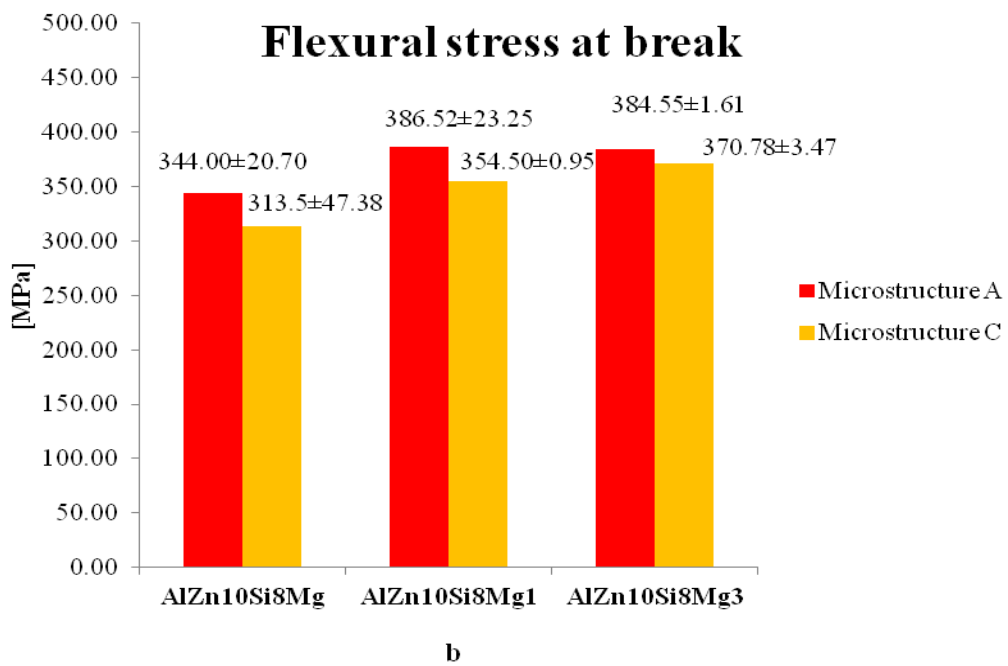
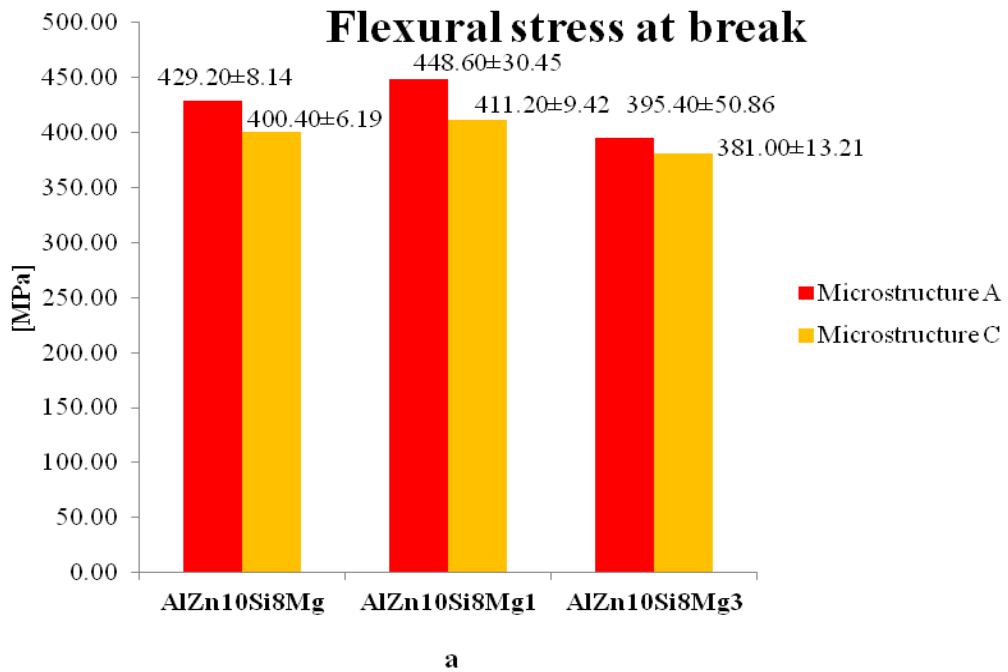
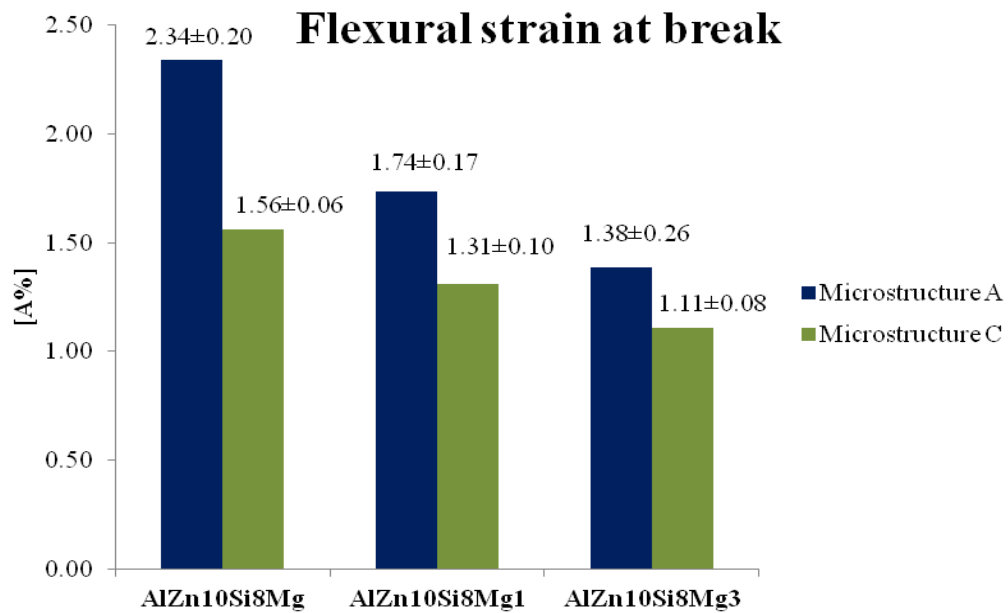
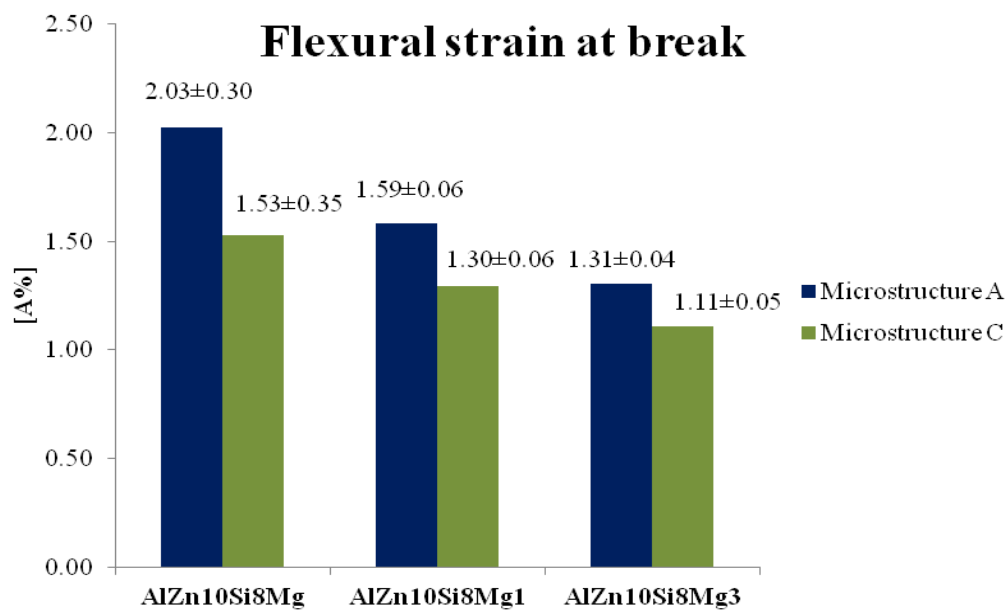


**Figure 91:** Three point bending tests, flexural stress at break results: a) before the intergranular corrosion test and b) after the intergranular corrosion test.



a

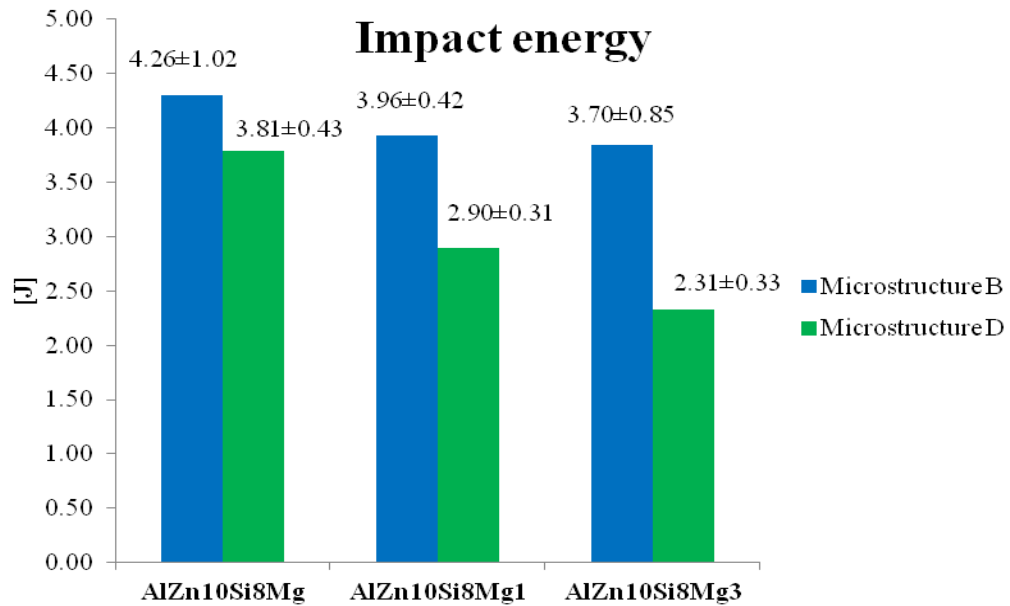


b

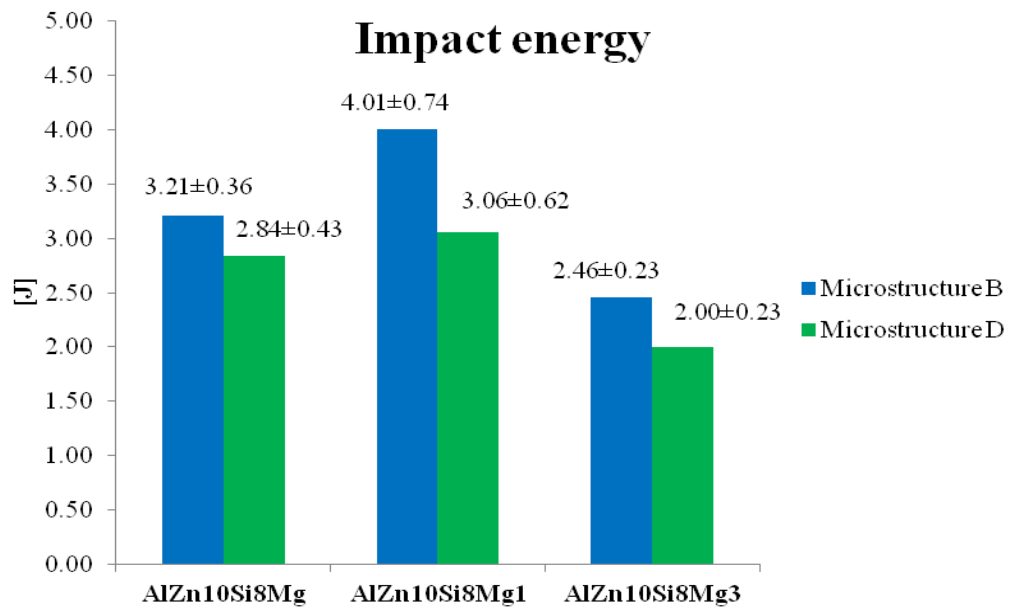
**Figure 92:** Three point bending tests, flexural strain at break results: a) before the intergranular corrosion test and b) after the intergranular corrosion test.

Moreover also the impact energy, in the case of the AlZn10Si8Mg and AlZn10Si8Mg3 alloys, has been subjected to a reduction of about 25%, because of the corrosion. On the contrary, the AlZn10Si8Mg1 alloy has the same impact energy before and after the

intergranular corrosion test. The results of impact test, before and after the intergranular corrosion test, are reported in Figure 93.



a



b

**Figure 93:** Charpy test results: a) before the intergranular corrosion test and b) after the intergranular corrosion test.

#### 4.4.5 Fatigue properties evaluation

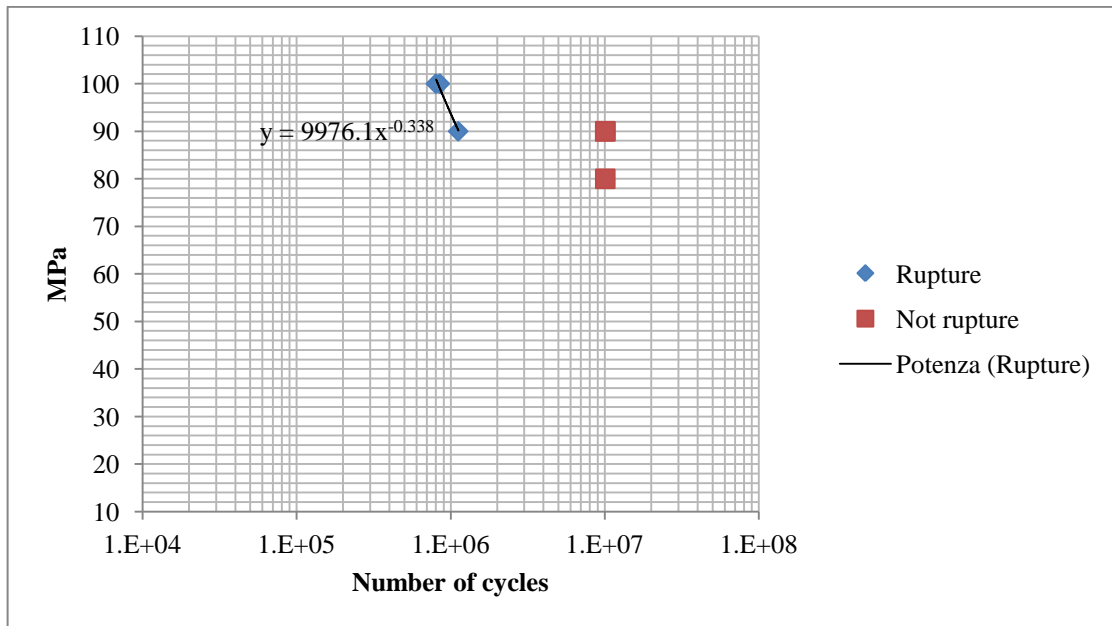
The obtained results till now suggest that at the moment the most promising alloy, that allows to obtain the right compromise between good mechanical properties and an increased corrosion resistance, is the AlZn10Si8Mg1 self-hardening aluminum alloy. For this reason has been decided to investigate as well the fatigue resistance of the AlZn10Si8Mg1 alloy.

The fatigue test have been realized by fatigue testing machine (TESTRONIC 100K RUMUL) under a load ratio of  $R = \sigma_{\min}/\sigma_{\max} = 0$  and a frequency between 130 Hz, at room temperature.

Fatigue limit was defined as the upper limit stress at which the specimens survived after a number of cycles  $N=10^7$  and, for all the tested samples, has been evaluated by stair case method.

Figure 94 reports the S-N curve and the survival probabilities obtained by the stair case method. In the S-N curve only two points are visible but really there are many points which are overlapped between themselves, this due to the scale used for the horizontal axis of the graph.

It can be observed that the AlZn10Si8Mg1 self hardening aluminum alloy has a fatigue limit of about 92 MPa. This fatigue limit value is comparable with that of A356 (AlSi7Mg0.3) alloy subjected to a T6 heat treatment and casting by permanent mold technique [3].



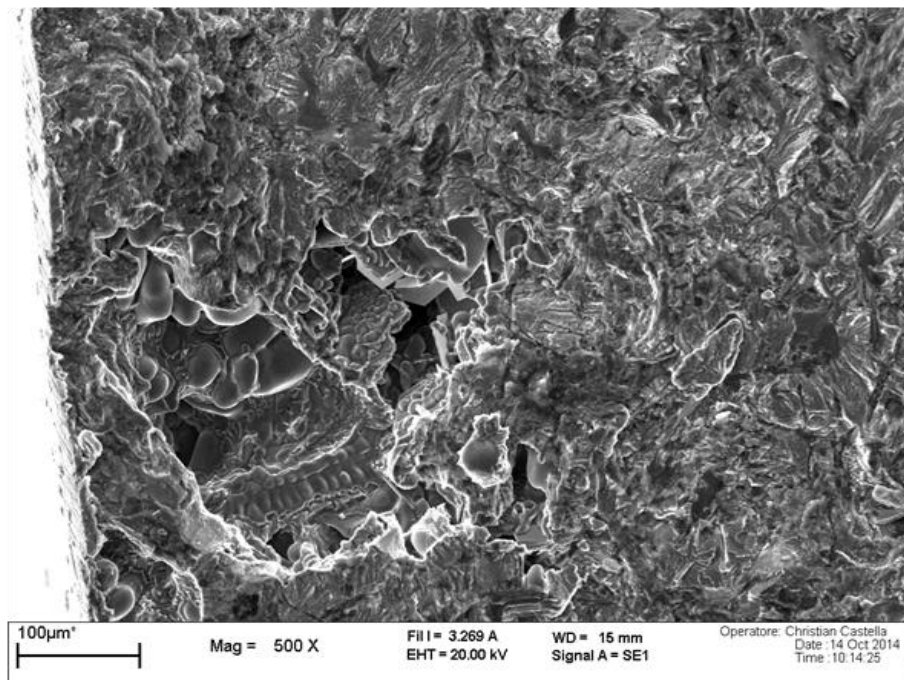
a

Stair case method for the AlZn10Si8Mg1			
	Survivor probability 90%	Survivor probability 50%	Survivor probability 10%
Fatigue limit [MPa]	84.9	91.7	98.45

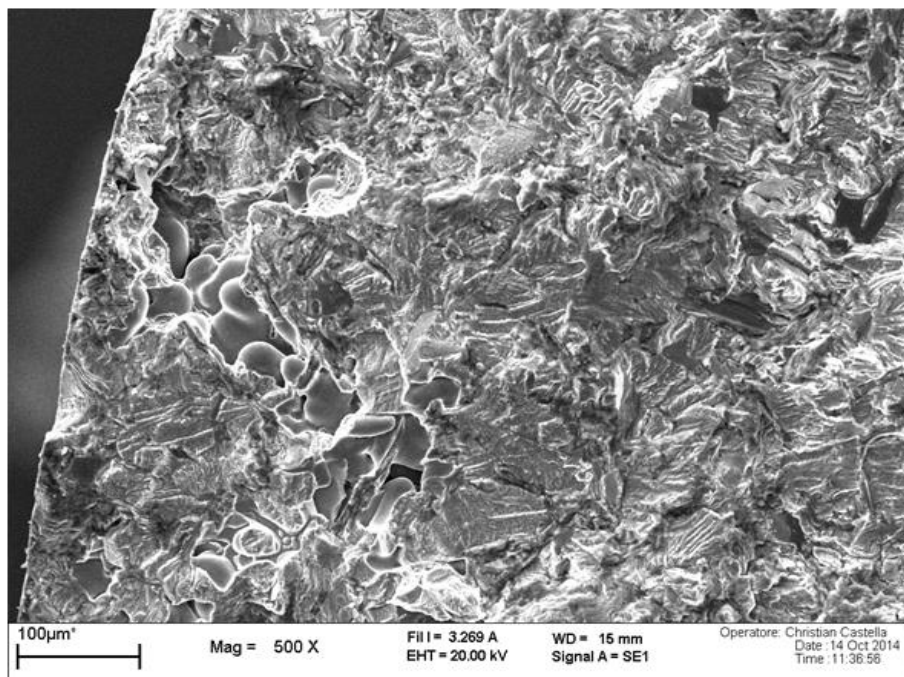
**Figure 94:** Fatigue test results: a) S-N curve and b) survival probabilities obtained by the stair case method.

#### 4.4.5.1 Fracture surface analysis

The fracture surface of sample after the fatigue tests is reported in Figure 95. The most frequently obtained defects, which have acted as nucleation site for the fatigue cracks development are shrinkage porosities, as shown in the SEM micrographs of Figure 95. These type of defects are generally considered as the main casting defects, originated during the casting operation or in the course of the mould feeding operations. Such imperfections can be solved, making some correction during the design and during the successive manufacturing process.



a



b

**Figure 95:** SEM micrographs showing shrinkage porosities that acted as crack initiation site.

Shrinkage porosities have been detected in many other areas of the fracture surfaces, as reported in the SEM micrograph of Figure 96. Fe-Mn intermetallics have been detected close to the shrinkage porosities. These intermetallics, that during the solidification of the aluminum alloy act as obstacle to the flow of liquid metal, are one of the principal causes of shrinkage porosities development.

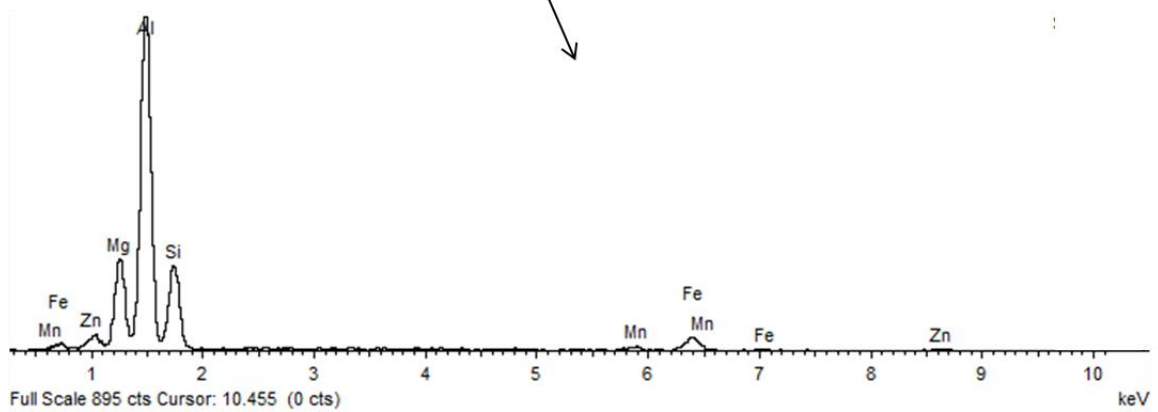
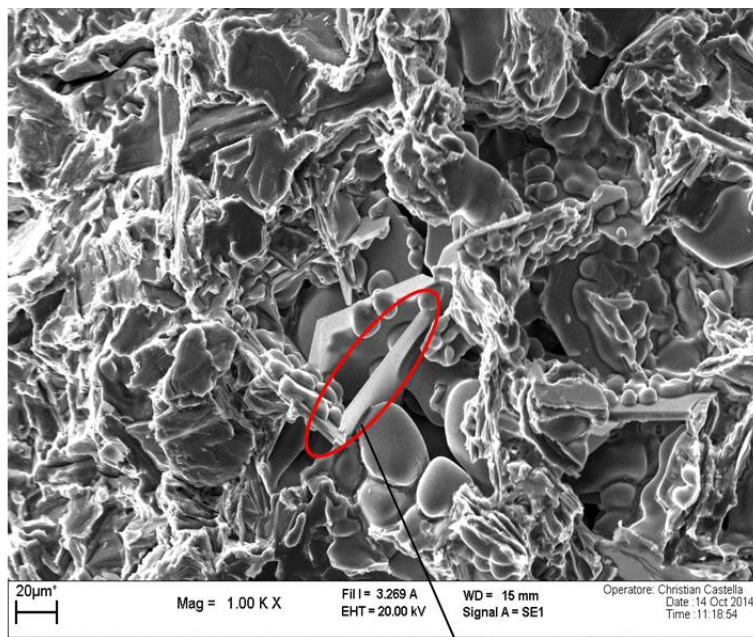


**Figure 96:** SEM micrograph that shows Fe-Mn intermetallics, which are one of the causes of shrinkage porosity development and EDS analysis results.

## 5 CONCLUSIONS

The goal of this PhD Thesis was to find an alternative solution to the actually used T6 heat-treated A356 alloy for automotive component production. The solution proposed is based on the use of an innovative class of light aluminum alloys and in particular a self-hardening Al-Zn-Si-Mg aluminum alloy. This class of alloy shows high mechanical properties which make them suitable for many applications in different industrial fields, especially in transport industry. The most important and relevant feature of the self-hardening alloys is related to their good performance, without the need of any heat treatment, because they are subjected to a natural ageing phenomenon at room temperature after a storage period of about 7-10 days.

The PhD Thesis includes a feasibility study of the development, of a knuckle suspension component, starting from the self hardening alloy which was evaluated and investigated. Actually, from economical point of view, the obtained results have demonstrated that the substitution of the A356 alloy, with the AlZn10Si8Mg self hardening alloy, for this specific application, is not a convenient choice. Despite this, the feature that makes this alloy interesting is the possibility to reach an important energy saving, especially in terms of gas and electricity consumption.

The microstructural analysis have revealed that the AlZn10Si8Mg alloy is made of a primary  $\alpha$ -aluminum matrix phase, an eutectic mixture of Al-Si, some Zn-rich areas and some intermetallics compounds. Especially MgZn<sub>2</sub> and Mg<sub>2</sub>Si precipitates, as well as Zn-rich areas into the  $\alpha$ -Al matrix, have allowed obtaining high mechanical properties, respectively, by the precipitation hardening and the solid solution strengthening mechanism. The obtained mechanical properties are perfectly comparable to those of the T6 heat treated A356 (AlSi7Mg0.3) aluminum alloy and they satisfy the properties requirements for the knuckle component. Currently, only the elongation to fracture (A%) does not satisfy the requirement for the knuckle suspension component. The alloy has achieved the highest mechanical performance after seven days of natural ageing.

## Conclusions

The composition of the basic alloy has been modified by Mg addition in order to promote the precipitation of  $Mg_2Si$  precipitates, that are anodic particles with respect to the  $\alpha$ -aluminum matrix and allow to enhance the corrosion resistance of the alloy.

Two modified self hardening alloys have been casted and investigated: one with 1wt% of Mg, labeled as AlZn10Si8Mg1 and the second one with 3wt% of Mg, labeled as AlZn10Si8Mg3.

The influence of both the Mg wt% and of the cooling rate, on the microstructure, on the mechanical properties and on the corrosion resistance of the alloys, was investigated.

High Mg content, with high cooling rate, have allowed achieving a fine microstructure, with modified silicon particles, with a partially fibrous structure. Moreover, high Mg content and low cooling rate values, promotes the precipitation of large Mg-Si precipitates and they negatively influenced the mechanical properties of the alloy.

The AlZn10Si8Mg1 alloy has the highest values of flexural stress at break, thanks to the presence of  $Mg_2Si$  and  $MgZn_2$  hardening precipitates. Increasing the Mg wt%, the Mg-Si based intermetallics, are became larger, and consequently contributes to the crack growths followed by the failure of the alloys. This is the reason why AlZn10Si8Mg3 alloy presents lower flexural stress at break values than those of the AlZn10Si8Mg and AlZn10Si8Mg1 alloys. The presence of Mg-Si compound has a detrimentally effect also on the flexural strain values and on the impact resistance of the alloys.

The increased Mg content has allowed increasing the corrosion resistance: the best corrosion resistance was reached by the AlZn10Si8Mg3 alloy as presented, thanks to the precipitation of Al-Fe-Si-Mg compounds and the high amount of  $Mg_2Si$  precipitates, which are anodic with respect to the Al-matrix.

Comparing the obtained results, in terms of mechanical properties and corrosion resistance, the AlZn10Si8Mg1 alloy, obtained with a cooling rate of about  $14^\circ C/s$ , results to be the most promising candidate. This alloy allows obtaining the right compromise between good mechanical properties and an increased corrosion resistance. Furthermore, the fatigue limit of this alloy is about 92 MPa. This results is comparable to that of the A356 alloy, subjected to the T6 heat treatment. Shrinkage porosities are the main defects affecting negatively the fatigue resistance of the alloy.

## Conclusions

### **ON-GOING ACTIVITIES**

Some on-going research activities are related to complete the evaluation of the mechanical properties. The further goal will be to increase the value of the elongation to fracture, in order to reach the standard required by the automotive industry for these alloys. Moreover, the fatigue resistance of the most promising alloy will be evaluated at high temperature.

## References

## **REFERENCES**

- [1] *Atlante metallografico delle leghe di alluminio da fonderia*, Ettore di Russo, Edimet.
- [2] *Corrosion of aluminum and aluminum alloys*, edited by J.R.Davis, The materials information society.
- [3] ASM handbook, volume 2 edited by Joseph R. Davis.
- [4] E.A. Starke Jr.; *Aluminum alloys: Alloy, Heat Treatment, and Temper Designation*; Encyclopedia of Materials: Science and Technology (Second Edition), 2001, Pages 106-107.
- [5] H.A. Elhadari, H.A. Patel, D.L. Chena, W. Kasprzak; *Tensile and fatigue properties of a cast aluminum alloy with Ti, Zr and V additions*; Materials Science and Engineering A 528 (2011) 8128–8138.
- [6] R. S. Rana, Rajesh Purohit, and S Das; *Reviews on the Influences of Alloying elements on the Microstructure and Mechanical Properties of Aluminum*; International Journal of Scientific and Research Publications, Volume 2, Issue 6, June 2012 .
- [7] G.Timelli, E.Fiorese, *Metodi di neutralizzazione del Fe in leghe Al-Si da fonderia*, La Metallurgia Italiana n.3 Marzo (2011) 9-23.
- [8] GUO Hong-min, YANG Xiang-jie; *Preparation of semi-solid slurry containing fine and globular particles for wrought aluminum alloy 2024*; Trans. Nonferrous Met. SOC. China 17(2007) 799-804.
- [9] D.G. Eskin, Suyitno, L. Katgerman; *Mechanical properties in the semi-solid state and hot tearing of aluminium alloys*; Progress in Materials Science 49 (2004) 629–711.
- [10] Emma Sjölander, Salem Seifeddine; *The heat treatment of Al-Si-Cu-Mg casting alloys*; Journal of Materials Processing Technology 210 (2010) 1249–1259.
- [11] M.F. Ibrahim, A.M. Samuel, F.H. Samuel, *A preliminary study on optimizing the heat treatment of high strength Al-Cu-Mg-Zn alloys*, Materials and Design 57 (2014) 342–350.
- [12] Higgins R.A., *Engineering metallurgy*, Second Edition, ELBS, ISBN 034018468X, (1986).

## References

- [13] J.S. Robinson, D.A. Tanner, C.E. Truman, A.M. Paradowska, R.C. Wimpory; *The influence of quench sensitivity on residual stresses in the aluminium alloys 7010 and 7075*; *Materials Characterization* 65 (2012) 73 – 85.
- [14] Jasim M. Salman, Shaymaa Abbas Abd Alsada and Khadim F. Al-Sultani; *Improvement Properties of 7075-T6 Aluminum Alloy by Quenching in 30% Polyethylene Glycol and Addition 0.1%B*; *Research Journal of Material Sciences* Vol. 1(6), 12-17, July (2013).
- [15] Diana A. Lados, Diran Apelian, Libo Wang; *Minimization of residual stress in heat-treated Al–Si–Mg cast alloys using uphill quenching: Mechanisms and effects on static and dynamic properties*; *Materials Science and Engineering A* 527 (2010) 3159–3165.
- [16] William D. Callister, Jr.; *Fundamentals of Materials Science and Engineering*; Fifth edition.
- [17] D.L. Cocks, *A proposed simple qualitative classification for die-casting defects*, Proc. Die-Casting Conference, Montreaux (1996), p. 19/1.
- [18] J. Campbell, R.A. Harding, *Casting Technology*, in TALAT 2.0 cd-rom, EEA, Brussels (2000).
- [19] *Manuale della difettologia nei getti pressocolati*, E.Gariboldi – F.Bonollo – P.Parona, Associazione Italiana di Metallurgia.
- [20] S.B. Ghanti, E.A. Druschitz, A.P. Druschitz, J.A. Griffin; *The effects of solidification underpressure on the porosity and mechanical properties of A206-T6 cast aluminum alloy*; Paper 11-048 page 1-8 AFS proceedings 2011 America Foundry Society Schaumburg, IL USA.
- [21] H.R. Ammar, A.M. Samuel, F.H. Samuel; *Porosity and the fatigue behavior of hypoeutectic and hypereutectic aluminum–silicon casting alloys*; *International Journal of Fatigue* 30 (2008) 1024–1035.
- [22] Bitu Ghaffari, George Mozurkewich, Larry A. Godlewski, Jacob W. Zindel; *Ultrasonic characterization of shrinkage microporosity in aluminum castings*; *Ultrasonics* 41 (2004) 699–707.

## References

- [23] C. Tian, J. Law, J. van der Touw, M. Murray, J.-Y. Yao, D. Graham, D. St. John; *Effect of melt cleanliness on the formation of porosity defects in automotive aluminium high pressure die castings*; Journal of Materials Processing Technology 122 (2002) 82–93.
- [24] O. Majidi, S.G. Shabestari, M.R. Aboutalebi; *Study of fluxing temperature in molten aluminum refining process*; Journal of Materials Processing Technology 182 (2007) 450–455.
- [25] Yun Wang, Hu-Tian Li, Zhongyun Fan; *Oxidation of Aluminium Alloy Melts and Inoculation by Oxide Particles*; Trans Indian Inst Met DOI 10.1007/s12666-012-0194-x.
- [26] J.Campbell, *Castings*, Butterworth, Oxford, 1991.
- [27] D.Dispinar, J.Campbell, International Journal of cast metal research 17,2004, 280-286.
- [28] Salem Seifeddine, Torsten Sjögren and Ingvar L Svensson; *Variations in microstructure and mechanical properties of cast aluminum EN AC 43100 alloy*; Metallurgical Science and Technology 12-22.
- [29] J. Hirsch, T. Al-Samman; *Superior light metals by texture engineering: Optimized aluminum and magnesium alloys for automotive applications*; Acta Materialia 61 (2013) 818–843.
- [30] European Aluminium Association.
- [31] Ju`rgen Hirsch; *Aluminium in Innovative Light-Weight Car Design*; Materials Transactions, Vol. 52, No. 5 (2011) pp. 818 to 824.
- [32] Jürgen HIRSCH; *Recent development in aluminium for automotive applications*; Trans. Nonferrous Met. Soc. China 24(2014) 1995–2002.
- [33]J.Hirsch; *Aluminium in innovative light-weight car design*; Proc Innovative Development for Lightweight Vehicle Structures; Wolfsburg, Germany: VW, 2009: 101.
- [34] SLC Super Light Car Project [EB/OL]. <http://www.superlightcar.com>.
- [35] K. Shimizu, R.C. Furneaux, G.E. Thompson, G.C. Wood, A. Gotoh and K. Kobayashi; *On the nature of “easy paths” for the diffusion of oxygen in thermal oxide films on aluminium*; Oxidation of Metals vol.35, Nos.5/6 pp.427-439, 1991.

## References

- [36] J.R. Davis; *Corrosion of aluminum and aluminum alloys*; Edited by J.R.Davis ASM International.
- [37] N. L. Sukiman, X. Zhou, N. Birbilis, A.E. Hughes, J. M. C. Mol, S. J. Garcia, X. Zhou and G. E. Thompson; *Aluminium Alloys - New Trends in Fabrication and Applications*; Edited by Zaki Ahmad, Intech.
- [38] G. M. Scamans, N. Birbilis, R. G. Buchheit; *Corrosion of Aluminum and its Alloys*; 2010 Elsevier B.V..
- [39] M.G. Alvarez, J.R. Galvele; *Pitting Corrosion*; Shreir's Corrosion Volume 2, 2010, Pages 772-800.
- [40] M.A. Pech-Canul, M.I. Pech-Canul, P. Bartolo-Pérez, M. Echeverría; *The role of silicon alloying addition on the pitting corrosion resistance of an Al-12 wt.%Si alloy*; *Electrochimica Acta* 140 (2014) 258–265.
- [41] S. Jain; *Corrosion and protection of heterogeneous cast Al-Si (356) and Al-Si-Cu-Fe (380) alloys by chromate and cerium inhibitors*; The Ohio State University, Ohio, USA, 2006.
- [42] K. Nisancioglu; *Electrochemical behavior of aluminum-base intermetallics containing iron*; *J. Electrochem. Soc.* 137 (1990) 69-77.
- [43] K.A. Yasakau, M.L. Zheludkevich, S.V. Lamaka, M.G.S. Ferreira; *Role of intermetallic phases in localized corrosion of AA5083*; *Electrochim. Acta* 52 (2007) 7651-7659.
- [44] R. Arrabal, B. Mingo, A. Pardo, M. Mohedano, E. Matykina, I. Rodriguez; *Pitting corrosion of rheocast A356 aluminium alloy in 3.5 wt.% NaCl solution*; *Corrosion Science* 73 (2013) 342–355.
- [45] H.C. Fang, H. Chao, K.H. Chen; *Effect of recrystallization on intergranular fracture and corrosion of Al-Zn-Mg-Cu-Zr alloy*; *Journal of Alloys and Compounds* 622 (2015) 166–173.
- [46] Fengxuan Song, Xinming Zhang, Shengdan Liu, Qi Tan, Dongfeng Li; *The effect of quench rate and overageing temper on the corrosion behaviour of AA7050*; *Corrosion Science* xxx (2013).

## References

- [47] Lanping Huang, Kanghua Chen, Song Li; *Influence of grain-boundary pre-precipitation and corrosion characteristics of inter-granular phases on corrosion behaviors of an Al–Zn–Mg–Cu alloy*; *Materials Science and Engineering B* 177 (2012) 862–868.
- [48] Amjad Saleh El-Amoush; *Intergranular corrosion behavior of the 7075-T6 aluminum alloy under different annealing conditions*; *Materials Chemistry and Physics* 126 (2011) 607-613.
- [49] W.J. Liang, P.A. Rometsch, L.F. Cao, N. Birbilis; *General aspects related to the corrosion of 6xxx series aluminium alloys: Exploring the influence of Mg/Si ratio and Cu*; *Corrosion Science* 76 (2013) 119–128.
- [50] Starink M.J., Li X M.; *A model for electrical conductivity of peak-aged and overaged Al–Zn–Mg–Cu alloys*; [J]. *Metallurgical and Materials Transactions A*, 2003, 34(4): 899–911.
- [51] Chen Song-yi, Chwn Kang-hua, Peng Guo-sheng, Liang Xin, Chen Xue-hai; *Effect of quenching rate on microstructure and stress corrosion cracking of 7085 aluminum alloy*; [J]. *Transactions of Nonferrous Metals Society of China*, 2012, 22(1): 47–52.
- [52] Knight S. P., Birbilis N., Muddle B. C., Trueman A. R., Lynch S. P.; *Correlations between intergranular stress corrosion cracking, grain-boundary microchemistry, and grain-boundary electrochemistry for Al–Zn–Mg–Cu alloys*; [J]. *Corrosion Science*, 2010, 52(12): 4073–4080.
- [53] Andreatta F., Terryn H., de Wit J. H. W.; *Effect of solution heat treatment on galvanic coupling between intermetallics and matrix in AA7075-T6*; [J]. *Corrosion Science*, 2003, 45(8): 1733–1746.
- [54] Zhang Ping, Li Qi, Zhao Jun-jun, Zeng Qing-qiang.; *Analysis of secondary phases and measurement of volta potential of 7A52aluminum alloy*; [J]. *The Chinese Journal of Nonferrous Metals*, 2011, 21(6): 1252–1257.
- [55] Venugopal A., Panda R., Manwatkar S., Sreekumar K., Rama Krishna L., Sundararajan G.; *Effect of micro arc oxidation treatment on localized corrosion behaviour of AA7075 aluminum alloy in 3.5% NaCl solution*; [J]. *Transactions of Nonferrous Metals Society of China*, 2012, 22(3): 700–710.

## References

- [56] Huan She, Wei Chu, Da Shu, Jun Wang, Bao-de Sun; *Effects of silicon content on microstructure and stress corrosion cracking resistance of 7050 aluminum alloy*; Trans. Nonferrous Met. Soc. China 24(2014) 2307–2313.
- [57] S. Geng, S. Joshi, W. Pinc, W.G. Fahrenholtz, M.J. O' Keefe, T.J. O' Keefe, P. Yu; *Influence of processing parameters on cerium based conversion coatings*; in: Proc. Tri-Service Corrosion Conference, Denver, CO, NACE International, 2007, p. 10.
- [58] B. Valdez, S. Kiyota, M. Stoytcheva, R. Zlatev, J.M. Bastidas; *Cerium-based conversion coatings to improve the corrosion resistance of aluminium alloy 6061-T6*; Corrosion Science 87 (2014) 141–149.
- [59] Peter Plagemann, Joerg Weise, Anja Zockoll; *Zinc-magnesium-pigment rich coatings for corrosion protection of aluminum alloys*; Progress in Organic Coatings 76 (2013) 616– 625.
- [60] Du Nan, Wang Shuai-xing, Zhao Qing, Shao Zhi-song; *Effects of boric acid on microstructure and corrosion resistance of boric/sulfuric acid anodic film on 7050 aluminum alloy*; Trans. Nonferrous Met. Soc. China 22(2012) 1655-1660.
- [61] J. Singh-Beemat, J.O. Iroh; *Effect of clay on the corrosion inhibition and dynamic mechanical properties of epoxy ester–polyurea–polysiloxane hybrid coatings*; Polym. Eng. Sci. (2012).
- [62] J. Singh-Beemat, J.O. Iroh; *Characterization of corrosion resistant clay/epoxy ester composite coatings and thin films*; Progress in Organic Coatings 74 (2012) 173–180.
- [63] Jaspreet Singh-Beemat, Jude O. Iroh, Linqian Feng; *Mechanism of corrosion protection of aluminum alloy substrate by hybrid polymer nanocomposite coatings*; Progress in Organic Coatings 76 (2013) 1576– 1580.
- [64] E. Tillová, E. Ďuriníková, M. Chalupová; *Structural analysis of secondary AlZn10Si8Mg cast alloy*; Acta Metallurgica Slovaca, Vol. 17, 2011, No. 1, p. 4-10.
- [65] E. Tillová, E. Ďuriníková, M. Chalupová; *Characterization of phases in secondary AlZn10Si8Mg cast alloy*; Materials Engineering - Materiálové inžinierstvo 18 (2011) 1-7.
- [66] [http://www.dietermann-guss.de/\\_pdf-Dateien/IN%20FORM\\_01\\_12%20eng.pdf](http://www.dietermann-guss.de/_pdf-Dateien/IN%20FORM_01_12%20eng.pdf).

## References

- [67] M.Rosso, I.Peter, C.Castella , R.Molina; *Investigation on AlZn10Si8Mg alloys for automotive application*; Metallurgical Science and Technology Vol. 31-1 - Ed. 2013.
- [68] M.Rosso, I.Peter, C.Castella , R.Molina; *Properties of AlZn10Si8Mg Alloys for High Performances Application*; Light metals 2014 p.213-218.
- [69] I.Peter, M.Rosso, C.Castella, R.Molina; *Self-hardening alloys for automotive application*; Materials Science Forum Vols. 794-796 (2014) pp 1221-1226.
- [70] <http://www.rheinfelden-alloys.eu/>.
- [71] C. Y. Song, J. Lee; *Reliability-based design optimization of knuckle component using conservative method of moving least squares meta-models*; Probabilistic Engineering Mechanics 26 (2011) 364–379.
- [72] J. L. Murray; *The Al-Zn (Aluminum-Zinc) System*; Bulletin of Alloy Phase Diagrams Vol. 4 No. 1 1983.
- [73] G.Timelli, E.Fiorese; *Metodi di neutralizzazione del Fe in leghe Al-Si da fonderia*; La Metallurgia Italiana n.3 Marzo 2011 9-23.
- [74] C. Mascré, Fonderie, 108 (1955), 4330-4334.
- [75] R. Arrabal, B. Mingo, A. Pardo, M. Mohedano, E. Matykina, I. Rodriguez, *Pitting corrosion of rheocast A356 aluminium alloy in 3.5 wt.% NaCl solution*, Corrosion Science 73 (2013) 342-355.
- [76] Kiryl A. Yasakau, Mikhail L. Zheludkevich ,Sviatlana V. Lamaka, Mario G.S. Ferreira; *Role of intermetallic phases in localized corrosion of AA5083*; Electrochimica Acta 52 (2007) 7651–7659.
- [77] V.A. Hosseini, S.G. Shabestari, R. Gholizadeh; *Study on the effect of cooling rate on the solidification parameters, microstructure, and mechanical properties of LM13 alloy using cooling curve thermal analysis technique*; Materials and Design 50 (2013) 7-14.
- [78] Deepak Singla, S.R. Mediratta; *Evaluation of mechanical properties of Al 7075-fly ash composite material*; International Journal of Innovative Research in Science, Engineering and Technology Vol. 2, Issue 4, April 201.
- [79] *Determination of resistance to IGC of solution heat-treatable aluminium alloys*, Standard BS11846:1995, British Standards Institution (1995).

Author's publications

- [1] *Investigation on AlZn10Si8Mg alloys for automotive application*; Mario Rosso, Ildiko Peter, Christian Castella, Roberto Molina; Metallurgical Science and Technology Vol. 31-1 - Ed. 2013, ISSN 0393-6074.
- [2] *Investigation on coatings of dies for advanced squeeze casting process*; Ildiko Peter, Mario Rosso, Christian Castella; Acta Metallurgica Slovaca, Vol. 20, 2014, No. 1, p. 18-27, doi 10.12776/ams.v20i1.207.
- [3] *Design and microstructure of innovative Cobalt base alloy*; Ildiko Peter, Mario Rosso, Dan Ioan, Brandusa Ghiban and Christian Castella; Materials Science Forum Vols. 790-791 (2014) pp 235-240, doi:10.4028/www.scientific.net/MSF.790-791.235.
- [4] *Self- hardening alloys for automotive application*; Ildiko Peter, Mario Rosso, Christian Castella, Roberto Molina; Materials Science Forum Vols. 794-796 (2014) pp 1221-1226; doi:10.4028/www.scientific.net/MSF.794-796.1221.
- [5] *Effects of thermal treatments on the behavior of AlSi7Cu3Mg alloy*; Mario Rosso, Ildiko Peter, Christian Castella, Roberto Molina; Metallurgical Science and Technology, vol.32-1 - Ed.2014.
- [6] *Properties of AlZn10Si8Mg Alloys for High Performances Application*; Mario Rosso, Ildiko Peter, Christian Castella, Roberto Molina; in Proceedings of the symposia sponsored by the TMS Aluminum Committee at the TMS 2014 Annual Meeting & Exhibition, February 16-20, 2014 San Diego, California, USA, Light metals 2014 pp .213-218, ISSN: 1096-9586.
- [7] *Studio e ottimizzazione del trattamento termico T6 per la lega 7068*, Proceedings 35° Convegno Nazionale AIM (Associazione Italiana di Metallurgia), Roma 5-7 Novembre 2014, Università degli studi di Roma Tor Vergata.
- [8] Presentazione su invito, *Light weight components for automotive application*, Proceedings RoMat 2014 - 5<sup>th</sup> International Conference on Materials Science and Technologies , 15<sup>th</sup>-17<sup>th</sup> October 2014, Bucharest - Romania, University Politehnica of Bucharest, Romania.